1-1-2000

Solid-state NMR studies of PEO in various environments : conformation, chemical shift, and dynamics.

Douglas J. Harris
University of Massachusetts Amherst

SOLID-STATE NMR STUDIES OF PEO IN VARIOUS ENVIRONMENTS: CONFORMATION, CHEMICAL SHIFT, AND DYNAMICS

A Dissertation Presented

by

DOUGLAS J. HARRIS

Submitted to the Graduate School of the
University of Massachusetts Amherst in partial fulfillment
of the requirements for the degree of

DOCTOR OF PHILOSOPHY

September 2000

Polymer Science & Engineering

SOLID-STATE NMR STUDIES OF PEO IN VARIOUS ENVIRONMENTS: CONFORMATION, CHEMICAL SHIFT, AND DYNAMICS

A Dissertation Presented

by

DOUGLAS J. HARRIS

Approved as to style and content by:

Klaus Schmidt-Rohr, Chair

Helmut Strey, Member

Scott Auerbach, Member

Richard J. Farris, Department Head
Polymer Science & Engineering

To Doodyhead, Lolly, Lily, and Zygomorphic Bilk.

ACKNOWLEDGMENTS

Many people have provided advice, assistance and encouragement. I would first like to thank Professor Klaus Schmidt-Rohr, a superior man and a rising star in applied physics. His tutelage and enthusiasm towards science has made my Ph.D. experience both exciting and enjoyable. His constructive criticism has greatly increased the quality of this thesis, and his many ideas has initiated my research. Radiating from this man is a passion for science that has inspired every member of Team Schmidt-Rohr.

I also would like to thank the members of my committee, Professor Helmut Strey and Professor Scott Auerbach, for their different prospective which has benefited my interpretation and understanding of my research. In addition, there are many members of the Polymer Science and Engineering department who have provided help with the research. I am grateful to Dr. L. Charles Dickinson for the help that he provided whenever I encountered problems with the NMR spectrometers. I am also thankful to Dr. Alan Waddon, and Mrs. Eileen Besse for their kind assistance in the past years.

I would like to express my appreciation to all of the current and past members of Team Schmidt-Rohr: Professor Kristin Kumashiro, Professor Tito Bonagamba, Professor Hironori Kaji, Prof. Dick Sandström, Dr. Ioannis Polios, Dr. Matt Dunbar, Mr. Mikhail Gelfer, Mr. Doug Harris, Mr. Dan Mowery, Mr. Eduardo deAzevedo, Mr. Fabio Becker-Guedes, and Ms. Gabi Menges. We have shared many late nights together in the Conte Building and their encouragement and advice has increased my passion towards science.

There are many people outside of the department who have contributed to my research. My father, since I was hatched, has encouraged me to study science. My mother has taught me to think, to dream, and never yield. My brother taught me that I must work hard or else he would be better than me. I would like to thank Dr. Robin Nissan who introduced NMR spectroscopy to me, and Professor Anne Mayes who challenged me to learn about polymer science. Finally, I sincerely thank my wife for her support during my Ph.D. studies. She is truly a superior woman. Her dedication, honesty, and love have made me strong despite the long distance that had separated us.

ABSTRACT

SOLID-STATE NMR STUDIES OF PEO IN VARIOUS ENVIRONMENTS: CONFORMATION, CHEMICAL SHIFT, AND DYNAMICS

SEPTEMBER 2000

DOUGLAS J. HARRIS, B.S., MASSACHUSETTS INSTITUTE OF TECHNOLOGY

B.S., MASSACHUSETTS INSTITUTE OF TECHNOLOGY

M.S., UNIVERSITY OF MASSACHUSETTS AMHERST

Ph.D., UNIVERSITY OF MASSACHUSETTS AMHERST

Directed by: Professor Klaus Schmidt-Rohr

In this dissertation, double-quantum NMR spectroscopy was employed to determine the torsion angle distributions of the OC-CO bonds in poly(ethylene oxide), PEO, in various environments: crystalline PEO, PEO–*p*-nitrophenol (PEO/PNP) and PEO-resorcinol molecular complexes, PEO nanocomposites with a smectite clay and MoS_2, and PEO-poly(α,L-glutamate) blends. The technique not only allowed quantitative determination of both the relative ratios and average torsion angles for the trans and gauche bonds, but also set an upper limit for the width of the torsion angle distribution. The studies confirmed that the OC-CO bonds in crystalline PEO all adopt a gauche torsion angle and determined an average angle of $\psi = 74 \pm 4^\circ$ with a distribution width of $\sigma_\psi < 9^\circ$. The spectra of the PEO-resorcinol and PEO-poly(α,L-glutamate)

blends showed little difference from that of crystalline PEO. PEO/PNP was shown to be a suitable model system for studying conformation because 1/3 of OC-CO bonds are trans and the complex has extremely slow dynamics at room temperature. Simulations of the double-quantum spectra set an upper limit for the trans torsion angle distribution width of $\sigma_\psi < 7^\circ$. Finally, the OC-CO bonds of the PEO chains in the nanocomposites were found to be $90 \pm 5\%$ gauche, which provides valuable constraints on the possible chain conformation in the intercalation gaps.

The effects of packing, hydrogen bonding, and conformation on ^{13}C chemical shift were studied in crystalline PEO and the PEO/PNP complexes. CP-MAS spectra of crystalline PEO at 200 K, acquired under strong ^{1}H decoupling and after filters to suppress the mobile components, resolved four distinct peaks. Deconvolution of the 1D spectrum showed chemical shifts ranging from 74.7 to 71.6 ppm for the 14 carbons in the 7_2 helical repeat unit. 2D ^{13}C exchange and INADEQUATE spectra suggested a possible assignment of the chemical shifts to the structure. 1D and 2D NMR techniques were also applied to assign chemical shifts to the carbons in the crystalline repeat unit of PEO/PNP. The solid-state INADEQUATE spectrum and spin-diffusion CODEX data of PEO/PNP show two chemical shifts for the gauche OC-CO bonds: 71.4 ppm and 69.8 ppm; the carbons in the trans OC-CO bonds both have a chemical shift of 69.2 ppm. ^{2}H-^{13}C REDOR experiments showed that the hydroxyl group of the PNP is closer to the 71.4-ppm gauche carbon than the average of the components in the 69.4-ppm peak, with a distance of 3.2 ± 0.2 Å. This is inconsistent with the previous hypothesis that

hydrogen bonding was responsible for the upfield shift of the 69.4-ppm peak. Instead, the chemical shift differences are now attributed to packing effects.

Dynamics of the conductive phase was studied in polymer electrolytes and block copolymers from poly(oligo(oxyethylene) methacrylate) macromonomer (POEM), lauryl methacrylate, *n*-butyl methacrylate, and methyl methacrylate. ^{1}H and ^{7}Li NMR spectroscopy was successful in showing that the enhanced conductivity of diblock copolymer electrolytes with a low T_g non-conductive phase is at least partially due to faster chain dynamics in the conductive phase. A higher T_g non-conductive block shifts the observed dynamics curves towards a higher temperature by approximately 5 °C. Finally, the dynamic inhomogeneity in the POEM side chain, observed in the nonexponential $T_{1\rho}$ decay, was determined by wideline separation (WISE) experiments to be on a length-scale of less than 5 nm.

TABLE OF CONTENTS

LIST OF TABLES

LIST OF FIGURES

Figure

CHAPTER 1

INTRODUCTION

1.1 Overview of the Dissertation

Modern material science optimizes a polymer based on an understanding of the relationships of structure, dynamics, and processing to the polymer's performance. For macromolecular materials, the need to understand the relationships from an atomic level has driven polymer physics to develop new techniques, but measurements of the conformation, short-range order, and dynamics are still vexing challenges. Wide-angle X-ray scattering cannot accurately probe the structure of amorphous polymers and has only limited resolution for solving the imperfect structure of crystalline polymers. Other techniques, such as infrared and Raman spectroscopy cannot be used to precisely determine the torsion angles of bonds and do not elucidate the relative orientations of functional groups that are not connected by chemical bonds. Many techniques have been developed to study polymer dynamics but most of them fail in complicated polymer systems or yield only unspecific information.

Solid-state nuclear magnetic resonance spectroscopy (NMR) is a powerful and rapidly evolving technique for determining conformation, short-range order, and dynamics in polymers. New pulse sequences, including two-dimensional (2D) double-quantum NMR (DQ-NMR), have been recently developed that correlate the relative orientations of two ^{13}C-labeled segments. Other techniques, such as rotational-echo double resonance (REDOR) and spin diffusion, are useful for determining distances and morphology on

length scales between Ångströms and tens of nanometers. The dynamics of polymer chains can be determined by NMR techniques including ^1H linewidth determination, ^1H $T_{1\rho}$ relaxation rates, and exchange NMR.

The central focus of this thesis is poly(ethylene oxide), PEO, and its copolymers, complexes, blends, and intercalates. The studies explore aspects of structure and dynamics and also the effects of hydrogen bonding, conformation, and packing on the chemical shift of the PEO carbons. The results provide insights to understand the behavior of polymer chains. The work describes both new and recently developed techniques used to answer detailed questions and more traditional solid-state NMR methods used to investigate more complicated systems. Some of the results are immediately applicable to understanding the structure-property relationships, while other results are principally beneficial as benchmarks for molecular simulations.

1.2 Conformation of PEO chains

Undoubtedly, the conformation of PEO is responsible for many of the desired properties of this polymer. The rotational isomeric state (RIS) description of amorphous PEO[1,2] is frequently used to estimate the torsion angles of the bonds. Results on model compounds and energy calculations suggest that the gauche conformation of the OC-CO bond is thermodynamically favored in the bulk state. On the basis of the temperature dependence of dipole moment and chain stiffness, RIS models calculate that the gauche bond is 400 cal/mol more favorable than the trans conformation; approximately 80% of

these bonds were calculated to be gauche in the amorphous state. Molecular dynamics simulations and small-angle neutron scattering experiments have also been used to determine the radius of gyration's characteristic ratio as a function of temperature and thus to calculate the conformational populations.[3] The results suggest that approximately 80% of OC-CO adopt the gauche conformation at all temperatures between 300 and 450 K. For higher temperatures, the increase of CO-CC gauche conformations inhibits the OC-CO bonds from having a higher percentage of trans torsion angles. Neither model, however, includes environmental effects. The conformation and torsion angle distribution of the OC-CO bonds of PEO in various environments are explored in this research by use of solid-state NMR spectroscopy.

1.3 Isotropic ^{13}C Chemical Shifts

Solution and solid-state NMR are routinely employed to determine the isotropic ^{13}C chemical shifts in a system. Therefore, one of the "Holy Grails" of multidimensional NMR techniques is to determine simple relationships between conformation or packing and the chemical shift that can be applied in future one-dimensional (1D) experiments. Many studies of PEO have attempted to yield a correlation between the observed chemical shifts of PEO chains and its conformation. Dioxane, which has a "boat" conformation with gauche OC-CO torsion angles has a ^{13}C chemical shift of 66.5 ppm, which is lower than that of dimethoxyethane, 72.3 ppm.[4] The effects of solvent and temperature on the ^{13}C chemical shift of PEO have also been studied, and the results

suggest that the gauche shift and the trans shift are 71.58 and 73.83 ppm, respectively.[5] These results were used to hypothesize that an increasing ^{13}C chemical shift of PEO upon addition of the surfactant sodium dodecyl sulfate is due to an increased population of trans OC-CO conformations.[6] The experiments presented in this thesis debunk the myth of a simple, systematic correlation between chemical shift and conformation in PEO.

1.4 Crystalline PEO

Crystalline PEO adopts a helical structure that is more complex than that of most other simple polymers. Previous X-ray scattering studies have suggested that the different OC-CO bonds in the distorted 7_2 helical conformation have discrete torsion angles ranging from 49° to 92°.[7] A distorted structure is also suggested by the ^{13}C cross polarization/magic-angle spinning (CP-MAS) spectrum.[8] At low temperatures, sufficiently high spinning rates, and strong proton decoupling fields, the spectrum has four ^{13}C maxima with frequencies ranging from 72 ppm to 76 ppm. The origin of the inequivalent chemical shift must be due to packing effects. Chapter 3 describes experiments that determined the upper limit of the torsion angle distortion and also presents possible assignments for the ^{13}C chemical shifts to the 14 carbons in each helical repeat unit.

1.5 PEO-Hydroxybenzene Molecular Complexes

The effects of hydrogen bonding on the conformation of the polymer are examined in PEO-hydroxybenzene crystalline complexes. Molecules including resorcinol (RES)[9-15] and *p*-nitrophenol (PNP)[9,15-20] form crystalline complexes with PEO, with structures previously studied by X-ray scattering and infrared spectroscopy. The proposed structures had not been previously studied by NMR spectroscopy. The PEO-PNP complex, which has extremely slow dynamics at room temperature, is model system for testing new techniques and determining the correlation between chemical shift, conformation, and hydrogen bonding. A new technique, CODEX[21,22] with exchange via spin diffusion,[23] is presented in Chapter 4 and was used as a novel one-dimensional approach to conformation determination.

1.6 PEO-Nanocomposites

The conformations of PEO intercalated in MoS_2[24-26] and in a smectite clay were studied by solid-state NMR spectroscopy. The PEO chains in these nanocomposites are confined to layers that are less than 1 nm thick. Several papers[27,28] have speculated about possible chain conformations. The DQ-NMR spectra presented in Chapter 5 show the OC-CO torsion angle conformation of the PEO chain in these nanocomposites. The results of this study have relevance to polymer physics questions about confined polymers.

1.7 PEO-PGNA Blends

Another system that was studied is PEO-PGNA. Recently, this surfactant, PEO, and a protein polyelectrolyte, poly(α-L-glutamic acid), sodium salt (PGNA), were reported to form a macromolecular complex.[29] Based on questionable interpretation of the experimental data, the paper suggested that the PEO chains tightly surround the protein to form complexes. It was claimed that the PGNA are induced to adopt an α-helical conformation in the complex. The conformation of the PEO chain and morphology of the system are reported in Chapter 6.

1.8 Block Copolymer Electrolyte Mobility

To improve mechanical properties while retaining excellent ionic conductivity, block copolymer electrolytes have been recently investigated.[30-32] The microphase separation in those block copolymer electrolytes confers solid-like mechanical properties to the material at macroscopic scales even when both polymer blocks reside above their glass-transition temperatures. The effects of composition on electrical conductivity has been determined,[31] but no experiment has been previously conducted to study the chain dynamics.

Chapter 7 describes solid-state NMR studies to determine the effects of the T_g of the non-conductive block on the local dynamics of the conductive phase. The ^1H $T_{1\rho}$ relaxation rates, and both ^1H and ^7Li linewidths are measured for several block copolymer electrolytes with various compositions. Also dynamic inhomogeneity in the conductive

block is investigated by wideline separation (WISE) experiments with spin-diffusion during a mixing time.

1.9 References

(1) Mark, J. E.; Flory, P. J. *J. Am. Chem. Soc.* **1965**, *87*, 1415-1422.

(2) Mark, J. E.; Flory, P. J. *J. Am. Chem. Soc.* **1966**, *88*, 3702-3707.

(3) Smith, G. D.; Yoon, D. Y.; Jaffe, R. L.; Colby, R. H.; Krishnamoorti, R.; Fetters, L. J. *Macromolecules* **1996**, *29*, 3462-3469.

(4) Ribeiro, A. A.; Dennis, E. A. *J. Phys. Chem* **1977**, *81*, 957-963.

(5) Björling, M.; Karlström, G.; Linse, P. *J. Phys. Chem.* **1991**, *95*, 6706-6709.

(6) Cabane, B. *J. Phys. Chem.* **1977**, *81*, 1639-1645.

(7) Takahashi, Y.; Tadokoro, H. *Macromolecules* **1973**, *6*, 672-675.

(8) Schilling, F. C.; Tonelli, A. E.; Cholli, A. L. *J. Polym. Sci., Part B: Polym. Phys.* **1992**, *30*, 91-96.

(9) Paternostre, L.; Damman, P.; Dosière, M. *Macromolecules* **1997**, *30*, 3946-3948.

(10) Myasnikova, R. M.; Titova, E. F.; Obolonska, E. S. *Polymer* **1980**, *21*, 403-407.

(11) Cheng, C.; Belfiore, L. A. *Polym. News* **1990**, *15*, 39-49.

(12) Belfiore, L. A.; J., L. T.; Cheng, C.; Bronnimann, C. E. *J. Polym. Sci., Part B: Polym. Phys.* **1990**, *28*, 1261-1274.

(13) Delaite, E.; Point, J. J.; Damman, P.; Dosière, M. *Macromolecules* **1992**, *25*, 4768-4778.

(14) Paternostre, L.; Damman, P.; Dosière, M.; Bourgaux, C. *Macromolecules* **1996**, *29*, 2046-2052.

(15) Spevácek, J.; Paternostre, L.; Damman, P.; Draye, A. C.; Dosière, M. *Macromolecules* **1998**, *31*, 3612-3616.

(16) Point, J. J.; Damman, P. *Macromolecules* **1992**, *25*, 1184-1188.

(17) Damman, P.; Point, J. J. *Macromolecules* **1993**, *26*, 1722-1728.

(18) Damman, P.; Point, J. J. *Macromolecules* **1994**, *27*, 3919-3925.

(19) Damman, P.; Point, J. J. *Macromolecules* **1995**, *28*, 2050-2053.

(20) Spevácek, J.; Suchopárek, M. *Macromol. Symp.* **1997**, *114*, 23-34.

(21) deAzevedo, E. R.; Hu, W.-G.; Bonagamba, T. J.; Schmidt-Rohr, K. *J. Am. Chem. Soc.* **1999**, *121*, 8411-8412.

(22) deAzevedo, E. R.; Hu, W.-G.; Bonagamba, T. J.; Schmidt-Rohr, K. *J. Chem. Phys* **(accepted)**.

(23) Harris, D. J.; Bonagamba, T. J.; Hong, M.; Schmidt-Rohr, K. *accepted to Macromolecules* **2000**.

(24) Oriakhi, C. O.; Nafshun, R. L.; Lerner, M. M. *Mater. Res. Bull.* **1996**, *31*, 1513-1520.

(25) Giannelis, E. *Adv. Mater.* **1996**, *8*, 29.

(26) Vaia, R. A.; Vasudevan, S.; Krawiec, W.; Scanlon, L. G.; Gianellis, E. P. *Adv. Mater.* **1995**, *7*, 154.

(27) Wu, J.; Lerner, M. M. *Chem. Mater.* **1993**, *5*, 835.

(28) Aranda, P.; Ruiz-Hitzky, E. *Chem. Mater.* **1992**, *4*, 1395-1403.

(29) Pemawansa, K. P.; Thakur, A.; Karikari, E. K.; Khan, I. M. *Macromolecules* **1999**, *32*, 1910-1917.

(30) Li, J.; Khan, I. *Makromol. Chem.* **1991**, *192*, 3043-3050.

(31) Soo, P. P.; Huang, B. Y.; Jang, Y.-I.; Chiang, Y.-M.; Sadoway, D. R.; Mayes, A. M. *J. Electrochem. Soc.* **1999**, *146*, 32-37.

(32) Gray, F. M.; MacCallum, J. R.; Vincent, C. A.; Giles, J. R. M. *Macromolecules* **1988**, *21*, 392-397.

CHAPTER 2

NMR TECHNIQUES

2.1 Nuclear Magnetic Resonance Techniques to Study Polymers

NMR spectroscopy detects the interactions between the nucleus and the surrounding electrons and nearby nuclei.[1] This information can be used to deduce the chemical structure and motion in polymers.[2,3] This chapter will discuss the solid-state NMR techniques used in this research.

2.2 ^{7}Li and ^{1}H Linewidth

In rigid organic polymers, the typical ^{1}H full-width-at-half-maximum (fwhm) is typically $2\pi \times 40$ kHz[1] due to ^{1}H-^{1}H dipolar couplings. Near the glass-transition temperature of polymers, motion results in narrowing of the observed linewidth. The relative linewidth of two polymers can be compared to qualitatively determine relative mobility.

2.3 $T_{1\rho}$ Relaxation Time

Relaxation times, including T_1, T_2, and $T_{1\rho}$, are commonly used to characterize the motional rates in polymers. $T_{1\rho}$ relaxation is the decay of the magnetization in the x-y plane when the nucleus is spin-locked in a particular direction by an applied magnetic field. Polymer motion with rates similar to the frequency of the locking field (~$2\pi \times 80$

kHz) results in a minimum value for the $T_{1\rho}$ relaxation time. Slower or extremely rapid motion results in longer relaxation times. The temperature dependence of the $T_{1\rho}$ relaxation times for a polymer can be analyzed with the Bloembergen-Purcell-Pound theory to determine motional frequency,[4] or qualitatively compared with other polymers. Slower dynamics in a polymer results in a horizontal displacement of the observed curve towards higher temperature.

2.4 Spin Diffusion Techniques

Homonuclear polarization transfer among protons occurs in polymer systems by a process called spin diffusion.[5,6] Transfer of z magnetization due to homonuclear coupling proceeds without radio frequency irradiation. Experimentally, ^{1}H magnetization of one component is initially suppressed and then stored in the ±z directions. A spin diffusion mixing time in the pulse sequence allows partial transfer of the magnetization back to the suppressed regions. Detection of the final magnetization can be accomplished by rotating the ^{1}H magnetization back into the x-y plane and either detecting the ^{1}H signal, or via cross polarization and detecting the resulting ^{13}C magnetization.

Spin diffusion can be used to determine domain size in polymer systems. The transfer of magnetization can be analyzed using Fick's second law of diffusion:[7]

$$\partial M(r,t)/\partial t = \nabla(D(r,t)\,\nabla M(r,t)) \qquad (2.2)$$

where D is the spin diffusion coefficient. Using this formula, domain sizes in a range of 1-100 nm[8,9] can be determined. The spin diffusion coefficient has been determined to be

$D = 0.8$ nm^2/ms for rigid polymer systems. For polymer systems above the glass transition temperature, the dependence of the spin diffusion coefficient on the ^{1}H transverse relaxation time, T_2, has been experimentally determined[10] for highly mobile polymers to be

$$D(T_2^{-1}) = 8.2*10^{-6}T_2^{-1.5} + 0.007 \text{ nm}^2/\text{ms}, \quad 0 < T_2^{-1} < 1000 \text{ Hz} \tag{2.3}$$

For polymers with an intermediate value of T_2^{-1}, the formula was also empirically determined to be:

$$D(T_2^{-1}) = (4.4 \times 10^{-4}T_2^{-1} + 0.26) \text{ nm}^2/\text{ms}, \quad 1000 < T_2^{-1} < 3500 \text{ Hz} \tag{2.3}$$

The T_2 of the mobile phase must be determined using a Carr-Purcell-Meiboom-Gill (CPMG)[11] sequence.

The effective spin diffusion coefficient, $\sqrt{D_{eff}}$, is the geometric average of $\sqrt{D_{mobile}}$ and $\sqrt{D_{rigid}}$, divided by the arithmetic average of their roots[2,12]:

$$\sqrt{D_{eff}} = \frac{\sqrt{D_{mobile}D_{rigid}}}{(\sqrt{D_{mobile}} + \sqrt{D_{mobile}})/2} \tag{2.4}$$

This calculated value of $\sqrt{D_{eff}}$ can be used to determine the dimension of the mobile phase, d_{mobile}, by extrapolating the initial loss of magnetization from the excited component. The intercept of the line with the x-axis, $\sqrt{t_m}^{s,0}$, is used in the following equation:

$$d_{mobile} = \frac{2 \in}{\sqrt{\pi}} \sqrt{D_{eff} t_m^{s,0}} \tag{2.5}$$

where $\in$ is the effective dimensionally for spin diffusion: one for lamellar systems, two for cylindrical morphology, and three for spherical geometries.

2.5 ^{1}H Wideline Separation (WISE)

The linewidth of ^{1}H nuclei bonded to carbons with different chemical shifts can be determined using wideline separation.[13] The simplest WISE experiment is similar to the standard CP-MAS experiment except that there is an incremented delay t_1 after the initial ^{1}H 90° pulse. The Fourier transformation over t_1 and t_2 results in a spectrum where the wideline ^{1}H spectrum is correlated with the isotropic chemical shifts of the ^{13}C nuclei. Thus, motional inhomogeneity in blends and copolymers can be detected. The length scale of this inhomogeneity can be determined by a 2D WISE experiment with ^{1}H spin diffusion. After the t_1 delay, the magnetization is flipped to the ±z direction and a spin diffusion mixing time allows transfer of magnetization from the more mobile protons to the more rigid regions. The spin diffusion mixing time required to equilibrate the magnetization provides an estimate of the thickness of the mobile and rigid domains.

2.6 REDOR ^{2}H-^{13}C Distance Determination Experiments

The distance between a ^{2}H nucleus and nearby ^{13}C nuclei can be determined using the REDOR (rotational-echo double resonance) technique.[14,15] The principle of the experiment is using rotor-synchronous 180° pulses on the ^{13}C channel and one ^{2}H 180° pulse to reintroduce ("recouple") the heteronuclear dipolar interaction between the two nuclei under MAS conditions. A stronger heteronuclear ^{2}H-^{13}C interaction results in a

more rapid echo decay. Comparison of the observed spectra with different lengths of recoupling to a reference spectrum with no ^{2}H pulse allows determination of the distance between the nuclei.

2.7 ^{13}C-^{13}C Dipolar/CSA Correlation Experiment

The ^{13}C-^{13}C dipolar coupling can be correlated with the ^{13}C chemical-shift anisotropy (CSA) using a 2D NMR experiment.[16,17] The ^{13}C-^{13}C dipolar couplings are decoupled during detection using a decoupling sequence with a 10-pulse cycle.[16,18] The observed spectrum can be used to deduce both the chemical-shift tensor orientation and the distance between ^{13}C nuclei.

2.8 Double-Quantum NMR Spectroscopy

The relative orientations of two ^{13}C nuclei can be determined using Double-Quantum NMR spectroscopy (DQ-NMR).[18,19] DQ-NMR yields 2D spectra in which the first dimension shows the sum of the orientation-dependent ^{13}C chemical shifts, while the second dimension shows the individual anisotropic chemical shifts and ^{13}C-^{13}C dipolar couplings. The relative orientation of the coupled sites, i.e. the torsion angles for bonded carbons, can be determined from simulations of these 2D spectra. Trans conformations are easily identified by a diagonal ridge with a slope of two.

2.9 Solid-State Dipolar INADEQUATE Spectroscopy under MAS

Dipolar-mediated INADEQUATE NMR experiments[20] using the dipolar recoupling sequence CMR7[21] to excite the double-quantum coherence under MAS can be used to determine the connectivities of carbon peaks with different chemical shifts. Signals at the same ω_1 value belong to a ^{13}C-^{13}C pair, and the chemical shifts of the two ^{13}C's in the pair can be read off in the ω_2 dimension. In addition, due to special magic-angle-spinning effects, the line broadening makes it possible to identify which peaks belong to gauche or trans conformations: a broadening arises if the two dipolar-coupled ^{13}C nuclei have different CSA orientations, as is the case for a gauche conformation. In that case, the dipolar coupling is not completely removed by MAS, since the sum of chemical shift difference and the dipolar coupling Hamiltonian, which have to be considered together, does not commute at different rotor orientations. In other words, the sum of the chemical-shift difference and the dipolar coupling represents a homogeneous Hamiltonian which produces broadened MAS peaks.[22]

2.10 ^{13}C CODEX Experiments

The ^{13}C CODEX technique[23,24] with ^{13}C spin diffusion in the mixing time was designed to calculate the fraction of trans bonds. For the two sites on a trans bond, the anisotropic chemical shift is the same; thus spin diffusion does not result in a frequency change and does not dephase the signal. For gauche bonds, we have a two-site exchange process. Exchange in the long-time limit results in a frequency change for half the

magnetization, while the other half still resides in the initial site. Therefore, dephasing reaches an asymptote of 50%. This technique has not been used previously to determine conformation, and may prove to be a useful and versatile one-dimensional NMR technique to determine conformation statistics.

2.11 2D Exchange Experiment

Multidimensional exchange NMR has been applied to study aspects of polymer dynamics for processes with correlation times between 10^{-5} and 10^{2} seconds.[2] The technique measures the NMR frequency of the molecular segment at two different times: before and after a mixing time.[25] Off-diagonal intensity in the resulting spectrum is indicative of motion. In static experiments, the observed pattern can be used to determine the geometry of motion, and exchange NMR under MAS identifies interconversion of atoms with inequivalent chemical shifts due to packing or environmental effects.

Many crystalline polymers undergo helical jumps including poly(oxymethylene, isotactic poly(propylene), polyethylene, and polyethylene oxide.[2] For crystalline PEO, the dynamics are very fast near room temperature; the rate of helical jumps is approximately 5/s.[26] Static 2D and 3D exchange ^{13}C spectra of PEO at 225 K, where the jump rate is approximately 225 K, were used to investigate the angle of motion, and thus determine the disorder in the system.[2] The experiments suggested that the crystalline repeat unit is distorted from an ideal 7_2 helix. However, the results suggested that the

proposed X-ray structure[27] overestimated the deviations from the average torsional angles.

The 2D exchange ^{13}C spectrum of PEO under MAS has not been previously reported. The experiment will determine the frequencies of the ^{13}C nuclei before and after the polymer undergoes a helical jump. Thus, the experiment can correlate the chemical shifts of the atoms in adjacent monomer units.

2.12 References

(1) Abragam, A. *Principles of Nuclear Magnetism*; Oxford University Press: Oxford, 1961.

(2) Schmidt-Rohr, K.; Spiess, H. W. *Multidimensional Solid-State NMR and Polymers*; Academic Press: San Diego, 1994.

(3) McBrierty, V. J.; Packer, K. J. *Nuclear Magnetic Resonance in Solid Polymers*; Cambridge University Press: London, 1993.

(4) Bloembergen, N.; Purcell, E. M.; Pound, R. V. *Phys. Rev.* **1948**, *73*, 679-712.

(5) Bloembergen, N. *Physica* **1949**, *XV*, 386-426.

(6) Goldman, M.; Shen, L. *Phys. Rev.* **1966**, *144*, 321-331.

(7) Cranks, J. *The Mathematics of Diffusion*; Clarendon Press: Oxford, 1975.

(8) Landfester, K.; Boeffel, C.; Lambla, M.; Spiess, H. W. *Macromolecules* **1996**, *29*, 5972-5980.

(9) Spiegal, S.; Landfester, K.; Lieser, G.; Boeffel, C.; Spiess, H. W.; Eidam, N. *Macromol. Chem. Phys.* **1995**, *196*, 985-993.

(10) Mellinger, F.; Wilhelm, M.; Spiess, H. W. *Macromolecules* **1999**, *32*, 4686-4691.

(11) Carr, H. Y.; Purcell, E. M. *Phys. Rev.* **1954**, *94*, 630-638.

(12) Clauss, J. S.-R., K.; Spiess, H. W. *Acta Polymer.* **1993**, *44*, 1-17.

(13) Schmidt-Rohr, K.; Clauss, J.; Spiess, H. W. *Macromolecules* **1992**, *25*, 3273-3277.

(14) Schmidt, M.; Maurer, F. H. J. *J. Polym. Sci., Polym. Phys. Edn.* **1998**, *36*, 1061-1080.

(15) Sandström, D.; Hong, M.; Schmidt-Rohr, K. *Chem. Phys. Lett.* **1999**, *300*, 213-220.

(16) Dunbar, M. G.; Novak, B. M.; Schmidt-Rohr, K. *Solid State Nuclear Magn. Reson.* **1998**, *12*, 119-137.

(17) Schmidt-Rohr, K.; Wilhelm, M.; Johansson, A.; Spiess, H. W. *Magn. Reson. Chem.* **1993**, *31*, 352-356.

(18) Schmidt-Rohr, K. *J. Magn. Reson.* **1998**, *131*, 209.

(19) Schmidt-Rohr, K. *Macromolecules* **1996**, *29*, 3975-3981.

(20) Hong, M. *J. Magn. Reson.* **1999**, *136*, 86-89.

(21) Rienstra, C. M.; Hatcher, M. E.; Mueller, L. J.; Sun, B. Q.; Fesik, S. W.; Griffin, R. G. *J. Am. Chem. Soc.* **1998**, *120*, 10602-10612.

(22) Maricq, M.; Waugh, J. S. *J. Chem. Phys.* **1979**, *70*, 3300.

(23) deAzevedo, E. R.; Hu, W.-G.; Bonagamba, T. J.; Schmidt-Rohr, K. *J. Am. Chem. Soc.* **1999**, *121*, 8411-8412.

(24) deAzevedo, E. R.; Hu, W.-G.; Bonagamba, T. J.; Schmidt-Rohr, K. *J. Chem. Phys* **(accepted)**.

(25) Jeener, J.; Meier, B. H.; Bachmann, T.; Ernst, R. R. *J. Chem. Phys.* **1978**, *71*, 4546-4553.

(26) VanderHart, D. L.; Earl, W. L.; Garroway, A. N. *J. Magn. Reson.* **1981**, *44*, 361-401.

(27) Takahashi, Y.; Tadokoro, H. *Macromolecules* **1973**, *6*, 672-675.

CHAPTER 3

CONFORMATION AND ^{13}C CHEMICAL SHIFTS OF CRYSTALLINE PEO

3.1 Introduction

Packing effects are solely responsible for the different chemical shifts in crystalline PEO, thus making this polymer a useful model system. The carbon atoms in the monoclinic unit cell have different environments: some carbons are closely packed to the neighboring helices while others have less steric interactions. The differences in interchain interactions which result in inequivalent chemical shifts are observable by solid-state NMR at low temperatures, sufficiently high spinning rates, and strong proton decoupling fields. The ^{13}C cross-polarization/magic-angle-spinning (CP-MAS) spectrum has four maxima with frequencies spreading over a 4-ppm range.[1]

PEO chains in the crystalline state have been studied by infrared, Raman, and X-ray techniques. The results show that the chains adopt 7_2 helical conformations with trans CO-CC bonds and gauche OC-CO bonds.[2-4] Therefore, γ-gauche effects cannot be responsible for the differences in chemical shifts. In addition to resulting in inequivalent chemical shifts for each carbon nucleus, interchain interactions also distort the 7_2 helix. A detailed analysis of the X-ray diffraction peak intensities[4] has presented a possible model for chain conformation: the helix is highly distorted with the OC-CO bonds having discrete torsion angles of 57.0°, 67.8°, 74.2°, 49.0°, 91.8°, 60.2° and 79.1°. This model was compared to the results of static 2D exchange ^{13}C spectra.[5] The NMR technique

determines the bond angles based on changes of orientation of the carbon atoms after a helical jump. Simulations of the observed spectra showed that the chains are indeed distorted, but concluded that the X-ray analysis overestimated the distortion of the 7_2 helix. The distortions shown in both studies are indicative that packing effects are significant in crystalline PEO. Thus, interchain steric interactions result in the observed inequivalent chemical shifts of the otherwise chemically equivalent carbons.

In this work, the distortion of the crystalline PEO helix is analyzed by measuring the OC-CO torsion angles using double-quantum solid-state ^{13}C nuclear magnetic resonance (DQ-NMR) spectroscopy.[6,7] The average torsion angle and an upper limit for the distortion of the OC-CO bonds are determined from simulations of the experimental spectra. Also, the chemical shifts of the 14 carbons in each 7_2 helix were determined from a ^{13}C CP-MAS spectrum. Due to stronger ^{1}H decoupling and the TPPM sequence,[8] the spectrum has higher resolution than previously reported. Furthermore, a possible assignment of the chemical shifts to the 14 carbons in the helical repeat unit was determined from a solid-state dipolar ^{13}C INADEQUATE spectrum[9-11] and a 2D ^{13}C exchange spectrum under MAS. The INADEQUATE spectrum determined the chemical shift of the bonded carbon neighbor while the 2D exchange NMR technique provided the chemical shift of the carbons in the adjacent monomer units.

3.2 Experimental

3.2.1 Synthesis of (-^{13}C-^{13}C-O-) PEO

Doubly ^{13}C labeled PEO was synthesized by anionic polymerization in THF. The monomer was a mixture of 3.5 g (79 mmol) unlabeled ethylene oxide gas and 0.5 g (11 mmol) ethylene-$^{13}C_2$ oxide gas. The reaction flask containing 20 mg (0.5 mmol) of potassium metal and 100 mg (0.78 mmol) of naphthalene was filled with 70 mL of anhydrous and O_2-free THF. After polymerizing for 72 hr. at ambient temperature, the PEO was precipitated in hexanes, redissolved in THF, and reprecipitated in hexanes. The molecular weight was determined by gel permeation chromatography with a light-scattering detector and using CH_2Cl_2 as the eluent. The instrument determined M_n = 27 000 g/mol and M_w = 30 000 g/mol (PDI = 1.10). The integration of the satellite peaks due to ^{13}C splitting in the ^{1}H NMR spectrum showed that 13% of the ethylene oxide units are -$^{13}CH_2$-$^{13}CH_2$-O-.

3.2.2 Static DQ-NMR

The static 2D DQ-NMR spectra were recorded on a Bruker MSL-300 spectrometer at a ^{13}C resonance frequency of 75.5 MHz in a 4.5-mm diameter coil of a static variable-temperature probe. The proton 90° pulse length was *ca.* 3.1 μs, corresponding to a radio frequency field strength of 80 kHz during cross-polarization. For decoupling, the field strength was increased to ≈ 100 kHz. Typical carbon 90° pulse lengths were 2.6 μs. A cross-polarization time of 500 μs and a signal-acquisition time of 2.6 ms were used.

In the t_1 dimension, 40 slices with increments of 20 μs were aequired; in the t_2 dimension, the dwell time was 10 μs, and the number of data points was 256 for the ^{13}C undccoupled spcetra and 80 for the decouplcd spcctrum. Thc doublc-quantum excitation and reeonvcrsion delay was $2\tau = 280$ μs.[6] A combination of phasc cycling and off-rcsonanec evolution was used to rcducc artifacts in the spcctra. All of the pulscs wcrc applied on-rcsonancc, but thc frequcncy was switchcd by 5.5 kHz during thc evolution timc,[12] which scparates zero and singlc quantum artifacts from the truc doublc-quantum speetrum. Thc phasc cyelc had 128 stcps, which varicd the phases of thc cross-polarization, double-quantum cxeitation, double-quantum rcconvcrsion, and thc z-filtcr pulses. The reeycle delay for thc PEO was 7 s and the T_1-filtcr was 0.5 s. The speetra of PEO were all measurcd at 220 K. Thc measuring time for each two-dimensional double-quantum spcetrum was onc day.

3.2.3 ^{13}C CP-MAS Speetrum

The CP-MAS spcctrum was measurcd on a Bruker DSX-300 spectrometer. A eylinder of unlabelcd 100K PEO was plaeed in a 4-mm ZrO_2 rotor. Thc spinning rate was 5 kHz and the 90° pulse lengths wcre 3.2 μs for ^{13}C and 3.6 μs for ^{1}H. TPPM ^{1}H decoupling with a field strength of 110 kHz was uscd to minimize the lincwidth. The temperature nccessary to minimizc lincwidth was 208 K. Thc rccyclc dclay was 8 s and the speetrum was the sum of 1024 seans. The dwell timc was 29 μs and thc number of data points was 2048, resulting in an acquisition time of 60 ms. Thc amorphous phase

was suppressed by a combination of a 10 ms $T_{1\rho}$ filter and a 5 ms Hahn echo. The chemical shift of an internal polyethylene reference was calibrated at 32.8 ppm.

3.2.4 ^{13}C Exchange NMR Spectrum

The 2D exchange spectrum was recorded under similar conditions as the CP-MAS spectrum except the temperature was 225 K. A 10 ms $T_{1\rho}$ filter was used, but the Hahn echo before detection was short, 23 μs. The dwell time in t_1 and the number of slices were 160 μs and 160, respectively. Twenty-four scans were recorded for each of the slices resulting in an experiment time of 8 hr.

3.2.5 Solid-State Dipolar ^{13}C INADEQUATE Spectroscopy under MAS

A dipolar-mediated INADEQUATE NMR experiment[9] using the dipolar recoupling sequence CMR7[10] to excite the double-quantum coherence under MAS was applied to determine the connectivities of the carbon peaks in the ^{13}C-^{13}C-O labeled PEO. The experiment was performed on the Bruker DSX-300 spectrometer with the following conditions: spinning rate = 5 kHz; temperature = 293 K; 90° ^{1}H and ^{13}C pulse lengths = 4 and 4.1 μs, respectively; ^{1}H decoupling field ≈ 80 kHz; recycle delay = 5 s; number of scans = 128; slices in t_1 dimension = 96; total experiment = 16 hours.

3.3 Torsion Angle Distribution in Crystalline PEO

Simulated static ^{13}C-^{13}C decoupled DQ-NMR spectra for each of the seven torsion angles suggested by the previous X-ray study[3] are shown in Figures 3.1 (b) through (h). The mean torsion angle is $\psi = 68^{\circ}$, and the root-mean-square deviation is $\sigma_{\psi} = 14^{\circ}$. The sum of the seven spectra is shown in Figure 3.1 (a). Due primarily to the simulated spectra of the highest and lowest torsion angles, 92° and 49°, the sum spectrum has significant intensity in the upper region and also does not have the depression and small peak in the center. These features are used to confirm or reject the hypothesized conformation and to set limits on the width of the torsion angle distribution.

The experimental spectra, Figures 3.2 (a) and (b), show that all of the OC-CO torsion angles are gauche: there is no evidence of trans conformations which would result in a ridge with a slope of two (see Chapter 4).[13,14] Furthermore, the observed spectra show that large deviation of torsion angles from 74° is not possible because there is no intensity in the upper region as predicted by the simulations using the torsion angles suggested by the X-ray results, Figure 3.2 (e) and (f). Another indication that the Gaussian width of the torsion angle distribution must be less than $\sigma_{\psi} = 14^{\circ}$ is the presence of the peak and depression in the center region of the triangular pattern. A consistent simulation for the experimental spectra was produced using an average angle of $\psi = 74^{\circ}$ and a relatively narrow distribution, $\sigma_{\psi} = 5^{\circ}$, Figures 3.2 (c) and (d). The confidence of the mean value is $\psi = 74 \pm 4^{\circ}$. Outside this interval, the central peak and depression disappear. The confidence interval for the width of the torsion angle

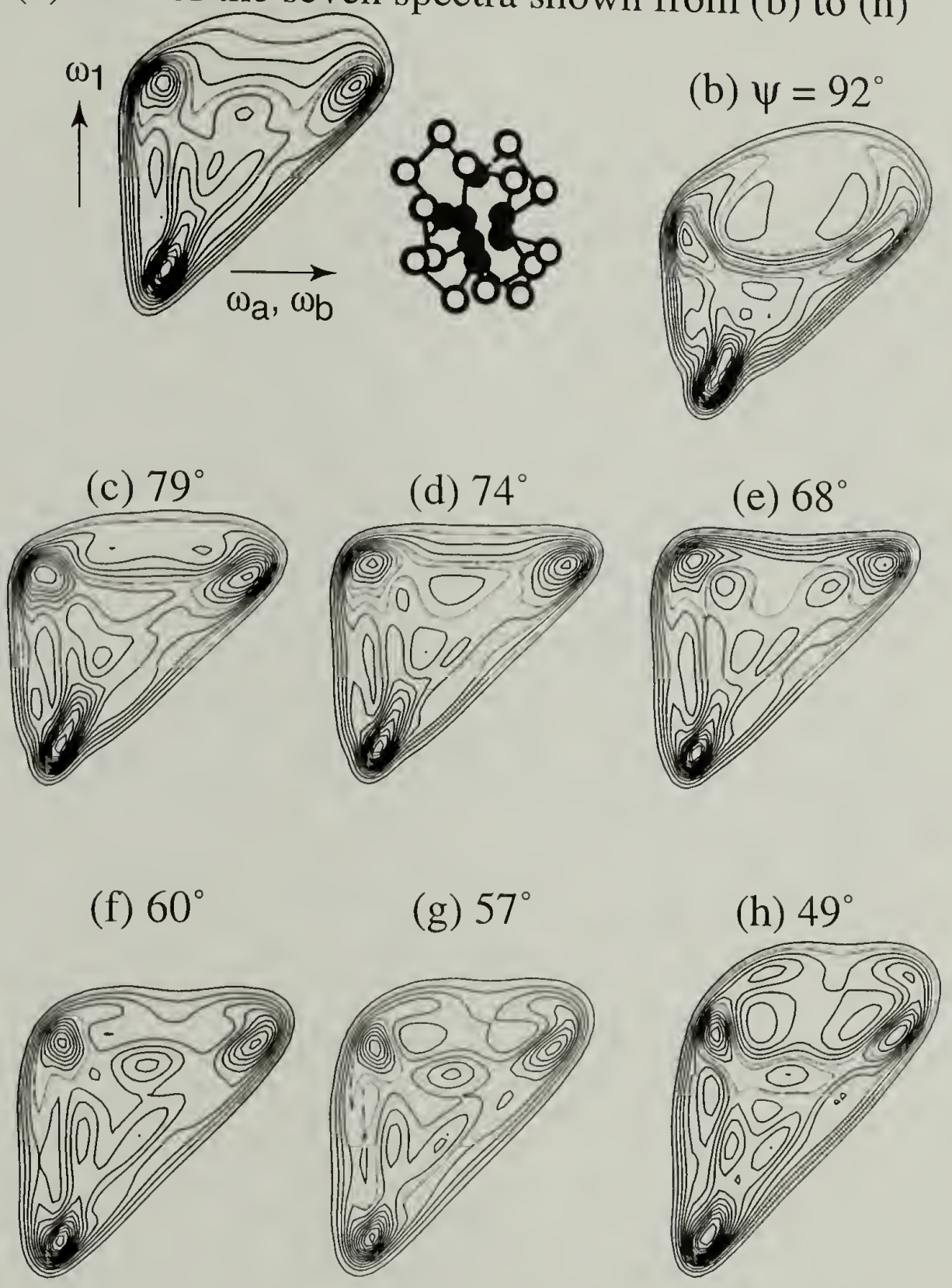

Figure 3.1: Simulated static DQ-NMR spectra with ^{13}C-^{13}C dipolar decoupling for torsion angles of structure suggested by X-ray analysis (Takahashi, 1973). The sum spectrum is shown in (a), while the spectra due to the seven individual torsion angles are shown in (b) 49°, (c) 57°, (d) 60°, (e) 68°, (f) 74°, (g) 79°, and (h) 92°. The prinsipal values of the chemical shift tensor used in the simulations were $\sigma_{11} = 95$ ppm, $\sigma_{22} = 86$ ppm, and $\sigma_{33} = 38$ ppm ($\sigma_{iso} = 73$ ppm) with the polar coordinates of the OC-CO bond in the chemical-shift principal-axis system (PAS) were $\alpha = -90°$, $\beta = 120°$.

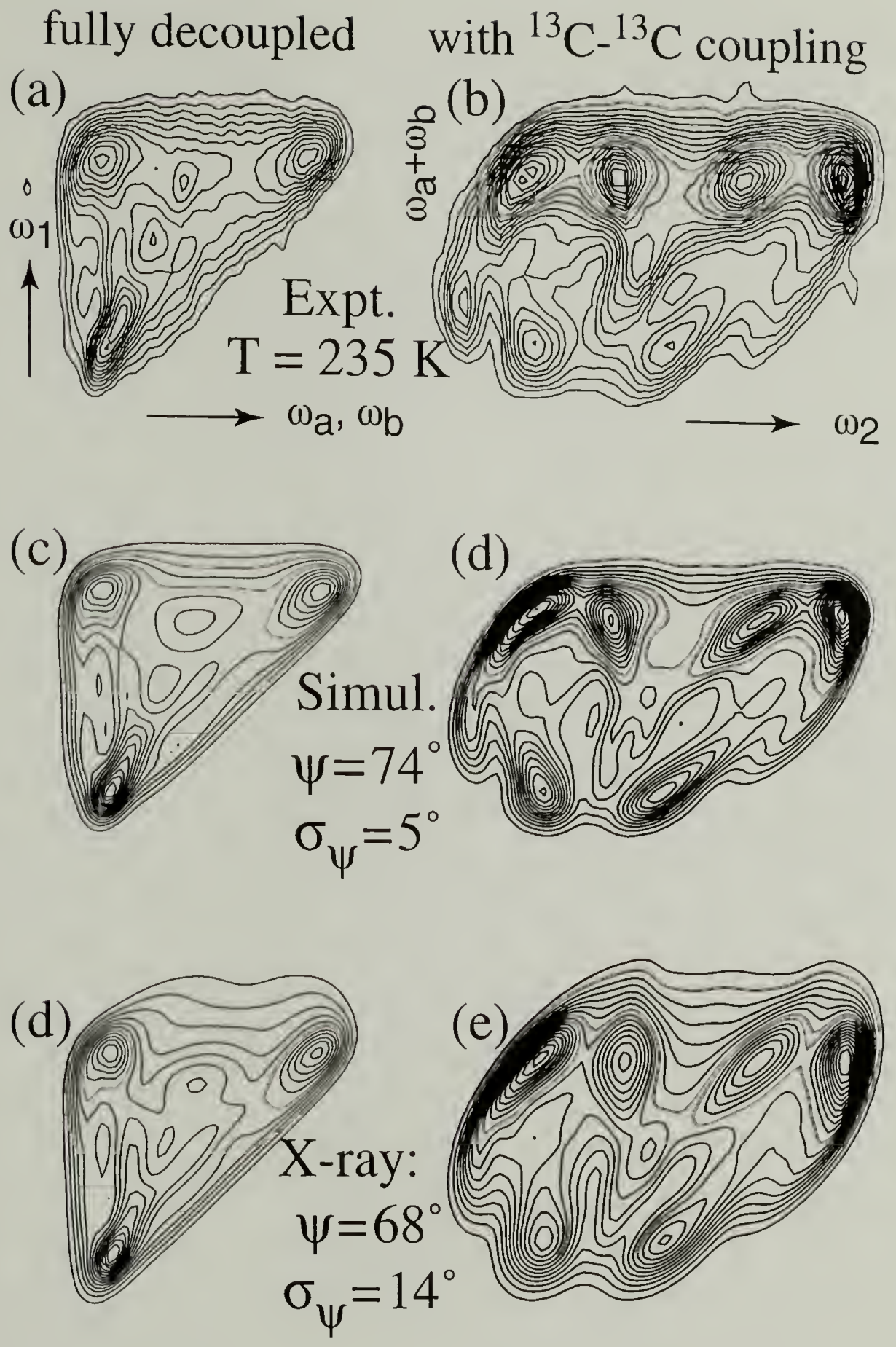

Figure 3.2: Static DQ-NMR spectra of labeled PEO measured at 75.5 MHz and 235 K: (a) with ^{13}C-^{13}C homonuclear decoupling and (b) without decoupling. The best simulations of both the fully decoupled (c) and CC undecoupled (e) spectra use a Gaussian torsion angle distribution with a mean gauche angle of $\psi = 74^\circ$ with a Gaussian width of $\sigma_\psi = 5^\circ$. The uncertainty of ψ is $\pm 4^\circ$ and the maximum allowable Gaussian width before obvious deviation from the observed spectra is $\sigma_\psi < 8^\circ$. Comparison with the simulation of the previously suggested structure (e) and (f) shows that the helix is not as highly disordered as previously suggested.

distribution is more difficult to quantify: other effects such as the multiple chemical shifts, insufficient ^{1}H decoupling, and chain motion broaden the spectrum and may result in an apparently wide torsion angle distribution in the experimental spectrum. Thus, only an upper limit to the distribution width can be determined: $\sigma_{\psi} < 8^{\circ}$.

The mean torsion angle of $\psi = 74^{\circ} \pm 4^{\circ}$ is different from the value of $\psi = 68^{\circ}$ suggested previously by the X-ray results.[4] Also, the torsion angle distribution, $\sigma_{\psi} < 8^{\circ}$, is narrower than the reported value of $\sigma_{\psi} = 14^{\circ}$. A highly distorted helical structure for crystalline PEO is still possible due to the 14 CO-CC torsion angles. The X-ray structure proposed that these torsion angles have an average value of $\psi = 186.0^{\circ}$ and a narrow torsion angle distribution, $\sigma_{\psi} = 7.6^{\circ}$. The CO-CC torsion angles were not determined in this study.

3.4 ^{13}C Chemical Shifts of Crystalline PEO

3.4.1 ^{13}C CP-MAS Spectrum

The observed CP-MAS spectrum, shown in Figure 3.3, has four distinct peaks. The chemical shifts were calibrated to the internal reference of polyethylene at 32.8 ppm. The resolution of the four peaks of PEO is better than in the previously published spectrum[1] due to lower temperature, higher magnetic field strength, and the filters used to destroy magnetization in the amorphous and mobile regions. The ^{1}H decoupling field strength, 110 kHz, is also critical for obtaining highly resolved spectra of the CH_2 group.[1,15] The TPPM decoupling pulse sequence provided a significant reduction in ^{13}C linewidth compared with spectrum obtained with continuous-wave ^{1}H decoupling.

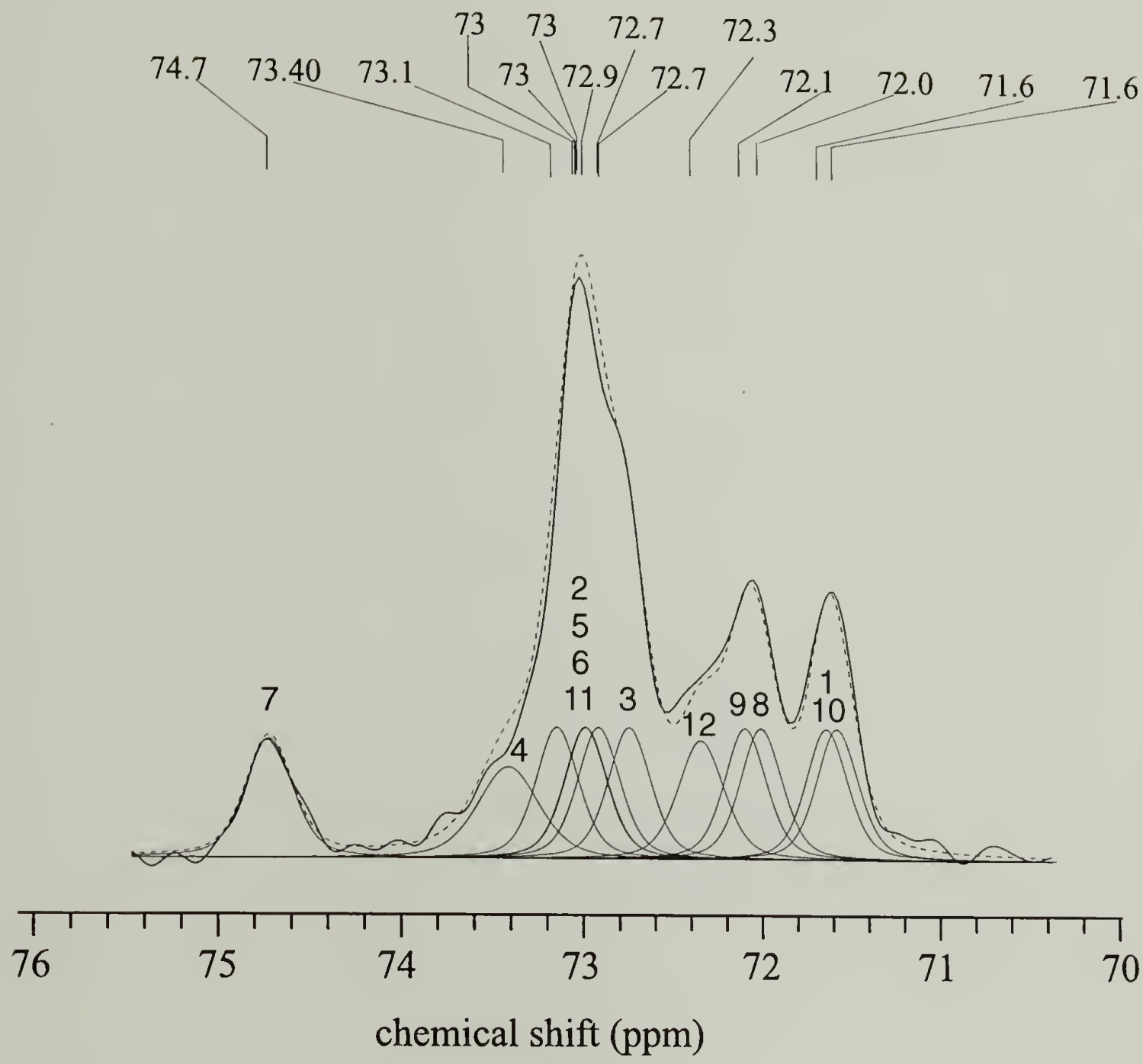

Figure 3.3: Deconvolution of the ^{13}C CP-MAS NMR spectrum of neat PEO. The spectrum was measured at 75.5 MHz. The temperature was 208 K and the spinning rate was 5 kHz. The chemical shift was referenced to the internal polyethylene standard that is assigned a chemical shift of 32.8 ppm. The 14 peaks in the deconvoluted have equal area, and typical linewidth of 22 Hz. The sum of simulated peaks is shown by the dashed curve.

The integrated area of the peak at 74.7 ppm is approximately 1/14th of the total area. This suggests that the signal arises from one of the 14 carbons in the 7_2 helical repeat unit. The probable chemical shifts of the other 13 carbons in the helical repeat unit were deconvoluted from the spectrum assuming that areas of all peaks are equal. The lineshapes were 40% Lorentzian and 60% Gaussian with typical full widths at half maximum of 22 Hz. The best-fit of the experimental spectrum used chemical shifts of 74.7, 73.4, 73.1, 73.0, 73.0, 73.0, 72.9, 72.7, 72.7, 72.3, 72.1, 72.0, 71.6, and 71.6 ppm. The chemical shifts were found to be slightly temperature dependent: the shifts of the peaks varied by ± 0.1 ppm between 225 K and 200 K.

3.4.2 Solid-State Dipolar ^{13}C INADEQUATE Spectroscopy under MAS

The 2D solid-state INADEQUATE spectrum of PEO at 203 K is shown in Figure 3.4 (a). A broadening arises because the dipolar-coupled ^{13}C nuclei have different instantaneous chemical shifts due to the gauche conformation. Therefore, the dipolar coupling is not completely removed by MAS.[16] This broadening for ^{13}C-^{13}C carbons connected with a gauche bond is discussed in more depth in Chapter 4.[14] In the spectrum, signals at the same ω_1 frequency belong to a ^{13}C-^{13}C pair, and the chemical shifts of each ^{13}C in the pair can be read off in the ω_2 dimension. Cross sections at 146.5, 145.8, 144.6, and 143.7 ppm are shown in Figure 3.4 (b). The spectrum and the cross section slices resolve six maxima. The peaks listed in this figure are labeled 1 to 14 on the

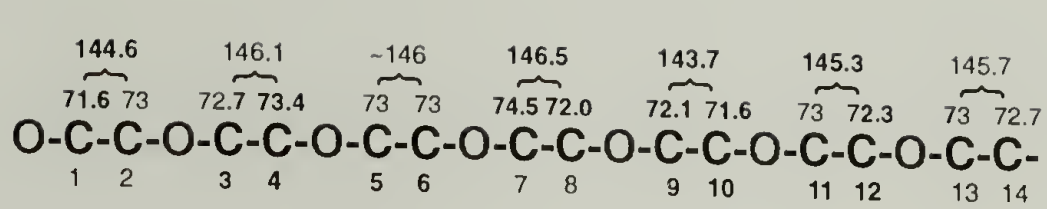

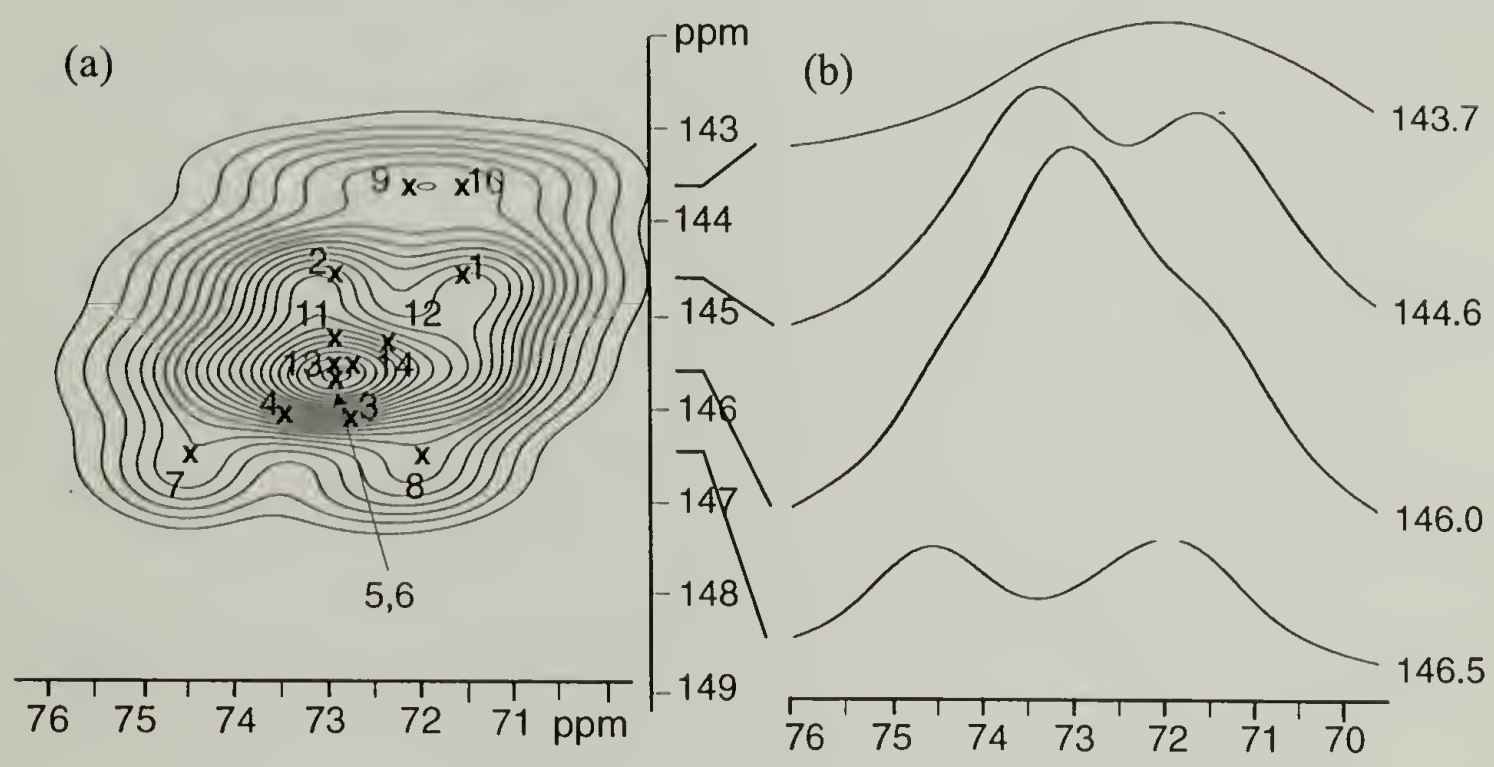

Figure 3.4: (a) 2D MAS ^{13}C INADEQUATE solid-state NMR spectrum of crystalline PEO. The spectrum was obtained at 203 K with a spinning rate of 5 kHz. The contour levels start at 10% and are in intervals of 4%. The expected peaks from the assignment of chemical shifts to the helical repeat unit are labeled. The assignment is derived from the results of this INADEQUATE spectrum, the deconvolution of the ^{13}C CP-MAS spectrum shown in Figure 3.3, and the exchange spectrum presented in Figure 3.5. The cross sections at 146.5, 146.0, 144.6, and 143.7 ppm are shown in (b).

basis of one possible interpretation of the results of this spectrum and both the ^{13}C CP-MAS and 2D exchange spectra. Three pairs of peaks are easily identifiable in the INADEQUATE spectrum: carbons **7** and **8** (74.5/72.0, 146.5 ppm), carbons **1** and **2** (71.6/73.0, 144.6 ppm), and carbons **9** and **10** (72.1/71.6, 143.7 ppm). There is a large peak centered at (≈ 73/≈ 73, 145.8 ppm) which is due to the many proximal pairs of peaks. Another set of chemical shifts was determined from the relatively high intensity at 144.6 ppm: thus, carbons **11** and **12** were assigned a sum shift of 145.3 ppm (73 and 72.3 ppm, respectively). Finally, the lack of intensity at 146.4 suggests that the neighbor of the 73.4 ppm carbon cannot have a chemical shift of 73 ppm. Thus the pair was assigned to the coordinates (72.7/73.4, 146.1 ppm). Other assignments could also be possible, but higher spinning speeds and a different pulse sequence would be necessary to clearly resolve all suspected peaks.

3.4.3 2D ^{13}C Exchange NMR

The exchange spectrum and a possible assignment of chemical shifts to the helical repeat unit are shown in Figure 3.5. There are many exchange peaks after the helical jumps. The assignment of chemical shifts to the 14 carbons in the helical repeat unit is also consistent with the INADEQUATE and CP-MAS spectra. A total of 28 exchange peaks are possible: 24 are resolvable and labeled in the spectrum and the other 4 may lay hidden beneath the high diagonal ridge. An unusual feature of this spectrum is that the intensities of the off-diagonal peaks are unequal. Another spectrum, with lower resolution but greater signal, obtained using a 7-mm MAS probe also show discrepancies

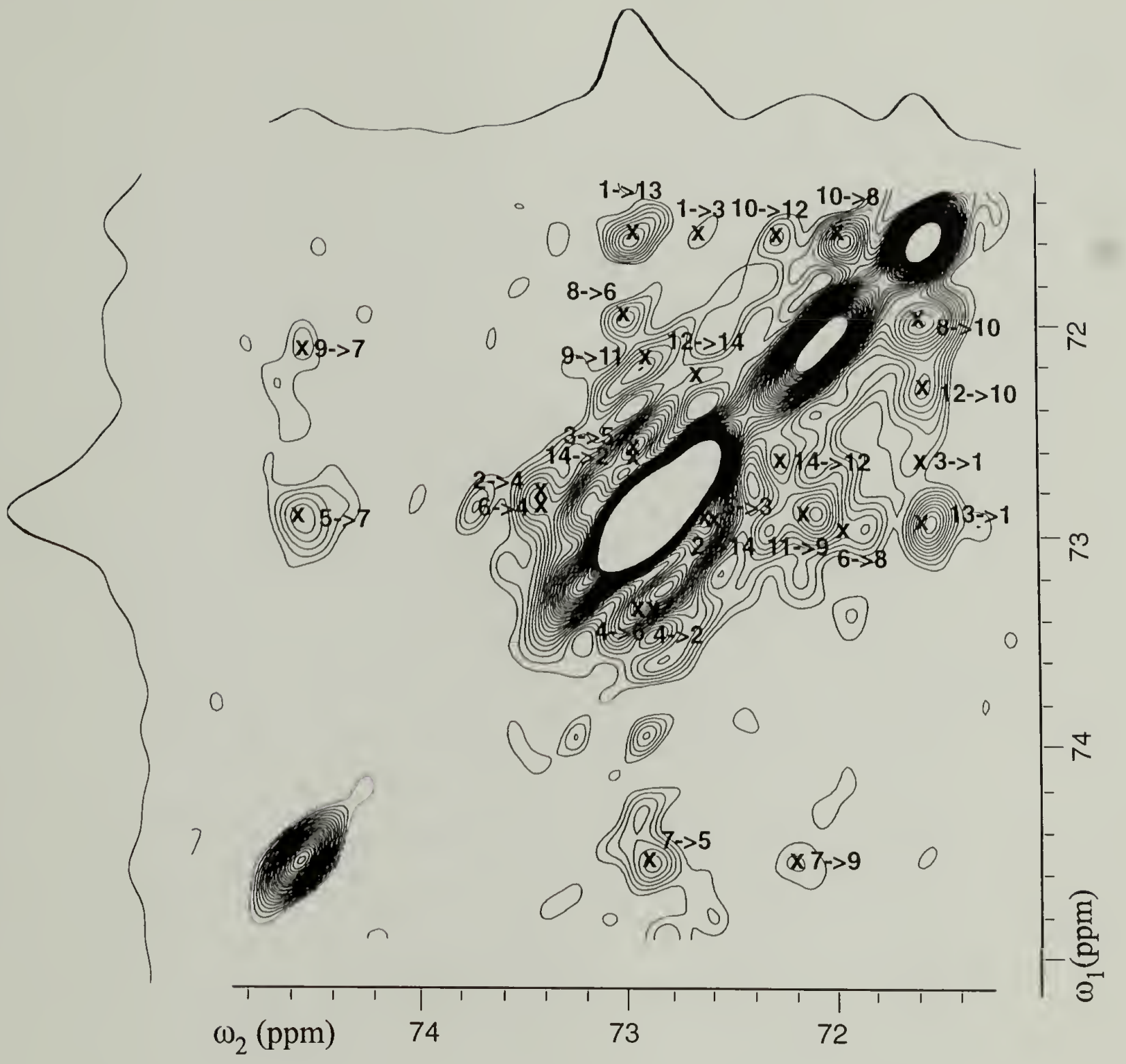

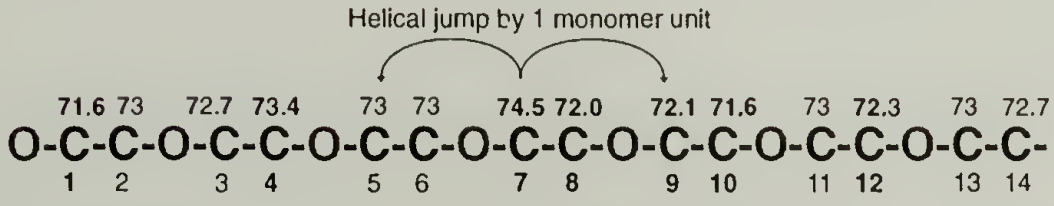

Figure 3.5: 2D exchange ^{13}C spectrum of crystalline PEO. The spectrum was obtained at 225 K with a spinning rate of 4 kHz and a mixing time of 600 ms. The contours are plotted from 1.77% to 23.2% in increments of 0.63%. The off-diagonal intensity arises from helical jumps during the mixing time where the helix rotates by one monomer unit. One possible assignment of chemical shifts is shown below the spectrum, and the expected exchange peaks are marked with x's.

in exchange intensity for the 74.5 ppm peaks. No explanation for this observation has been offered.

The assignment of chemical shifts to the helix began with carbon **7** at 74.5 ppm and its neighbor, resolved in the INADEQUATE spectrum, at 72.0 ppm. The exchange peaks at (74.5, 73 ppm), and (74.5, 72.1 ppm) results from helical jumps to carbons **5** and **9**, respectively. This assignment is arbitrary because there is no analysis to determine either the direction of the jump, or the torsion angles of the OC-CO and CO-CC bonds. The chemical shift of carbons **6** and **10** can also be determined to be 73 and 71.6 ppm, respectively, on the basis of the exchange intensity at (72.0, 71.6 ppm) and (72.0, 73.0 ppm). These pairs are also expected from the INADEQUATE spectrum. The other eight peaks in the assigned by a similar manner.

This assignment is unique: no other combination of the pairs of chemical shifts can be assigned that would result in the observed 22 off-diagonal intensities. However, the assignment of the chemical shifts in the INADEQUATE and CP-MAS spectra are critical for the interpretation.

3.5 Summary

Several multidimensional NMR techniques were used to study the OC-CO torsion angles and to assign the ^{13}C chemical shifts for crystalline PEO. Simulations of both ^{13}C-^{13}C undecoupled and decoupled static DQ-NMR spectra determined that the average torsion angle of the OC-CO bonds is $74^{\circ} \pm 4^{\circ}$, larger than the 68° average angle of the

previously suggested structure.[4] The Gaussian half-width of the torsion angle distribution is less than 8°, which is smaller than the previously suggested value of 14°.[4]

Packing effects were shown by the CP-MAS, MAS-INADEQUATE, and 2D exchange spectra to produce the different chemical shifts for the 14 carbons in each helical repeat unit. Deconvolution of the CP-MAS spectra based on observed peaks in the 2D spectra suggest that the carbon nuclei in each helical repeat unit have chemical shifts of 74.7, 73.4, 73.1, 73.0, 73.0, 73.0, 72.9, 72.7, 72.7, 72.3, 72.1, 72.0, 71.6, and 71.6 ppm. The connectivity between the carbons were studied by INADEQUATE and 2D exchange spectroscopy. The spectra show that the chemical shifts correspond to specific carbons in the helical unit cell. A possible assignment of chemical shifts is presented that is consistent with the observed intensities.

3.7 References

(1) Schilling, F. C.; Tonelli, A. E.; Cholli, A. L. *J. Polym. Sci., Part B: Polym. Phys.* **1992**, *30*, 91-96.

(2) Yoshihara, T.; Tadokoro, H.; Murahashi, S. *J. Chem. Phys.* **1964**, *41*, 2902-2911.

(3) Tadokoro, H.; Chatani, Y.; Yoshihara, T.; Tahara, S.; Murahashi, S. *Makromol. Chem.* **1964**, *73*, 109-127.

(4) Takahashi, Y.; Tadokoro, H. *Macromolecules* **1973**, *6*, 672-675.

(5) Schmidt-Rohr, K.; Spiess, H. W. *Multidimensional Solid-State NMR and Polymers*; Academic Press: San Diego, 1994.

(6) Schmidt-Rohr, K. *Macromolecules* **1996**, *29*, 3975-3981.

(7) Schmidt-Rohr, K. *J. Magn. Reson.* **1998**, *131*, 209.

(8) Bennett, A. E.; Rienstra, C. M.; Auger, M.; Lakshmi, K. V.; Griffin, R. G. *J. Chem. Phys.* **1995**, *103*, 6951-6958.

(9) Hong, M. *J. Magn. Reson.* **1999**, *136*, 86-89.

(10) Rienstra, C. M.; Hatcher, M. E.; Mueller, L. J.; Sun, B. Q.; Fesik, S. W.; Griffin, R. G. *J. Am. Chem. Soc.* **1998**, *120*, 10602-10612.

(11) Lee, Y. K.; Kurur, N. D.; Helmle, M.; Johannessen, O. G.; Nielsen, N. C.; Levitt, M. H. *Chem. Phys. Lett.* **1995**, *242*, 304-309.

(12) Kaji, H.; Schmidt-Rohr, K. **to be published.**

(13) Harris, D. J.; Bonagamba, T. J.; Schmidt-Rohr, K. *Macromolecules* **1999**, *32*, 6718.

(14) Harris, D. J.; Bonagamba, T. J.; Hong, M.; Schmidt-Rohr, K. *accepted to Macromolecules* **2000**.

(15) VanderHart, D. L.; Earl, W. L.; Garroway, A. N. *J. Magn. Reson.* **1981**, *44*, 361-401.

(16) Maricq, M.; Waugh, J. S. *J. Chem. Phys.* **1979**, *70*, 3300-3316.

CHAPTER 4

CONFORMATION OF PEO-HYDROXYBENZENE MOLECULAR COMPLEXES

4.1 Introduction

The conformation of PEO when complexed with various small molecules, such as alkali metal salts,[1] urea,[2] thiourea,[3] and mercuric halides[4] is distorted from the *TTG* sequence found in crystalline PEO. Recently, there has been much interest in the complexes of PEO with *p*-dihalogenobenzenes[5,6] and hydroxybenzenes including resorcinol (RES)[7-13] and *p*-nitrophenol (PNP).[7,13-18] WAXD and IR data suggest that the conformation of the PEO in many of the complexes with *p*-dihalogenobenzene or RES is only slightly distorted from the original 7_2 helix. The conformation of the chains in these systems remains *TTG* but the periodicity of the helix changes slightly.[8]

Contrary to the PEO/RES complex, the conformation of the chains in PEO/PNP complexes is very different from the 7_2 helical conformation.[5] IR and WAXD analyses suggest that 1/3 of the OC-CO bonds are in the trans conformation. The hydrogen bonding between the host and guest molecules is believed to induce the chain to adopt a *TTGTTGTTT TTG'TTG'TTT* structure.[16] It should be noted that up to now this "unusual" conformation was not further confirmed. Another unusual property of the PEO/PNP complex is that there are two broad ^{13}C peaks at 71.4 and 69.4 ppm,[18] compared with a median of 72 ppm for neat PEO. The relative integrated intensities of these peaks are equal to 1:2. In this complex, there are two PNP molecules for every

three ethylene oxide repeat units so the 67%-peak was attributed to the carbons adjacent to an ether oxygen with a hydrogen bond with the OH of the PNP.[13]

In this chapter,[19] the OC-CO conformation of PEO in PEO/PNP and PEO/RES is determined using ^{13}C homonuclear undecoupled and decoupled DQ-NMR. In addition to torsion-angle determination, the information content of the isotropic chemical shifts in the PEO/PNP complex is also studied. A ^{13}C CODEX experiment[20,21] with spin diffusion is employed to identify the trans and gauche peaks. The assignments are confirmed by the linewidths in a magic-angle-spinning INADEQUATE ^{13}C NMR experiment with recoupling of ^{13}C-^{13}C interactions by the CMR7 sequence,[22-24] which also yields the connectivities of the ^{13}C peaks of PEO in the complex. A ^{2}H-^{13}C rotational-echo double-resonance (REDOR) NMR experiment[25-27] is used to determine the distances between the hydroxyl deuteron in d-PNP and the ^{13}C nuclei in the PEO.

4.2 Experimental

4.2.1 Complexation with Hydroxybenzenes

RES and PNP (both from Aldrich) were used as received. The molecular complexes of the ^{13}C-^{13}C labeled PEO and the hydroxybenzenes were prepared by heating a stoichiometric mixture at 120 °C for 24 hours under nitrogen and then recrystallizing. The molar ratio of PEO monomeric units and the PNP was 3:2 (68 wt% PNP) and the ratio for RES was 2:1 (55 wt% RES). The ^{13}C CP-MAS NMR spectra of the complexes, Figure 4.1, were similar to previous reported spectra[18] with peaks at 71.4

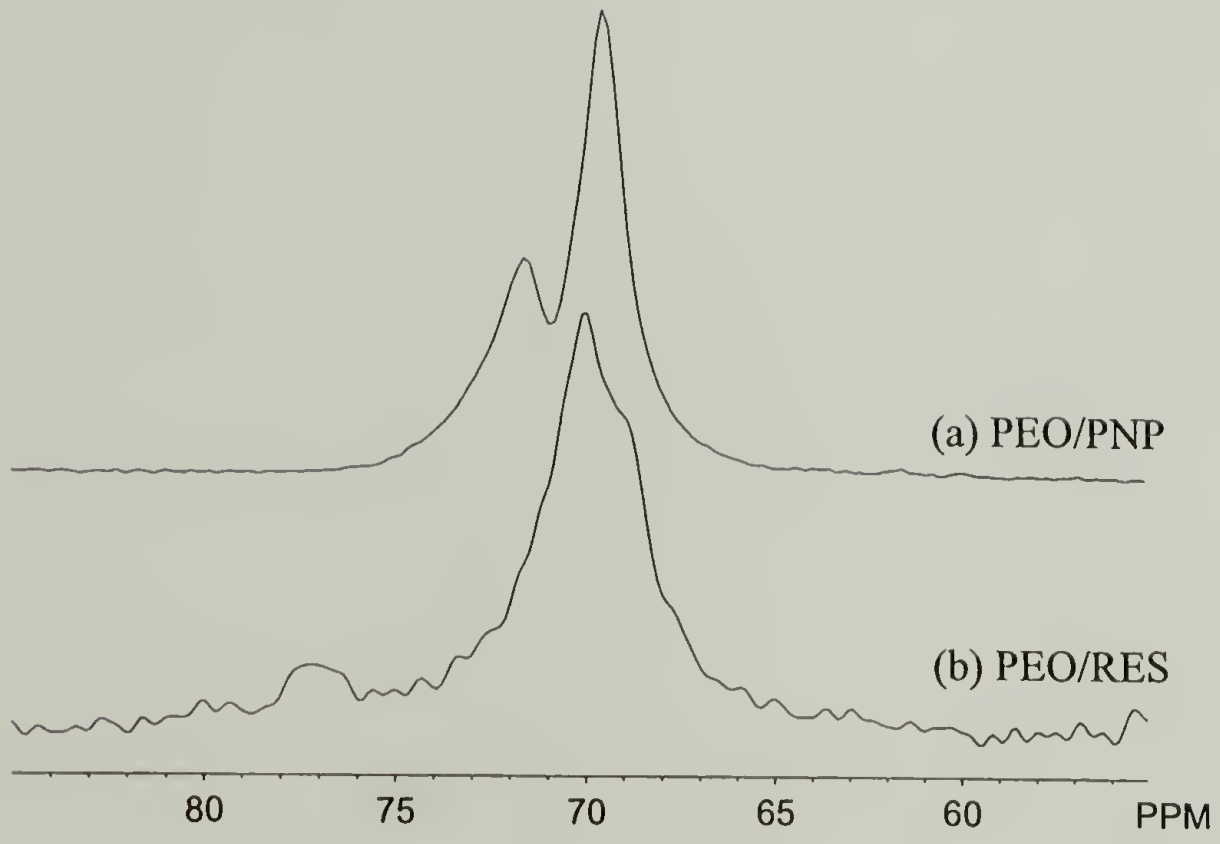

Figure 4.1: PEO resonances in the ^{13}C CP/MAS NMR spectra at 245 K of (a) PEO/PNP, and (b) PEO/RES. All spectra were measured at 75.5 MHz. The PEO/PNP and PEO/RES were measured with spinning rates of 5 kHz, and 4 kHz, respectively.

and 69.4 ppm for the PEO/PNP complex and 69.7 ppm for the PEO/RES complex. Differential scanning calorimetry (DSC) showed melting endotherms at 93 °C for PEO/PNP and 98 °C for PEO/RES, and a weak melting endotherm at 50 °C which corresponds to about 5% uncomplexed PEO crystalline phase in the samples. WAXD confirmed that little uncomplexed crystalline PEO phase was present in the samples and the correct complexed phases had been formed. The uncomplexed crystalline PEO will not contribute to the DQ-NMR spectra due to its high chain mobility that results in a short ^{1}H $T_{1\rho}$ relaxation time.

4.2.2 Wide-Angle X-Ray Diffraction

WAXD was performed using a Siemens D500 instrument with Ni-filtered Cu Kα radiation source in transmission mode.

4.2.3 Differential Scanning Calorimetry (DSC)

DSC measurements were performed with 10-mg samples loaded in Al pans on a DuPont Instruments DSC 2910. Samples were heated at 10 °C/min from 25 to 130 °C.

4.2.4 Static DQ-NMR

The static 2D DQ-NMR spectra were recorded on a Bruker MSL-300 spectrometer at a ^{13}C resonance frequency of 75.5 MHz in a 4.5-mm diameter coil of a static variable-temperature probe. The proton 90° pulse length was *ca.* 3.1 μs,

corresponding to a radio frequency field strength of 80 kHz during cross-polarization. For decoupling, the field strength was increased to ~100 kHz. Typical carbon 90° pulse lengths were 2.6 μs. A cross-polarization time of 500 μs and a signal-acquisition time of 2.6 ms were used. A 1.3 second T_1-filter suppressed the signal from the amorphous and uncomplexed regions.

In the t_1 dimension, 40 slices with increments of 20 μs were acquired. In the t_2 dimension, the dwell time was 10 μs and the number of data points was 256 for the ^{13}C undecoupled spectra and 80 for the decoupled spectrum. The double-quantum excitation and reconversion delay was $2\tau = 280$ μs.[28] A combination of phase cycling and off-resonance evolution was used to reduce artifacts in the spectra. The recycle delay for the PEO/PNP complex was 5 s, while the delay for the PEO/RES complex was 20 s. The spectra of the PEO/PNP complex were obtained at 293 K, those of PEO/RES at 255 K. The PEO/PNP spectra and the PEO/RES spectrum were taken with 512 and 128 scans per t_1 slice, respectively. The measuring time for each two-dimensional double-quantum spectrum was *ca.* 30 hours.

4.2.5 Dipolar/CSA Correlation Experiment

The ^{13}C chemical-shift anisotropy (CSA) is used as a probe of segmental orientation. The orientation of the chemical-shift tensor relative to the bonds is dependent on the electronic environment around the nucleus and has to be determined experimentally. Therefore, the orientations of the CSA tensors of the ^{13}C-^{13}C-O- units in PEO/PNP relative to the C-C bond were measured by a C-C/CSA correlation

experiment.[29,30] Since both the C-C dipolar coupling and the pure CSA are independent of the torsion angle, the spectral line shape depends only on the chemical-shift tensor orientation relative to the C-C bond. The ^{13}C-^{13}C dipolar couplings were decoupled during detection using a decoupling sequence with a 10-pulse cycle.[29,31] The spectrum was measured on the Bruker MSL-300 spectrometer. The number of slices in the t_1 dimension was 32, and 196 scans were averaged per slice to obtain the 2D spectrum. The recycle delay was 7 s and the total experiment time was 12 hours.

4.2.6 Chemical Shift Tensors

Three slightly different chemical shift tensors were used in the simulations of the PEO/PNP spectra, since the experimental spectra show clear differences in the principal values. In the static double-quantum ^{13}C decoupled spectrum, the right edge of the trans pattern is 6 ppm upfield from that of the gauche pattern. The MAS ^{13}C double-quantum experiment for PEO/PNP (see below) shows different isotropic chemical shifts of 71.4 ppm and 69.8 ppm for the gauche and of 69.2 ppm for the trans conformations. On this basis, the principal values of the chemical shift tensors for the two gauche components were obtained as $\sigma_{11} = 93$ ppm, $\sigma_{22} = 84$ ppm, and $\sigma_{33} = 36$ ppm ($\sigma_{iso} = 71$ ppm) and $\sigma_{11} = 91$ ppm, $\sigma_{22} = 82$ ppm, and $\sigma_{33} = 34$ ppm ($\sigma_{iso} = 69$ ppm). The trans component was simulated with a chemical shift anisotropy of $\sigma_{11} = 92$ ppm, $\sigma_{22} = 87$ ppm, and $\sigma_{33} = 28$ ppm ($\sigma_{iso} = 69$ ppm). Based on the dipolar/chemical shift anisotropy (CSA) correlation experiment, the polar coordinates of the C-C bond in the

chemical-shift principal-axis system (PAS) were $\alpha = -60^\circ$ and $\beta = 120^\circ$ for the gauche components, and $\alpha = -60^\circ$ and $\beta = 117^\circ$ for the trans component. The effective distance between two adjacent carbons was set equal to 1.56 Å. Examples of simulated spectra obtained for torsion angles of 60°, 70°, 80°, 160°, 170°, and 180° are shown in Figure 4.2.

4.2.7 Solid-State Dipolar ^{13}C INADEQUATE Spectroscopy under MAS

A dipolar-mediated INADEQUATE NMR experiment[22] using the dipolar recoupling sequence CMR7[23] to excite the double-quantum coherence under MAS was applied to determine the connectivities of the carbon peaks in PEO/PNP. The experiment was performed on a Bruker DSX-300 spectrometer at a frequency of 75.5 MHz in a 7-mm ZrO_2 rotor. The spinning rate was 5 kHz and the temperature was 293 K. The ^1H decoupling field was ~80 kHz. The 90° pulse lengths were 4 ms for ^{13}C and 4.1 ms for ^1H. The recycle delay was 5 s and the number of scans was 128. A total of 96 t_1-slices were acquired. The total experiment time was 16 hours.

4.2.8 ^{13}C CODEX Experiment

In order to identify the gauche and trans peaks in the PEO/PNP spectrum, a ^{13}C CODEX experiment[20,21] with ^{13}C spin diffusion in the mixing time was performed and the normalized peak intensities in the resulting spectra were plotted as a function of the spin-diffusion time. For the two sites on a trans bond, the anisotropic chemical shift is the same; thus spin diffusion does not result in a frequency change and does not dephase

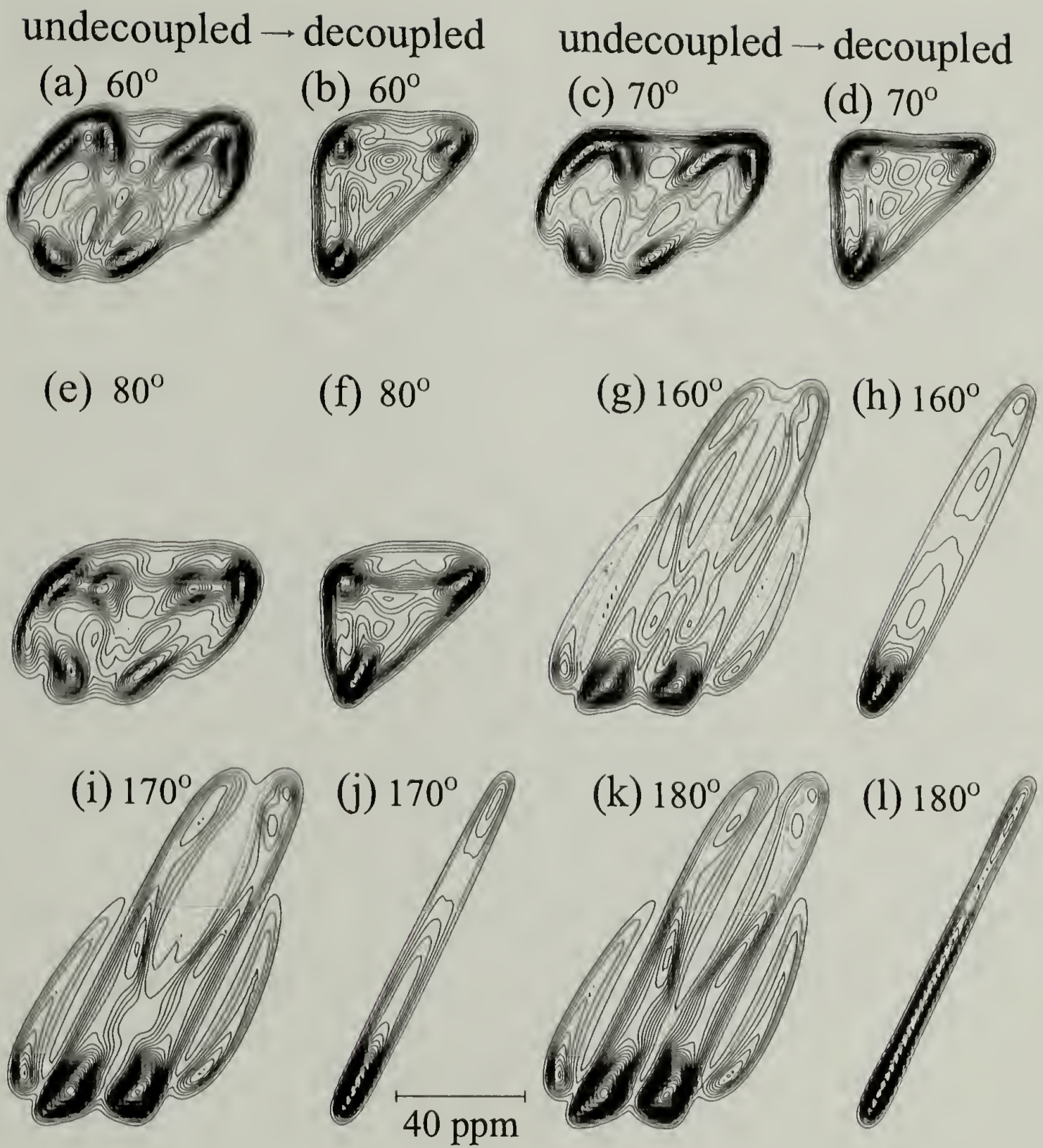

Figure 4.2: Simulated static double-quantum ^{13}C NMR spectra of ^{13}C-^{13}C labeled PEO with and without ^{13}C dipolar decoupling for torsion angles of (a/b) 60°, (c/d) 70°, (e/f) 80°, (g/h) 160°, (i/j) 170°, and (k/l) 180°. The tensor parameters are those of the gauche component as given in the caption of Figure 4.3.

the signal. For gauche bonds, we have a two-site exchange process. Exchange in the long-time limit results in a frequency change for half the magnetization, while the other half still resides in the initial site. Therefore, dephasing reaches an asymptote of 50%. The ^{13}C CODEX experiment was carried out on a Bruker DSX spectrometer at a ^{13}C resonance frequency of 75.5 MHz using a 4-mm double-resonance MAS probe. The ^{13}C and ^{1}H 90° pulse lengths were 2.3 μs and 3.3 μs, respectively. A cross-polarization time of 500 μs, a signal-acquisition time of 10 ms, and a recycle delay of 4 s were used. The spectra were acquired with a spinning frequency of 10 kHz at room temperature.

4.2.9 REDOR ^{2}H-^{13}C Distance Determination Experiments

The hydroxyl hydrogen in PNP was exchanged with deuterium by dissolving in CH_3OD and then drying under vacuum. This deuterated PNP was used to prepare PEO/d-PNP. A ^{2}H-^{13}C REDOR experiment[26,27] was performed and the dipolar recoupling-time-dependent peak intensities in the resulting spectra were used to determine ^{13}C-^{2}H distances. The NMR experiments were performed at a frequency of 75.5 MHz on a Bruker DSX-300 spectrometer using a 4-mm triple-resonance MAS probe. The ^{1}H decoupling field strength was 80 kHz. The 90° pulse length was 3.5 ms for ^{13}C and 2.1 ms for ^{2}H. A ^{1}H-^{13}C CP time of 500 ms was used. The spectra were acquired with a spinning frequency of 4.7 kHz at room temperature. The acquisition time was 38 ms and the number of scans was typically 6000. ^{2}H-^{13}C dipolar recoupling times of 0.43, 0.85, 1.28, and 2.13 ms were used.

4.3 Results and Discussion

4.3.1 Dipolar/CSA Correlation

This 2D experiment was used to analyze the orientations of the CSA tensor by correlating it with the C-C bond direction. The experimental spectrum is shown in Figure 4.3 (a) and compared with the best-fit simulated spectrum in Figure 4.3 (b). The orientations of the gauche and trans chemical shift tensors were allowed to be slightly different. The best-fit simulation, which was also consistent with the DQ-NMR spectra, required a trans tensor orientation of $\alpha = -60^\circ$ and $\beta = 117^\circ$, and a gauche tensor orientation of $\alpha = -60^\circ$ and $\beta = 120^\circ$. The uncertainty in the more important angle parameter β is $\pm 5^\circ$; that in α is $\pm 30^\circ$. These results are similar to previous measurements on PET[29,30] and consistent with C-H/CSA correlation results on PEO.[30]

The effect of α is seen mostly on the left-hand side of the pattern. From the local symmetry of the CH_2 group, $\alpha = 0^\circ$, $\pm 90^\circ$ or 180° would be expected. However, the $\alpha = 0^\circ$ value is excluded by measurements on oriented samples.[30] For $\alpha = -90^\circ$, reduced agreement with the experimental dipolar/CSA spectrum is observed. In addition, better fits of the double-quantum spectra are obtained with $\alpha = -60^\circ$. Nevertheless, overall the differences between $\alpha = -90^\circ$ and $\alpha = -60^\circ$ double-quantum patterns are small and do not change the torsion angle determination significantly.

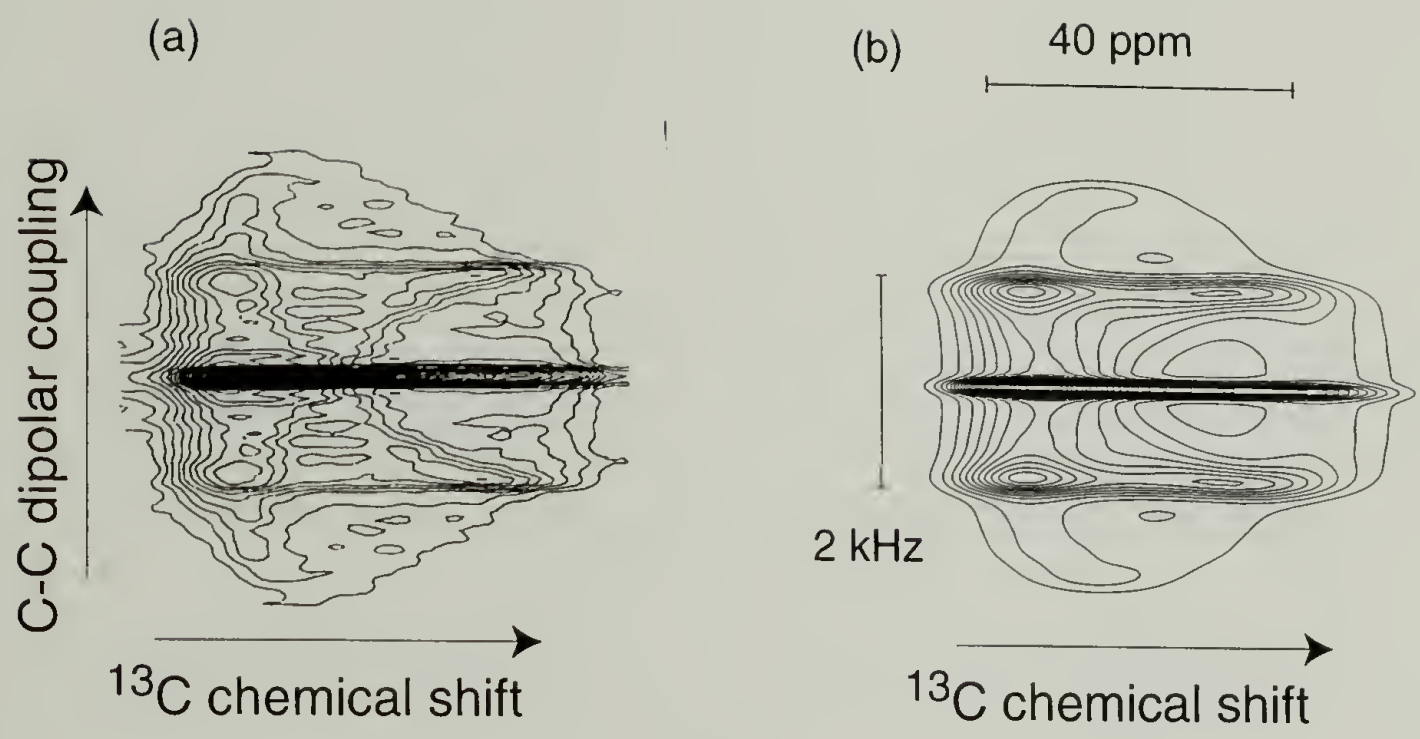

Figure 4.3: ^{13}C CSA-dipolar coupling correlation NMR spectrum (a) of PEO/PNP complex at 293 K. (b) Best-fit simulation using a trans:gauche ratio of 1:2. The tensor orientation (C-C bond in the PAS) was α = -60° and β = 117° for the trans component with principal values of (σ_{11} = 92 ppm, σ_{22} = 87 ppm, σ_{33} = 28 ppm), and of α = -60° and β = 120° with principal values of (σ_{11} = 93 ppm, σ_{22} = 84 ppm, σ_{33} = 36 ppm) and (σ_{11} = 91 ppm, σ_{22} = 82 ppm, σ_{33} = 34 ppm) for the gauche components.

These orientations were used as parameters for the static double-quantum ^{13}C NMR simulations. The undecoupled double-quantum spectra, which reflect both chemical shift and dipolar coupling in the ω_2 dimension, provide additional confirmation of the validity of this tensor orientation.

4.3.2 Static Double-Quantum ^{13}C NMR Measurements

The observed and simulated C-C undecoupled static double-quantum spectra of PEO/RES are shown in Figure 4.4. The observed spectrum shows that all of the OC-CO torsion angles are gauche. The simulation suggests that the average torsion angle is $\psi = 74 \pm 9^\circ$ with an angle distribution width of $\sigma_\psi < 10^\circ$. Other effects, such as insufficient ^1H decoupling or slow chain motion, may broaden the spectrum and result in an apparently broadened torsion angle distributions in the simulations. On the other hand, torsional librations that are fast on the NMR timescale of ~100 μs should be invisible to the experiment and not be taken into account in the quoted width of the distribution.

The observed and simulated undecoupled and decoupled static double-quantum spectra of PEO/PNP are shown in Figure 4.5. The spectra show a strong slope-two diagonal ridge due to trans OC-CO bonds. The simulations of the observed spectra were produced by factoring 0.33 for trans and 0.67 for gauche conformers. Both the undecoupled and decoupled static double-quantum spectra are consistent with one third

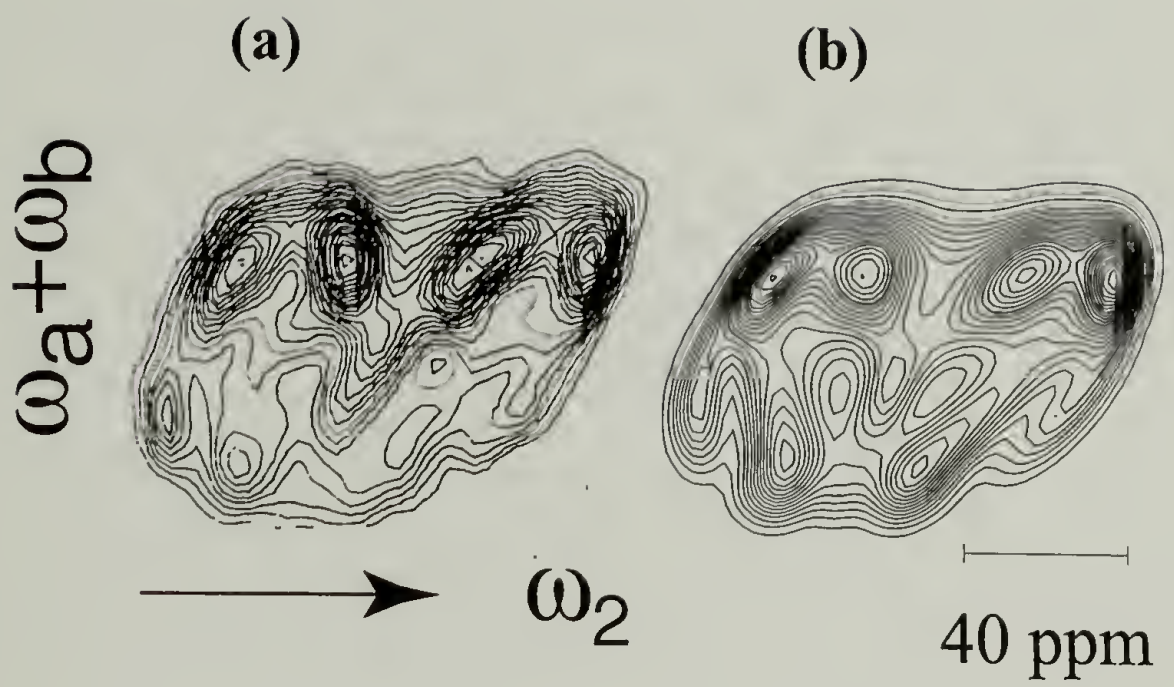

Figure 4.4: Static double-quantum ^{13}C NMR spectrum of labeled PEO/RES without ^{13}C homonuclear dipolar decoupling (a) measured at 75.5 MHz and 250 K. The best simulation (b) has an average gauche angle $\psi = 74 \pm 9^\circ$ with a distribution of width $\sigma_\psi = 7^\circ$.

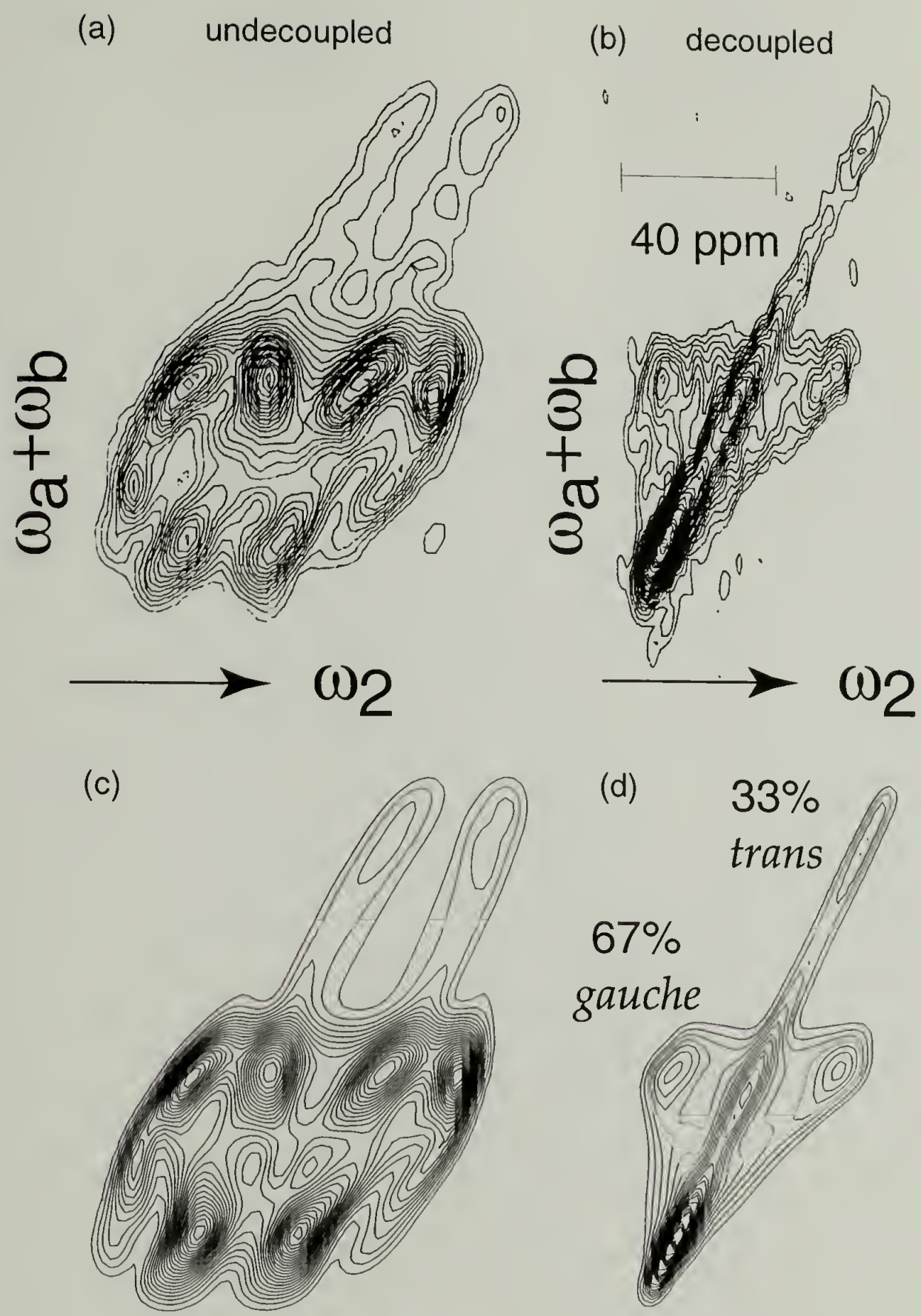

Figure 4.5: Static double-quantum ^{13}C NMR spectra of labeled PEO/PNP measured at 75.5 MHz and 293 K. (a) Without ^{13}C homonuclear decoupling and (b) with decoupling. The best simulations of both the undecoupled (c) and decoupled (d) spectra use a trans:gauche ratio of 1:2. The average gauche angle is $\psi = 70 \pm 9^\circ$ with a Gaussian width of $\sigma_\psi < 10^\circ$; a value of $\sigma_\psi = 5^\circ$ was used in the shown simulation. As seen from Figure 4.2(j), significant deviation from 180° results in broad diagonal ridges which was not experimentally observed. The narrow diagonal ridge indicates that the Gaussian width of the trans torsion angle distribution is $\sigma_\psi < 7^\circ$.

of OC-CO bonds of the PEO/PNP in the trans conformation ($\psi = 180^\circ$, $\sigma_\psi < 7^\circ$), and two thirds in the gauche conformation ($\psi = 70 \pm 9^\circ$, $\sigma_\psi < 10^\circ$).

4.3.3 Dipolar ^{13}C INADEQUATE Spectroscopy under MAS

The 2D INADEQUATE MAS spectrum of PEO/PNP is shown in Figure 4.6. Three peaks, a doublet and a singlet, are observed in the spectrum. Signals at the same ω_1 value belong to a ^{13}C-^{13}C pair, and the chemical shifts of the two ^{13}C's in the pair can be read off in the ω_2 dimension. In addition, due to special magic-angle-spinning effects, the line broadening makes it possible to identify which peaks belong to gauche or trans conformations: a broadening arises if the two dipolar-coupled ^{13}C nuclei have different CSA orientations, as is the case for a gauche conformation.[32] This was previously discussed in Chapter 2.

The doublet of broad peaks at (71.4, 141.3 ppm) and (69.8, 141.3 ppm) corresponds to two bonded ^{13}C nuclei with inequivalent chemical shifts. The strong broadening of the peaks shows that they are connected by a gauche bond. The singlet peak at (69.2, 138.4 ppm) is much sharper, which means that it must be due to a ^{13}C spin pair around a trans bond. The peak position shows that the isotropic chemical shifts of both ^{13}C nuclei of the trans bond are 69.2 ppm. This equivalence suggests that the chain structure is point-symmetric around the trans bond. The integrated area of the two gauche peaks is $73 \pm 5\%$ and the area of the trans peak is $27 \pm 5\%$.

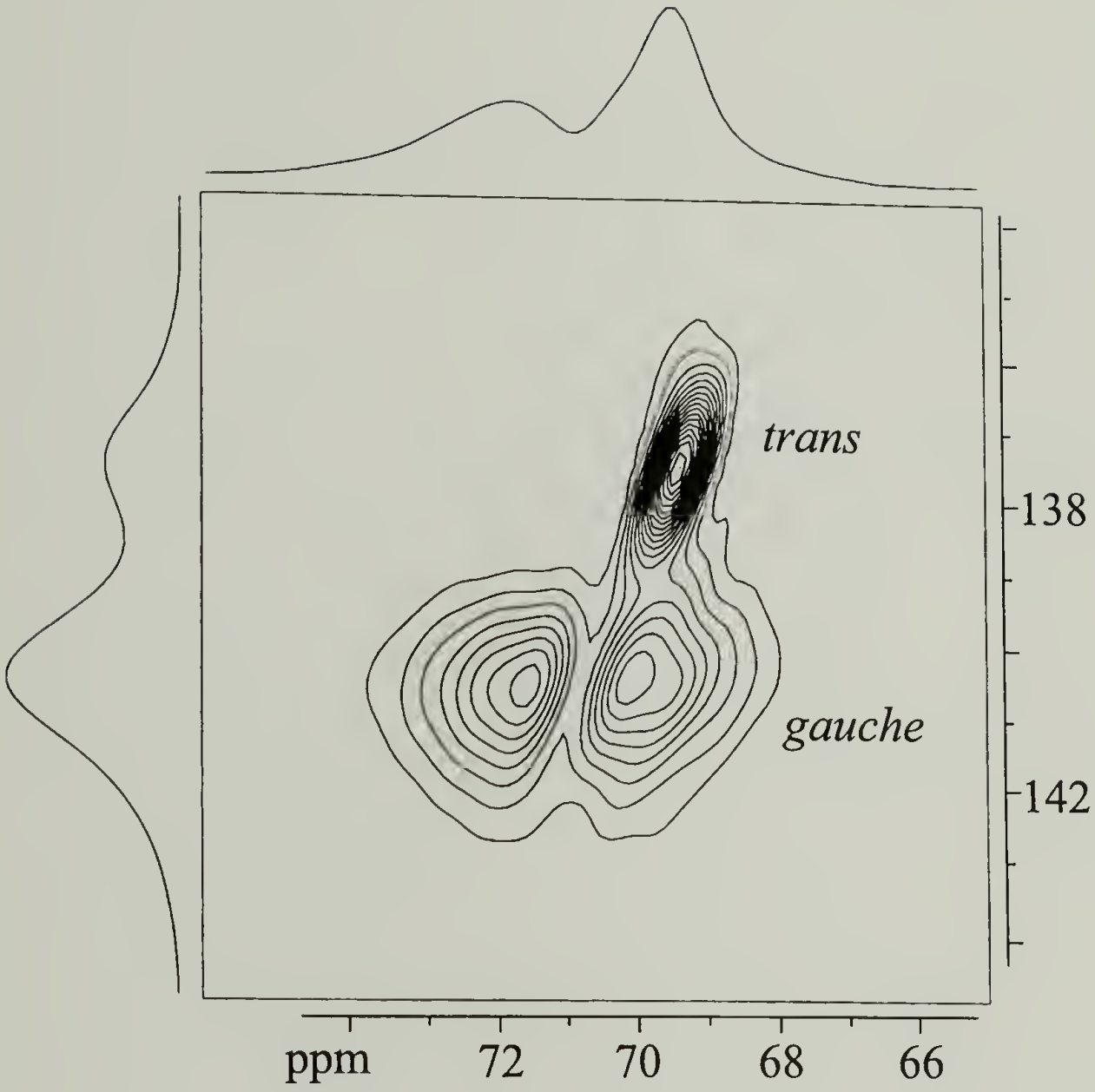

Figure 4.6: INADEQUATE spectrum of PEO/PNP. The spectrum was obtained at 293 K with a spinning rate of 5 kHz. There are peaks at (71.4, 141.3 ppm) (g_a) and (69.8, 141.3 ppm) (g_b) which correspond to the carbons of the gauche OC-CO bonds. The narrower peak at (69.2 ppm, 138.4 ppm) belongs to the magnetically equivalent carbons of the trans OC-CO bond.

The conformational effects on the chemical shift of PEO have previously been considered based on NMR spectra of alkyl chains. The ^{13}C chemical shift for alkyl chains is predominantly affected by conformational effects rather than packing effects.[33,34] Gauche bonds in alkyl chains result in γ-gauche effects which lower the chemical shifts of adjacent carbons by approximately 4 ppm. Studies of the temperature dependence of the chemical shift of PEO in water[35,36] have suggested that the gauche conformation of PEO also results in a lower chemical shift than the trans conformation. The gauche and trans chemical shifts were estimated to be 71.58 and 73.83 ppm, respectively. However, the INADEQUATE spectrum for PEO/PNP shows that there may not be a simple relationship between C-C bond conformation and chemical shift. In fact, the signal in crystalline PEO, where all OC-CO bonds are gauche and all CC-OC bonds trans, shows peaks separated by several ppm, which suggests that packing effects can result in significant chemical shift differences. Also, γ-gauche effects are not expected to occur in PEO/RES and PEO/PNP because only CC-OC bonds are relevant for γ-gauche shifts in PEO, and they are all trans.

4.3.4 ^{13}C CODEX Experiment

The assignment of the peaks to gauche and trans conformations is confirmed by the ^{13}C CODEX experiment with exchange by spin diffusion. As observed in Figure 4.1 (a), the PEO/PNP 1D ^{13}C spectrum consists of two broad peaks. The ^{13}C CODEX spectrum obtained with a mixing time of 100 ms, and the reference spectrum obtained

with the same pulse sequence but a mixing time of only 0.5 ms, are presented in Figures 4.7 (b) and (a), respectively. The spectra are scaled to equal heights of the 69.4 ppm line to highlight the greater effect of the spin diffusion on the 71.4-ppm line. To understand this difference, it has to be noted that spin diffusion between trans sites is not detectable because it does not introduce a change in the frequency of the involved ^{13}C nuclei; thus a spin-diffusion-induced decay is observed only for the two gauche sites. In Figure 4.7 (c), the mixing-time dependence of the CODEX spin diffusion is plotted for both peaks. The relative intensity of the 71.4-ppm gauche signal for long mixing times (> 100 ms) decays to a constant value of $E_\infty \sim 0.5$. Meanwhile, the relative intensity for the other peak, as expected for a two-site spin-diffusion process in the absence of slow chain motion, decays to approximately 0.75. The same plot also shows the decay for the pure trans conformation, obtained by determining the difference between the intensities of the left and the right line and taking the ratios of the differences obtained from reference and spin-diffusion CODEX spectra. This ratio is very close to unity, as expected for the trans conformation. From the values of the relative intensities obtained at t_m = 200 ms for both lines, Figure 4.7 (c), the gauche-trans ratio is estimated to be two, which confirms the result obtained from the double-quantum spectra, where 1/3 of the OC-CO torsion angles are trans and 2/3 are gauche.

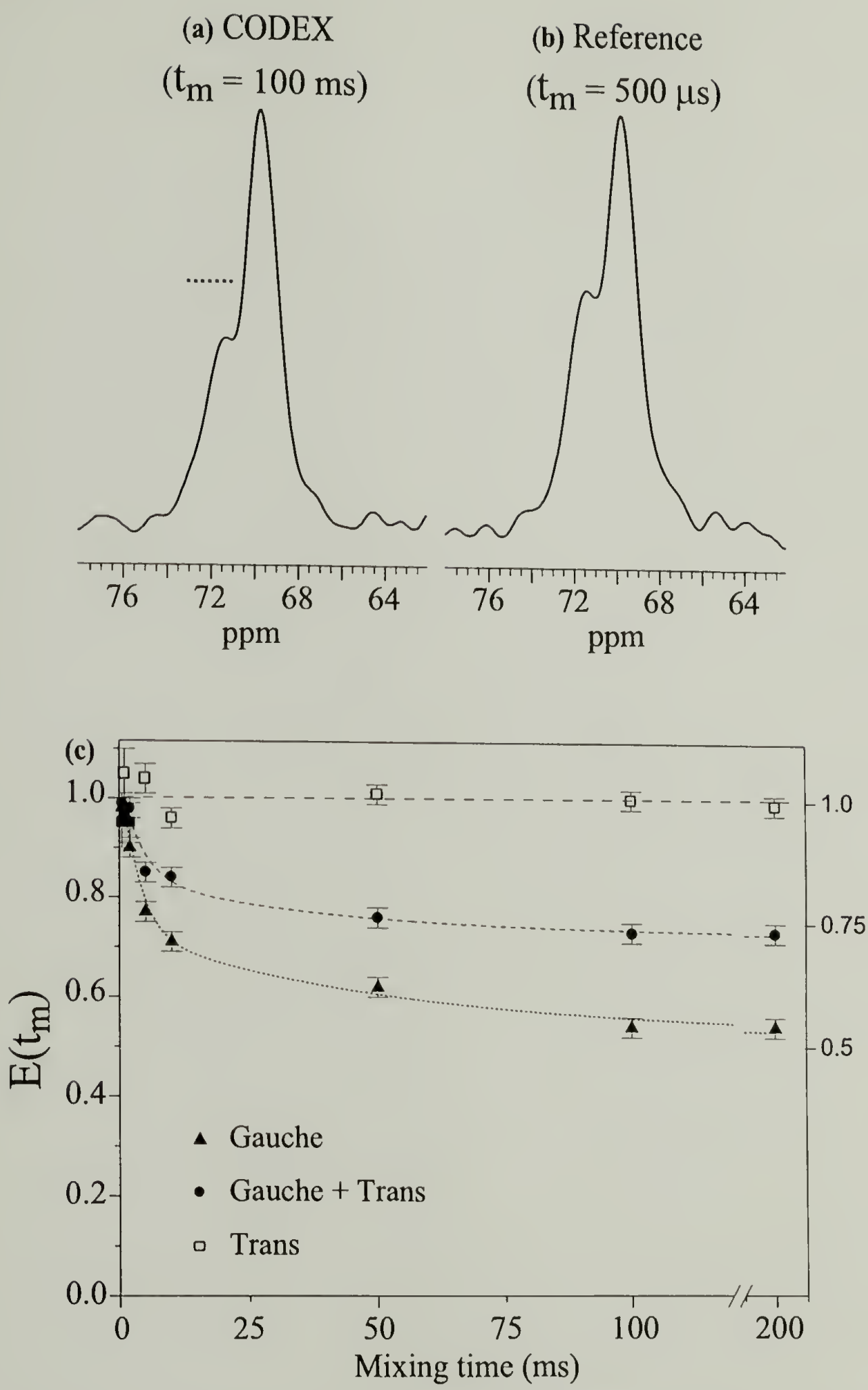

Figure 4.7: ^{13}C CODEX spectra used to determine the trans-gauche ratio in PEO/PNP. (a) Reference spectrum with a mixing time of 0.5 ms, and (b) CODEX spectrum with a mixing time of 100 ms. The right peak was scaled to equal height to enable comparison of the relative intensities. The decay of the peak intensities in (c) shows that the downfield peak at 71.4 ppm is gauche while the upfield 69.4-ppm line is 50% gauche and 50% trans.

4.3.5 ^{2}H-^{13}C Distance Estimates from REDOR

Information on PNP-PEO hydrogen bonding is obtained by measuring distances between OD deuterons and PEO carbons. Known earbon-deuteron distances within the d-PNP molecules are used as internal referenees. The ^{2}H-^{13}C differenee speetra with reeoupling times of 2.13 and 0.85 ms are shown in Figures 4.8 (b) and 4.8 (e). The spectra are sealed to equal heights of peak 1. For reference, the CP/TOSS-MAS speetrum is shown in Figure 4.8 (a). The PEO peak at 71.4 ppm has a relatively higher intensity than that at 69.4 ppm when compared with the CP-MAS spectrum. The CP-MAS referenee speetrum has a ratio of 1 : 1.90 for the intensities of the 71.4 ppm : 69.4 ppm peaks. At a short recoupling time of 0.85 ms, this ratio is 1 : 1.46, and in the spectrum with a longer recoupling time of 2.13 ms this ratio is 1 : 1.60. This suggests that the 71.4 ppm gauche carbon is closer to the OD group of d-PNP than the eombination of the trans and gauehe carbons in the 69.4 ppm peak. The earbon-deuteron distanees ean be estimated by comparison with the signal build-up of the various d-PNP sites. At shorter recoupling times, the signal of carbon 1, which is at only 2.3 Å from the deuteron, is mueh stronger than that of the other aromaties. At intermediate mixing times, the signals of carbon 2 (at 3.0 Å from the ^{2}H), carbon 6 (at 3.7 Å), and partly carbon 3 (at 4.4 Å) are also observed. The REDOR build-up curves for the important peaks are shown in Figure 4.9. Using the intensity build-up of the d-PNP peaks as referenees, the distanees of the carbons in the PEO ehain for the deuteron were estimated. Thus, the distanee from the ^{2}H to the ^{13}C with the chemical shift of 71.4 ppm (g_a) was determined to be

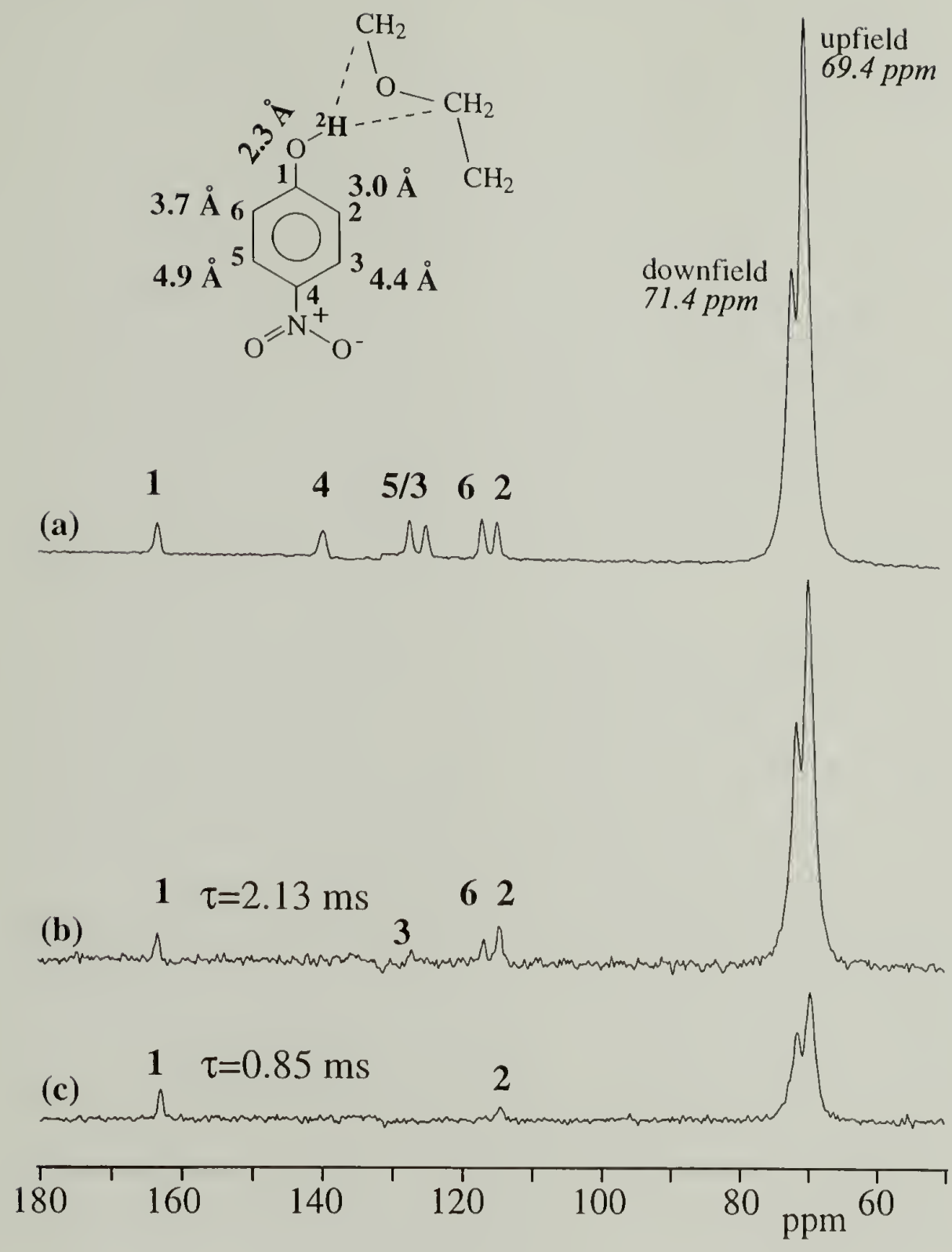

Figure 4.8: ^{2}H-^{13}C dipolar recoupling NMR spectra to determine the distances between the deuterated-PNP OD deuteron and the PEO carbons in the PEO/PNP complex. The CP/TOSS spectrum (a) is compared with the intensities of the peaks after recoupling times of (b) 2.13 ms and (c) 0.85 ms (spectra scaled to equal height of peak 1). The relative intensities of the 71.4-ppm peaks are greater than the peaks near 69.4 ppm when compared to the CP/TOSS spectrum. The intensity build-ups of the PNP peaks were used as references to determine internuclear distances.

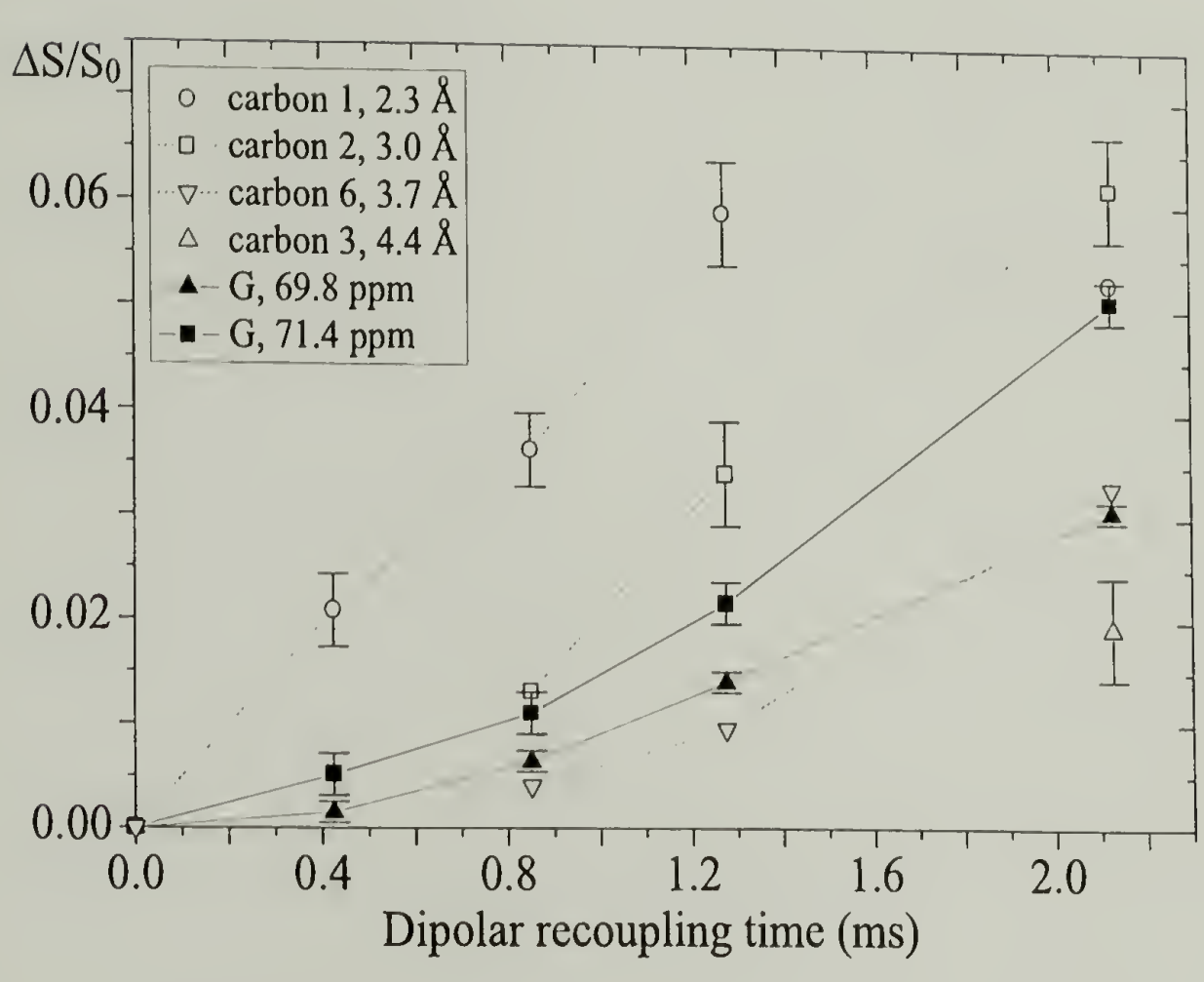

Figure 4.9: Normalized REDOR difference signal intensities ($\Delta S/S_0$) of the four carbons of PNP and the two observed peaks from the PEO chain were used to determine internuclear distances. The PEO peak at 69.4 ppm was assumed to be composed of two components: a trans carbon that is equally distant from the deuteron as the 71.4 ppm gauche peak, and a gauche carbon, with an isotropic chemical shift of 69.8 ppm, that is more distant. The value of $\Delta S/S_0$ for the 69.8-ppm gauche component was calculated to be $[\Delta S(69.4)-\Delta S(71.4)]/[S_0(69.4)-S_0(71.4)]$. The ^{2}H-^{13}C distances were calculated to be 3.2 ± 0.2 Å for the 71.4-ppm gauche peak and 3.6 ± 0.3 Å for the 69.8-ppm gauche component.

3.2 ± 0.2 Å. The observed REDOR build-up curves are steeper than simulated curves, not shown, which may be due to the high abundance of deuterons in the system.

The distances for the gauche and trans carbons with chemical shifts near 69.4 ppm can be estimated using the REDOR spectra and the predicted crystal structure of PEO/PNP, shown in Figure 4.10. If there is strong hydrogen bonding between the OD of the d-PNP and the ether oxygens as indicated in Figure 4.10, carbons labeled g_b are further from the OD groups. The distance between the deuterons and the gauche carbons g_a was assumed to be approximately equal to the distance between the deuterons and the trans carbons t. Using this assumption, the intensity of the 71.4 ppm peak was subtracted from the 69.4 ppm peak in the REDOR spectra. The resulting intensity was used to estimate that the distance from the deuteron to the carbon g_b is 1.13 ± 0.06 times larger than that to the carbon g_a; this yields a value of 3.6 ± 0.3 Å.

4.4 Summary

Five state-of-the-art solid-state NMR techniques were employed to study the chain conformation, hydrogen bonding, and chemical shifts of ^{13}C-labeled PEO in complexes with hydroxybenzenes. A two-dimensional double-quantum spectrum confirmed that the OC-CO torsion angles in PEO/RES are all gauche. In contrast, one third of the OC-CO torsion angles in PEO/PNP are trans, with $\psi = 180 \pm 7^\circ$, and two thirds are gauche, with $\psi = 70 \pm 9^\circ$. This confirms the previously suggested structure.[16] The solid-state INADEQUATE spectrum and spin-diffusion CODEX experiments of

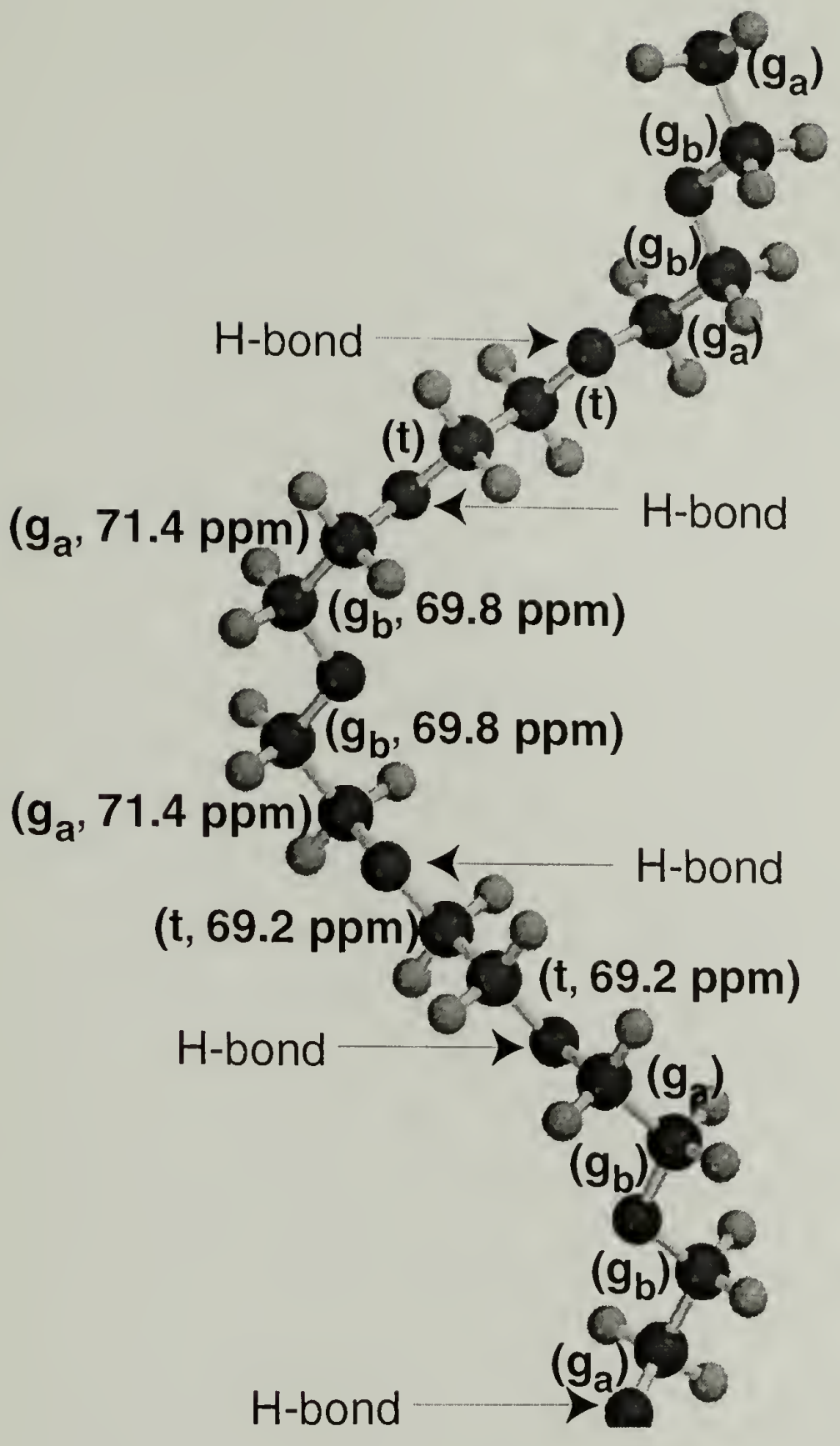

Figure 4.10: Crystal structure of PEO/PNP with assignment of chemical shifts. The structure shown has the OC-CO gauche torsion angles of ±70° determined here, and reproduces the 1.56-nm repeat period determined by X-ray diffraction, with ±5° deviations of the CC-OC torsion angles from exact trans. The assignment is based on the ^{2}H-^{13}C dipolar recoupling NMR spectra and the 2D MAS ^{13}C double-quantum solid-state NMR spectrum of PEO/PNP. The two different types of gauche carbons in the crystal structure are expected to have different distances from the OH group of the PNP. The carbons g_a, which have a chemical shift of 71.4 ppm, are close to the d-PNP's deuteron while the carbons g_b are more distant and have a chemical shift of 69.8 ppm.

PEO/PNP show that the carbons in the gauche OC-CO bonds have different chemical shifts of 71.4 ppm and 69.8 ppm, while the carbons in the trans OC-CO bonds both have a chemical shift of 69.2 ppm. The ^{2}H-^{13}C REDOR experiments showed that the hydroxyl group of the PNP is closer to the 71.4-ppm gauche carbon than the average of the components in the 69.4-ppm peak, with a distance of 3.2 ± 0.2 Å. This is inconsistent with the previous hypothesis that hydrogen bonding was responsible for the upfield shift of the 69.4-ppm peak. Instead, the chemical shift differences is attributed to packing effects, which in crystalline PEO were found to result in shifts of several ppm. The combination of all the information obtained allows chemical shift assignment for the three types of conformationally inequivalent carbons in the PEO/PNP complex.

4.5 References

(1) Papke, B. L.; Ratner, M. A.; Shriver, D. F. *J. Phys. Chem. Solids* **1981**, *42*, 493-500.

(2) Tadokoro, H.; Yoshihara, T.; Chatani, Y.; Murahashi, S. *J. Polym. Sci., Part B* **1964**, *2*, 363-368.

(3) Tadokoro, H. *Macromol. Rev.* **1966**, *1*, 119.

(4) Iwamoto, R.; Saito, Y.; Ishihara, H.; Tadokoro, H. *J. Polym. Sci., Part A-2* **1968**, *6*, 1509-1525.

(5) Point, J. J.; Coutelier, C. *J. Polym. Sci.: Polym. Phys. Ed.* **1985**, *23*, 231.

(6) Point, J. J.; Jasse, B.; Dosière, M. J. *J. Phys. Chem.* **1986**, *90*, 3273-3277.

(7) Paternostre, L.; Damman, P.; Dosière, M. *Macromolecules* **1997**, *30*, 3946-3948.

(8) Myasnikova, R. M.; Titova, E. F.; Obolonska, E. S. *Polymer* **1980**, *21*, 403-407.

(9) Cheng, C.; Belfiore, L. A. *Polym. News* **1990**, *15*, 39-49.

(10) Belfiore, L. A.; J., L. T.; Cheng, C.; Bronnimann, C. E. *J. Polym. Sci., Part B: Polym. Phys.* **1990**, *28*, 1261-1274.

(11) Delaite, E.; Point, J. J.; Damman, P.; Dosière, M. *Macromolecules* **1992**, *25*, 4768-4778.

(12) Paternostre, L.; Damman, P.; Dosière, M.; Bourgaux, C. *Macromolecules* **1996**, *29*, 2046-2052.

(13) Spevácek, J.; Paternostre, L.; Damman, P.; Draye, A. C.; Dosière, M. *Macromolecules* **1998**, *31*, 3612-3616.

(14) Point, J. J.; Damman, P. *Macromolecules* **1992**, *25*, 1184-1188.

(15) Damman, P.; Point, J. J. *Macromolecules* **1993**, *26*, 1722-1728.

(16) Damman, P.; Point, J. J. *Macromolecules* **1994**, *27*, 3919-3925.

(17) Damman, P.; Point, J. J. *Macromolecules* **1995**, *28*, 2050-2053.

(18) Spevácek, J.; Suchopárek, M. *Macromol. Symp.* **1997**, *114*, 23-34.

(19) Harris, D. J.; Bonagamba, T. J.; Hong, M.; Schmidt-Rohr, K. *accepted to Macromolecules* **2000**.

(20) deAzevedo, E. R.; Hu, W.-G.; Bonagamba, T. J.; Schmidt-Rohr, K. *J. Chem. Phys* **(accepted)**.

(21) deAzevedo, E. R.; Hu, W.-G.; Bonagamba, T. J.; Schmidt-Rohr, K. *J. Am. Chem. Soc.* **1999**, *121*, 8411-8412.

(22) Hong, M. *J. Magn. Reson.* **1999**, *136*, 86-89.

(23) Rienstra, C. M.; Hatcher, M. E.; Mueller, L. J.; Sun, B. Q.; Fesik, S. W.; Griffin, R. G. *J. Am. Chem. Soc.* **1998**, *120*, 10602-10612.

(24) Lee, Y. K.; Kurur, N. D.; Helmle, M.; Johannessen, O. G.; Nielsen, N. C.; Levitt, M. H. *Chem. Phys. Lett.* **1995**, *242*, 304-309.

(25) Gullion, T.; Schaefer, J. *J. Magn. Reson.* **1989**, *81*, 196-200.

(26) Schmidt, A.; McKay, R. A.; Schaefer, J. *J. Magn. Reson.* **1992**, *96*, 644-650.

(27) Sandström, D.; Hong, M.; Schmidt-Rohr, K. *Chem. Phys. Lett.* **1999**, *300*, 213-220.

(28) Schmidt-Rohr, K. *Macromolecules* **1996**, *29*, 3975-3981.

(29) Dunbar, M. G.; Novak, B. M.; Schmidt-Rohr, K. *Solid State Nuclear Magn. Reson.* **1998**, *12*, 119-137.

(30) Schmidt-Rohr, K.; Wilhelm, M.; Johansson, A.; Spiess, H. W. *Magn. Reson. Chem.* **1993**, *31*, 352-356.

(31) Schmidt-Rohr, K. *J. Magn. Reson.* **1998**, *131*, 209.

(32) Maricq, M.; Waugh, J. S. *J. Chem. Phys.* **1979**, *70*, 3300-3316.

(33) Cheney, V. B.; Grant, D. M. *J. Am. Chem. Soc.* **1967**, *89*, 5319-5327.

(34) Persson, B.-O.; Drakenberg, T.; Lindman, B. *J. Phys. Chem.* **1976**, *80*, 2124-2125.

(35) Björling, M.; Karlström, G.; Linse, P. *J. Phys. Chem.* **1991**, *95*, 6706-6709.

(36) Ahlnäs, T.; Karlström, G.; Lindman, B. *J. Phys. Chem.* **1987**, *91*, 4030-4036.

CHAPTER 5

CONFORMATION OF PEO INTERCALATED IN CLAY AND MoS_2

5.1 Introduction

The intercalation of organic compounds in layered inorganic solids such as smectite clay minerals (montmorillonite and hectorite) and transition metal dichalcogenides (MoS_2 and TiS_2) has been widely studied during the last years.[1-16] Recently, the interest in the nanocomposites of PEO increased due to their unique electronic, ionic (without counter-ions), mixed electronic and ionic, structural, and mechanical properties.[6,9] The knowledge of the conformational characteristics of PEO in these nanocomposites is therefore a prerequisite to understanding the above-cited important properties. Nevertheless, the structure of PEO in the less than 1-nm wide gaps between the inorganic layers is not well characterized.

The PEO conformation in the intercalates may differ from the 7_2 helical structure. WAXD measurements[1,5,8] show that the formation of PEO intercalates involves a gallery expansion by 0.4 nm or 0.8 nm, depending on the polymer mass fraction used to prepare the intercalated material, Figures 5.1 and 5.2. The estimated width of the galleries, including the alkali ions, in a smectite clay (hectorite) and in a transition metal dichalcogenide (MoS_2) is 0.80-1.00 nm and 0.85 nm, respectively.

In the nanocomposites, the polymer conformation may be affected by the limited space between layers and by the polymer interaction with the charged surfaces of the

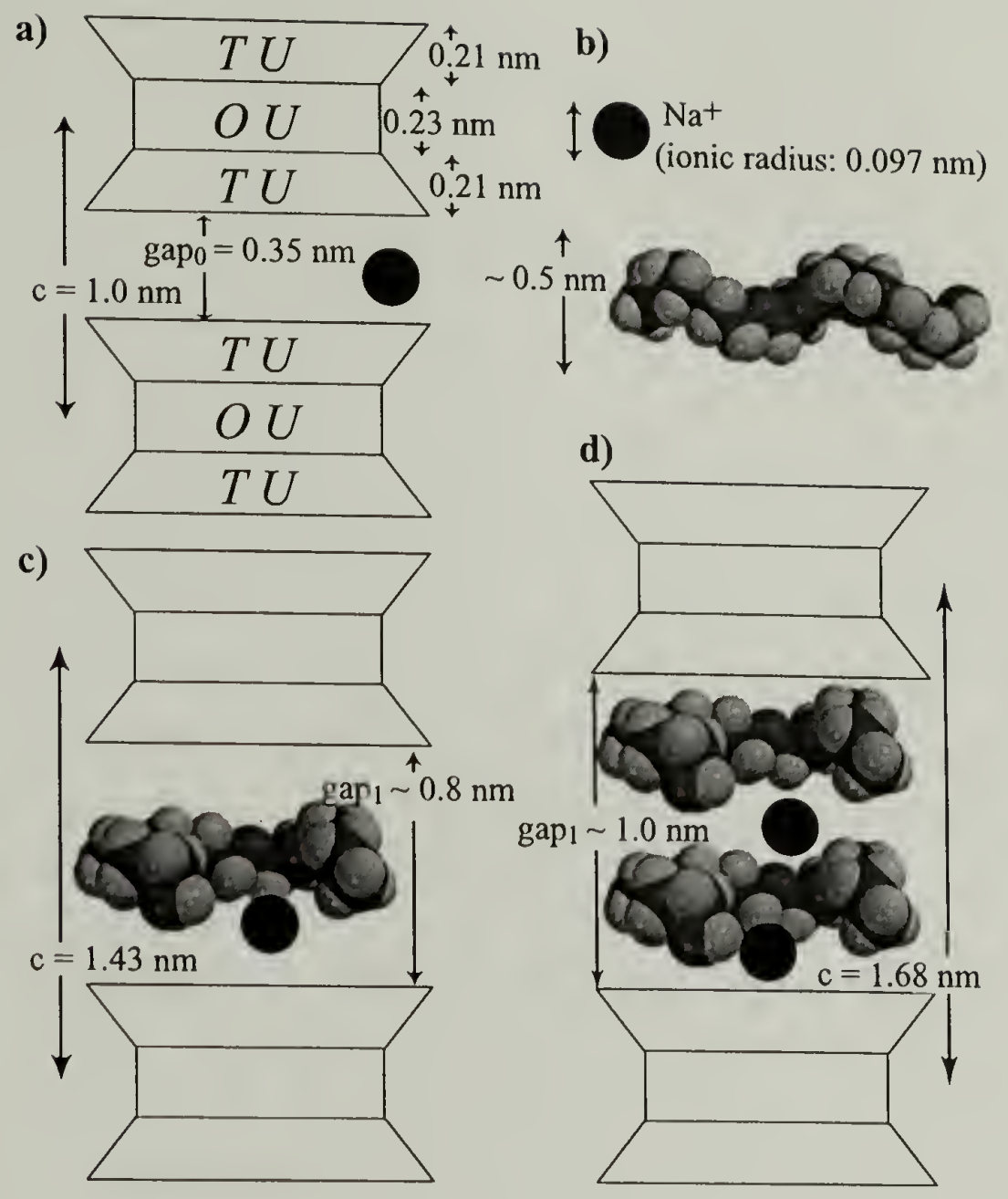

Figure 5.1: Idealized structures of smectite clays (montmorillonite and hectorite), PEO, and the respective intercalated nanocomposites. Smectite silicate clay minerals have layer lattice structures in which two-dimensional oxyanions are separated by layers of hydrated cations. (a) The oxygen atoms define the upper and lower sheets of tetrahedral units (TU) and the central sheet of octahedral units (OU). Si and sometimes Al normally occupy the tetrahedral positions in the oxygen framework. Al, Mg, or Li may occupy octahedral sites. In montmorillonite, the layer charge originates from the substitution of octahedral Al^{3+} by Mg^{2+}, while in hectorite from the substitution of octahedral Mg^{2+} by Li^{+}. The naturally occurring clays contain other ions by isomorphous substitution such as iron. Typically, the charge deficiency in the layers of smectites ranges from 0.4 to 1.2e per Si_8O_{20}, which is balanced by interlayer ions (Na^{+} in MMT and HCT). (b) PEO conformation proposed by Tadokoro. (c) and (d) Idealized structures for the intercalated nanocomposites PEO/HCT(0.45) and PEO/HCT(0.70), taking into consideration the information obtained from the WAXD and double-quantum NMR measurements. The main purpose is the representation of the relevant length scales; many details of the polymer conformation and cation distribution are hypothetical.

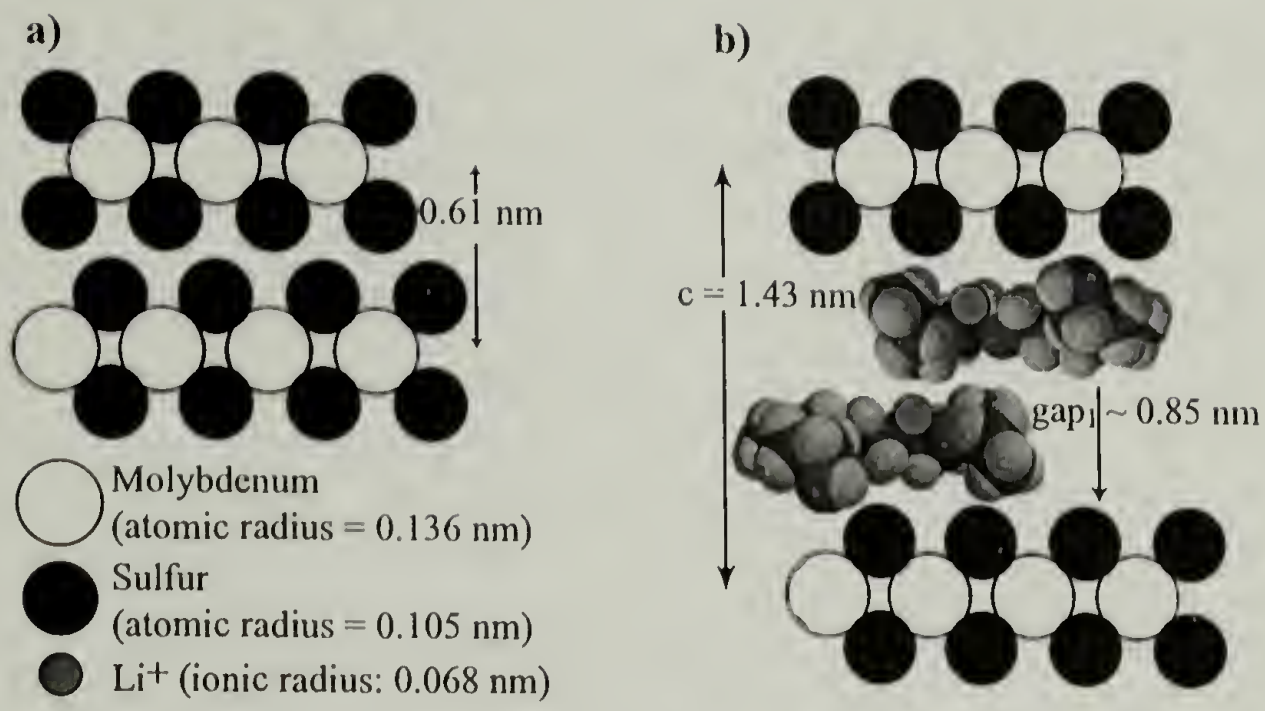

Figure 5.2: Idealized structures of MoS_2 and the respective PEO intercalated nanocomposites. (a) In the MoS_2 layer structure, the molybdenum is sandwiched between two sulfur sheets with six atoms of S surrounding a Mo atom, forming a trigonal prism. These layers are stacked along the c axis, with a long period c = 0.615 nm. (b) Idealized structure of the intercalated nanocomposite PEO/MoS_2(0.82), based on the WAXD and double-quantum NMR measurements.

inorganic host layers and interlayer cations[1,4], such as Li^+ or Na^+. Three particular models have been proposed: 1) preservation of the PEO helical conformation for the 0.8 nm compounds;[5] 2) double-polymer-layer planar zigzag disposition for the 0.8 nm compounds;[5] and 3) adsorption of the polymer layer on the inorganic host surfaces for both 0.4 nm or 0.8 nm compounds, resulting in single or double polymer layers, respectively.[1]

Various thermal studies[1-5,7-10] show no evidence of a crystalline melting transition or a glass transition in the nanocomposites, which indicates that the confinement of the polymer chain between the inorganic layers prohibits bulk-like crystallization. This also suggests that the polymer conformation within the galleries may be different than that of neat PEO. Adsorption isotherms show only one plateau,[5] indicating that the chains do not form double-layers in these nanocomposites.

In this chapter, the conformations of the OC-CO bonds of PEO intercalated in hectorite and in MoS_2 are investigated using DQ-NMR.[17] By matching the experimental 2D spectrum with simulated 2D patterns, the fraction of trans and gauche OC-CO torsion angles can be quantified.[18] The PEO used for these studies has 13% of the repeat units ^{13}C-^{13}C labeled, as described in Chapter 3.

5.2 Experimental

5.2.1 PEO Intercalation in Clays

The Na^+-hectorite (SHCa-1) and Na^+-montmorillonite (Swy-1), both from University of Missouri – Columbia, Source Clay Minerals Repository, were prepared for the intercalation process using procedures similar to those described elsewhere.[1,5] Na^+-Hectorite (HCT) was first treated with 0.5 N acetic acid in order to eliminate carbonate impurities. Afterwards, the clay was dissolved in deionized water and filtered several times.[5] Na^+-Montmorillonite (MMT), which was used as an important reference material, was dissolved in deionized water and filtered several times in order to remove noncolloidal impurities such as quartz and feldspar[1]. No ion exchange was performed. After this purification process, the Na^+-clays were dried in an oven at 65 °C, and then were heated to 80 °C under vacuum for several days. These dried Na^+-clays, sealed in capillary tubes, were analyzed by WAXD in order to determine the interlayer gap.

Nanocomposites were obtained by the stoichiometric addition of PEO and Na^+-clays in acetonitrile. Two reaction stoichiometries were used for the preparation of layered nanocomposites:[1] R = 0.1 and 0.4 (R = g PEO/g clay), in order to obtain uniform gallery expansions of 0.4 and 0.8 nm, respectively. These reactions involved 300 or 150 mg of clay and 30 or 60 mg of PEO dissolved in 20 mL of acetonitrile. The colloidal suspension was stirred for *ca.* 24 hours at room temperature, filtered, and then the nanocomposite was dried following the procedure described above. These Na^+-clay nanocomposites were immediately sealed in appropriate glass tubes for NMR and

WAXD and aluminum pans for DSC. For the stoichiometry of R = 0.4, excess PEO was eliminated by repeatedly washing with deionized water[5] and the DSC did not show a melting peak.

Like most naturally occurring silicates, montmorillonite contains some Fe^{3+} substitutionally situated in lattice Al^{3+} sites. The presence of this paramagnetic impurity induces strong line broadening in ^{13}C NMR.[19] For this reason, the intercalated PEO-montmorillonite nanocomposites could not be studied by ^{13}C NMR. However, given that montmorillonite is one of the most widely studied clay materials while hectorite is less commonly used, the scattering curves for montmorrillonite are included as references for those of the hectorite samples that were used for NMR spectroscopy due to their lower abundance of paramagnetic elements.[5]

5.2.2 PEO Intercalation in MoS_2

MoS_2 (Aldrich) was dried and then immediately analyzed by WAXD in order to determine the width of the gap between layers. The MoS_2 nanocomposites were obtained by reduction to $LiMoS_2$ and reaction with aqueous PEO.[2,6,20] To prepare the Li_xMoS_2 ($x \approx 1$) the host (0.5 g) was reduced with about 35% mole excess of butyllithium (1.67 mL, 2.5 M in hexane) in a solution of 100 mL of dry and O_2-free hexane.[21] This solution was stirred for about 1 day under nitrogen atmosphere. The solution was filtered and the $LiMoS_2$ was then immersed in deionized and O_2-free water (60 mL) containing a stoichiometric amount of PEO and stirred for *ca.* 30 hours.[2,6,21] Since there is no

evidence of intercalation producing 0.4 nm gallery expansion, only one reaction stoichiometry was used for the preparation of layered nanocomposites derived from MoS_2: R = 0.45. The solid product was separated by centrifugation at 12 000 rpm and washed several times with deionized and O_2-free water to ensure removal of LiOH and other soluble impurities. During the intercalation of PEO in MoS_2, all manipulations were performed under an N_2 atmosphere to exclude oxygen. The products were carefully dried under vacuum at a temperature of ca. 80 °C for several days. After that, the fine powdered samples were sealed in appropriate glass tubes for NMR and WAXD and aluminum pans for DSC.

Table 5.1 summarizes the characteristics of all samples prepared, including the abbreviation for each intercalate.

Table 5.1: Composition and interlayer distances of the samples studied.

Sample	R	Host c (nm)	Nanocomposite c (nm)	Δc (nm)	gap_0 (nm)*	gap_1 (nm)*
1) PEO/MMT(0.40)♦	0.10	0.97	1.37	0.40	0.35	0.75
2) PEO/MMT(0.80)	0.40	0.97	1.77	0.80	0.35	1.15
3) PEO/ HCT(0.45)	0.10	0.98	1.43	0.45	0.35	0.8
4) PEO/ HCT(0.70)	0.40	0.98	1.68	0.70	0.35	1.0
5) PEO/MoS_2(0.82)	0.45	0.61	1.43	0.82	0.02	0.85

♦ *The number between parenthesis is the parameter* **Δc** in nm.

* *Estimated interlayer gap before,* gap_0, *and after intercalation,* gap_1.

5.2.3 Wide-Angle X-Ray Diffraction

WAXD was performed using a Siemens D500 instrument with Ni-filtered Cu Kα radiation source in transmission mode.

5.2.4 Differential Scanning Calorimetry (DSC)

DSC measurements were performed with 10-mg samples loaded in Al pans on a DuPont Instruments DSC 2910. Samples were heated at 10 °C/min from -90 to +100 °C.

5.2.5 Static DQ-NMR

The static 2D DQ-NMR spectra were recorded on a Bruker MSL-300 spectrometer at a ^{13}C resonance frequency of 75.5 MHz in a 5-mm diameter coil of a static variable-temperature probe. The ^{13}C and ^{1}H 90° pulse lengths were *ca.* 3.5 μs. A cross-polarization time of 500 μs and a signal-acquisition time of 2.8 ms were used. For the PEO/HCT intercalated nanocomposites the recycle delay was 0.5 s (short T_1 due to the presence of paramagnetic impurities) and the spectra were obtained at 225 K, while for the PEO/MoS_2 it was 1 s and T = 220 K. These low temperatures were necessary to avoid motion of the PEO chains during the double-quantum excitation and reconversion delays. In the t_1 dimension, 30 slices with increments of 28 μs were acquired. Only one value of double-quantum excitation and reconversion delay was utilized, 2τ = 280 μs. The measuring time for each two-dimensional double-quantum spectrum was *ca.* 24 hours. To improve the signal-to-noise ratio of the spectra, two acquisitions of 24 hours were added.

The simulations of PEO/MoS_2 and PEO/HCT all used the principal values of σ_{11} = 93 ppm, σ_{22} = 84 ppm, and σ_{33} = 36 ppm. Based on the dipolar/CSA correlation experiment, the polar coordinates of the C-C bond in the chemical-shift principal-axis system (PAS) were α = -60° and β = 120°.

5.2.6 Sample Characterization

Elemental analysis for C, H and Li in the PEO/MoS_2(0.82) is given in Table 5.2. The ratios of these atoms are similar to those presented in a previous study.[2]

Table 5.2: Elemental analyses for C, H, and Li in PEO/MoS_2(0.82)

R	Li wt %	C wt %	H Wt %	H/C	Composition
0.45	0.30	14.18	2.29	1.92	$Li_{0.09}(PEO)_{1.28}MoS_2$

WAXD data of the nanocomposites show an increase in the separation of the original inorganic galleries by *ca.* 0.4 nm or 0.8 nm, indicating that the PEO and the hosts formed nanocomposites;[1] see parts (a) and (b) of Figures 5.3 and Figure 5.4 (a). The long period of the inorganic layers, c, is obtained from the (001) peak. Additional information about structure and intra- and interlayer atomic distances for pure and intercalated smectite clays and transition metal dichalcogenides were obtained from references.[22-25] The long period of the inorganic layers, c, obtained from the X-ray experiments for each sample studied, as well as the estimated free interlayer gap width before and after intercalation, gap_0 and gap_1, respectively, were summarized previously in Table 5.1.

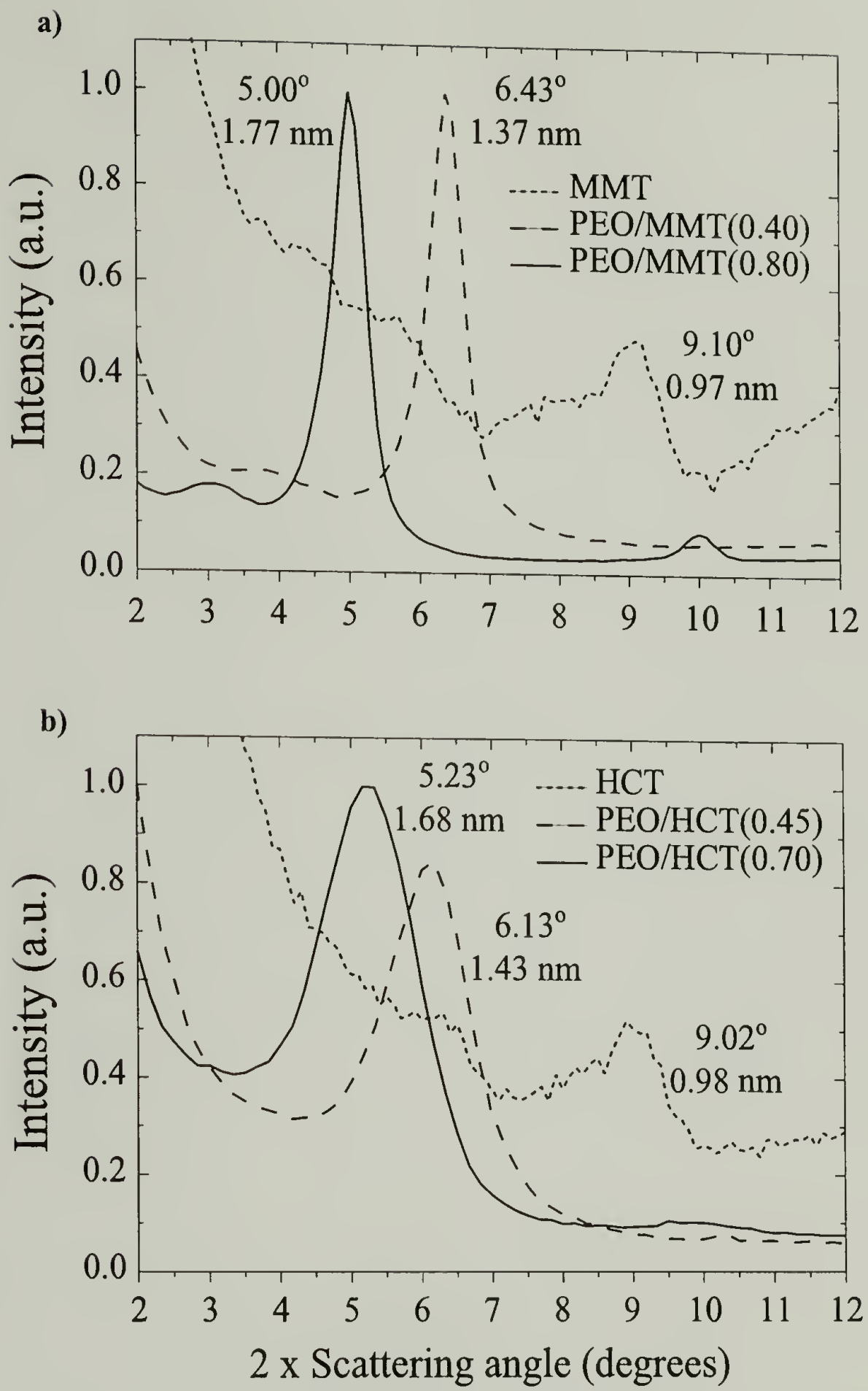

Figure 5.3: X-ray diffractograms of (a) HCT, PEO/HCT(0.45), and PEO/HCT(0.70) as studied by NMR, and, for reference, (b) MMT, PEO/MMT(0.40), and PEO/MMT(0.80). These X-ray patterns show an increase in the separation of the original inorganic galleries by ca. 0.40 nm or 0.80 nm, indicating that the guest and the host have formed a nanocomposite.

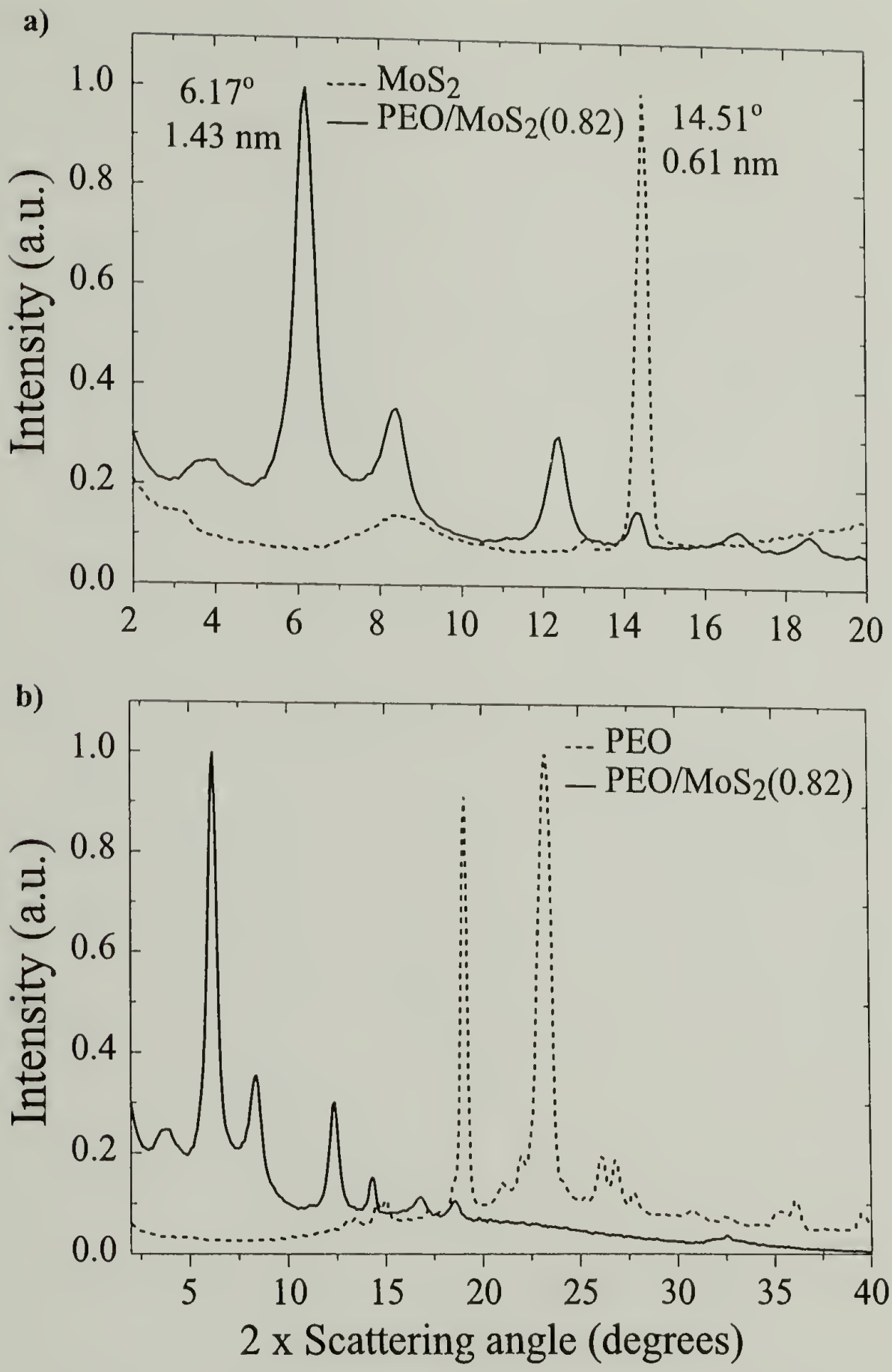

Figure 5.4: X-ray diffractograms of (a) MoS_2 and PEO/MoS_2(0.82), and, for comparison, (b) PEO/MoS_2(0.82) and neat PEO. The X-ray patterns in (a) show an increase in the separation of the original inorganic gallery by ca. 0.80 nm, indicating that the guest and the host formed a nanocomposite. In (b), the suppression of the PEO crystalline phase is observed for PEO/MoS_2(0.82).

WAXD also confirms the suppression of the crystalline phase of PEO. In Figure 5.4 (b) it is seen that the peaks characteristic of crystalline PEO are absent in the PEO/MoS_2(0.82) data.

Figure 5.5 shows the DSC curves recorded in the range of -90 to 100 °C for neat PEO and intercalated nanocomposites. Figure 5.5 (a) shows the characteristic behavior of neat PEO, where the large endotherm at 67 °C corresponds to the melting of the crystalline regions. The absence of a melting transition for all nanocomposites, Figure 5.5 (b) through (d), confirms that the confinement of polymer chains between the inorganic layers prevents crystallization[1-5,7-10] and indicates that all the polymer is intercalated.

5.3 Results and Discussion

5.3.1 Double-Quantum NMR Spectra

Figures 5.6 and 5.7 show the double-quantum 2D NMR spectra of the ^{13}C-^{13}C labeled PEO for the samples PEO/MoS_2(0.82), PEO/HCT(0.45) and PEO/HCT(0.70), with the corresponding simulations. The spectra show predominantly the pattern of the gauche conformation. Nevertheless, the extended features of the trans spectrum are also observed faintly at the upper region of the spectra.

The 2D double-quantum spectra for both clay nanocomposites are similar. The trans:gauche ratios are 8:92(±5), with average gauche and trans angles equal to 70°±15° and ~180°, respectively. Due to the low trans content, a reliable estimate of the uncertainty of the trans torsion angle is difficult. For the PEO/MoS_2(0.82) compound, the trans:gauche ratio was found to be 12:88(±5), with average gauche and trans angles

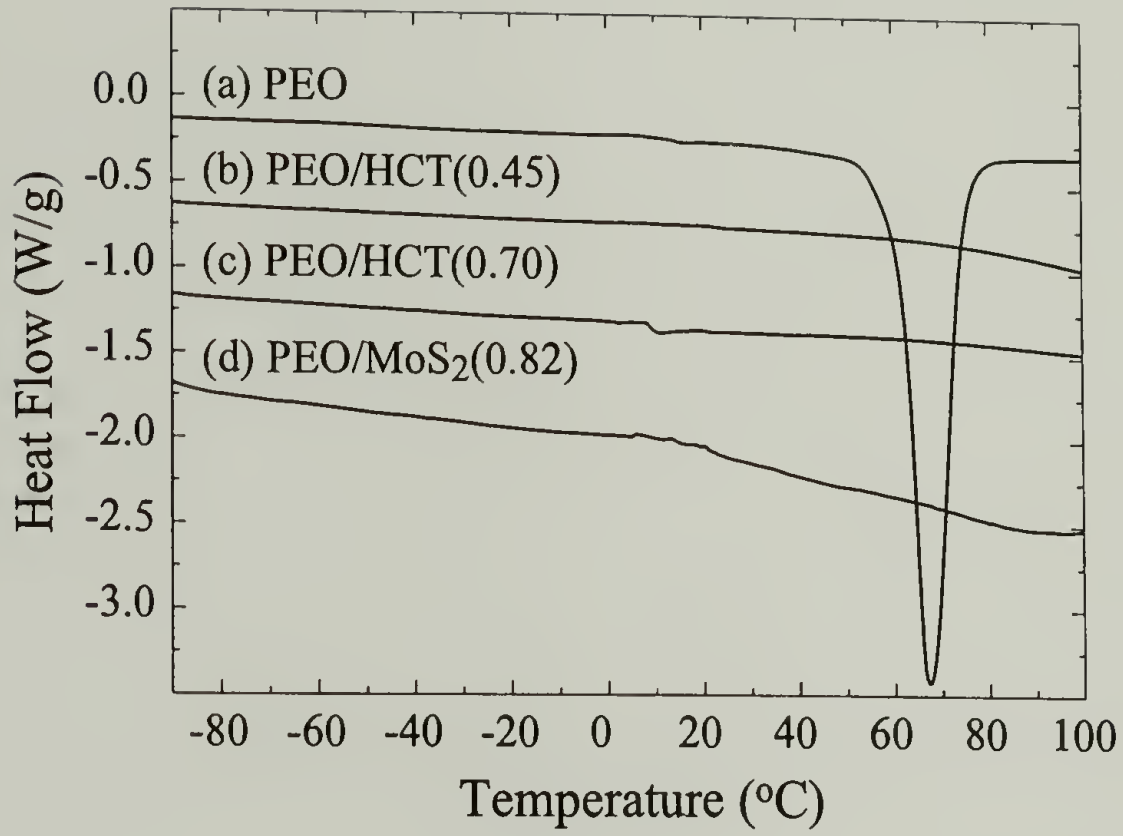

Figure 5.5: Differential scanning calorimetry traces for (a) neat PEO, (b) PEO/HCT(0.45), (c) PEO/HCT(0.70), and (d) PEO/MoS_2(0.82). Samples were heated at rate of 10 °C/min.

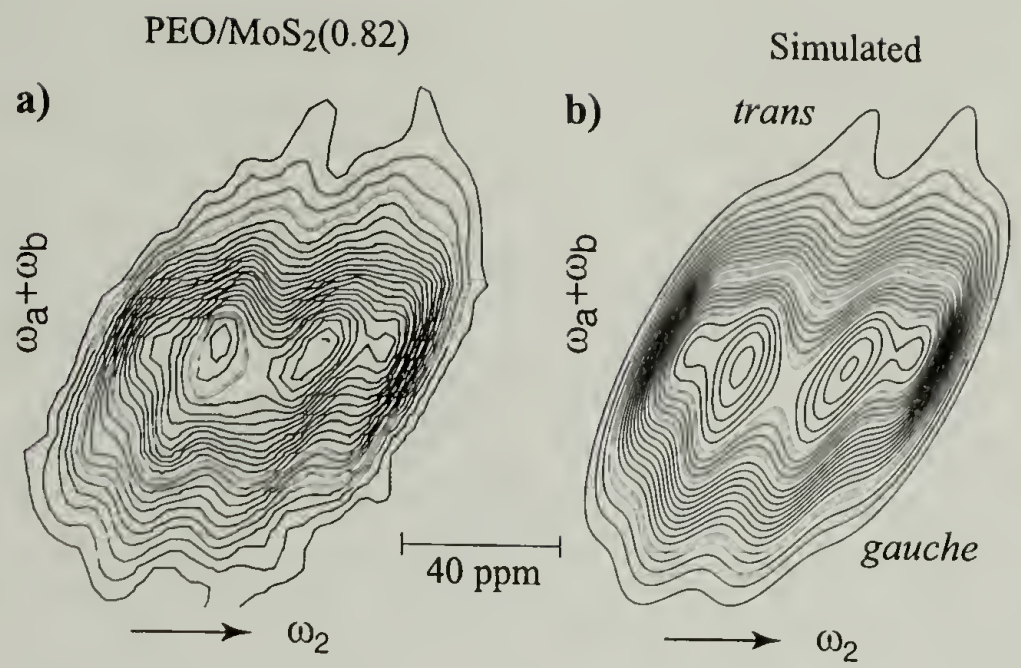

Figure 5.6: Experimental 2D double-quantum NMR spectrum of (a) PEO/MoS_2(0.82) and (b) the corresponding simulation using a trans content of 12%. The trans and gauche angles were distributed within ±10° around 180° and 70°, respectively. Contour lines were plotted between 5 and 98% of the maximum.

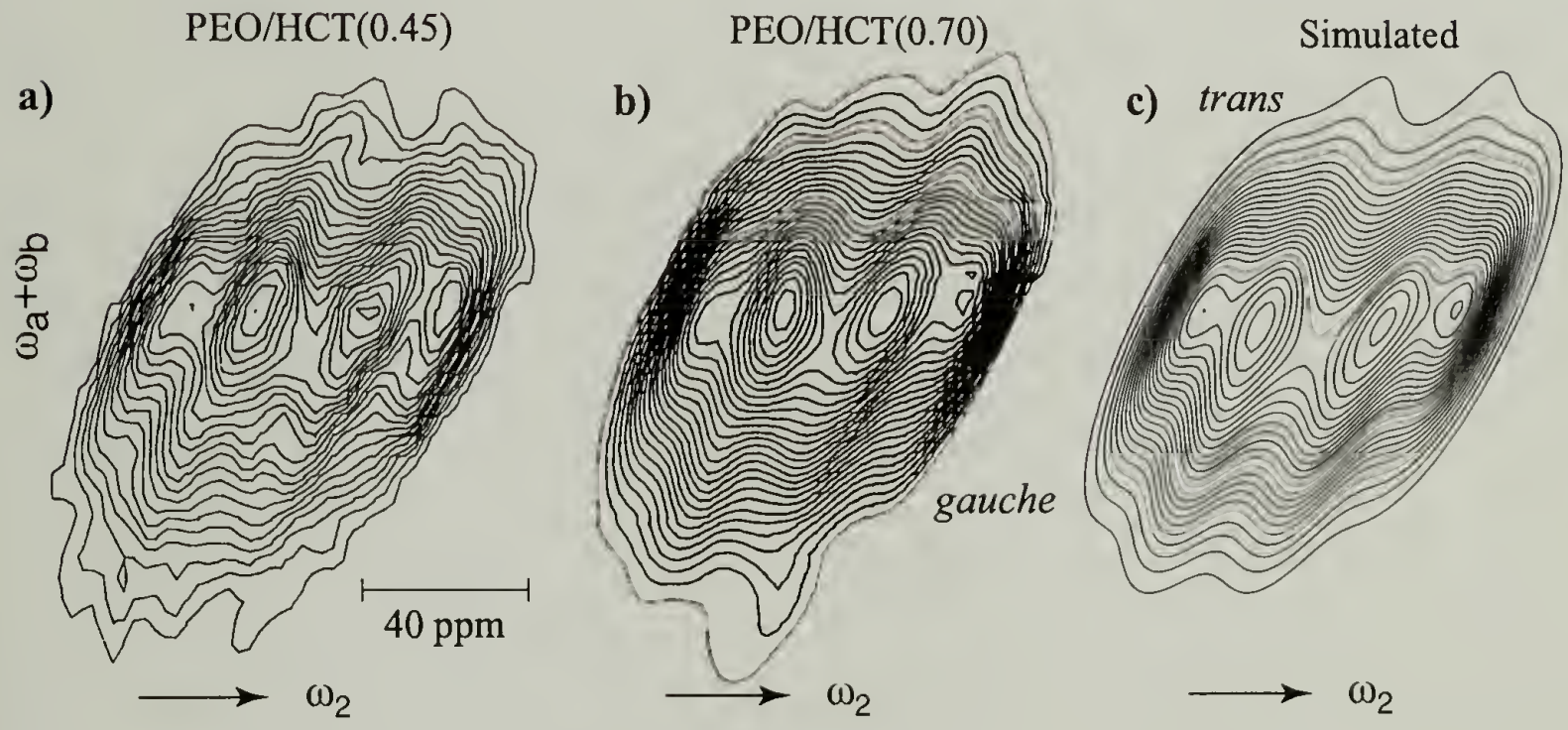

Figure 5.7: 2D double-quantum NMR spectra of (a) PEO/HCT(0.45), (b) PEO/HCT(0.70) with (c) corresponding simulation using a trans content of 8%. The trans and gauche angles were distributed within ±10° around 180° and 70°, respectively. The uncertainty in the average gauche torsion angle is ±15°.

equal to 70°±15° and ~180°. In the simulations, distributions with widths of 10° around the average trans and gauche torsion angles of 180° and 70° were used.

The experimental spectra show significant broadening, in particular along the line of slope two, which shows that the broadening for both coupled spins is correlated. It is probably due to paramagnetic impurities or to susceptibility effects. The chemical-shift dispersion due to conformational and packing effects is a less likely reason. These effects would not cause such large linewidths and the broadenings for the two bonded sites would be expected to be mostly uncorrelated. To avoid distortion of the lineshape by segmental dynamics, the samples were cooled to 220-225 K. Cooling to lower temperatures did not lead to significant lineshape changes.

The high gauche content clearly excludes a planar all-trans conformation. The low trans:gauche ratio also indicates that a regular planar structure with 33% trans as found in the complex of PEO with *p*-nitrophenol is not predominant. The conformational statistics and upper limits on the width of the gauche-conformation peak in the torsion-angle distribution will be useful as benchmarks for simulations of intercalated PEO chains.

5.3.2 Comparison with Previous Spectroscopic Results

Aranda and Ruiz-Hitzky[5] had shown that the ^{13}C CP/MAS NMR spectrum of PEO/Na^+-hectorite with gallery expansion of 0.8 nm had only one peak at 69.6 ppm which was assigned to the gauche conformation of methylene groups, suggesting that the helical conformation is maintained after intercalation. However, given the range of the

chemical shift resonances in neat PEO, the relation between the chemical shift and the C-C torsion is tentative at best[26]. Actually, in PEO the torsion angle of the C-C bond cannot lead to a γ-gauche shielding; only C-O torsion angles can lead to this effect. In addition, the MAS lines of PEO in hectorite and MoS_2 nanocomposites are 15 ppm broad, which makes it impossible to observe any fine structure indicative of specific conformations or packing.

Aranda and Ruiz-Hitzky[5] also had analyzed the interaction between ether oxygens and interlayer cations using ^{23}Na NMR spectroscopy for PEO/Na^+-hectorite with gallery expansion of 0.8 nm. The comparison of the ^{23}Na spectra of dry, hydrated, and PEO intercalated hectorites had shown an 11 ppm downfield shift of the ^{23}Na peak after intercalation of hectorite with PEO, suggesting that the Na^+ ions interact strongly with the ether oxygens. A dibenzo-24-crown-8/hectorite intercalate had a similar ^{23}Na spectrum (d = -10.3 ppm) to PEO/hectorite intercalates. A high OC-CO gauche content as found in this study is consistent with PEO segments in crown-ether like conformations. On the other hand, ^7Li NMR linewidths observed by Yang and Zax[27] suggest that Li^+ ions are restricted to the silicate surface.

^7Li and ^2H solid-state NMR had been used by Wong *et al.*[19,28] to probe the dynamics of the Li^+ ion and the polymer in deuterated PEO/Li^+-fluorohectorite intercalates. The temperature dependences of the quadrupolar NMR powder patterns of both nuclei indicate that PEO, even at 220 K, possesses some small-amplitude dynamics. At higher temperatures, even above the bulk melting point of PEO (65 °C), the spectra

exhibit residual powder patterns in addition to an intense single line, indicating restricted polymer motion between silicate layers. In addition, they indicate that there is a competition of the oxygen ethers of PEO with the surface oxygens of the silicate layers for interaction with the Li^+ cation. IR studies also indicate interaction between polymer and interlayer cations.[5]

Papke *et al.*[29] and Yokoyama *et al.*[30] had used vibrational-spectroscopy to study PEO in metal salt complexes to elucidate chain conformations. The analysis of CH_2 deformation bands of O-CH_2-CH_2-O groups reveals trans or gauche conformations, and consequently it was possible to ascribe a helical structure for alkaline metal salt complexes ($TTGTT\bar{G}$),[29] or alternatively, a nearly planar conformation in certain PEO/$HgCl_2$ salt complexes ($TGGT\bar{G}\,\bar{G}$).[30] Aranda and Ruiz-Hitzky[5] had used vibrational-spectroscopy studies to elucidate PEO chain conformations in intercalated clays. In PEO intercalates with gallery expansion of 0.8 nm, the spectra suggest a gauche conformation, which was taken to show that the matrix structure of PEO is preserved after intercalation. While the NMR results agree with a dominance of gauche, the observed trans content shows that very long helical sections are not possible.

5.3.3 Possible Chain Conformations

The rotational isomeric state (RIS) description of amorphous PEO[31,32] can be used to understand the chain conformations in the intercalated materials. The RIS model for amorphous PEO suggests that approximately 25% of the CO-CC bonds are gauche in

amorphous PEO and 20% of the OC-CO bonds are trans. The 10±5% trans population of the OC-CO bonds observed for intercalated PEO is less than the predicted value from the RIS description of amorphous PEO. If this difference is correct and the values of the RIS description are accurate, it may be due to either interaction with interlayer ions and the interface, or steric requirements. Regarding the latter, it is interesting to note that RIS simulations of PEO chains confined to channels of 0.8-nm diameter[33] predict a trans fraction of 50%, even though the crystalline 7_2 helix, with 100% gauche OC-CO bonds, would fit the channels.

To accommodate the large fraction of OC-CO bonds in the gauche conformation yet allowing the chain to remain mostly planar, some sequences of conformations will be restricted. The gauche OC-CO bonds cannot be randomly gauche$^+$ and gauche$^-$, but rather will be strongly correlated with nearby gauche bonds. If all of the gauche OC-CO bonds in a long chain section have the same sign, i.e. either all are gauche$^+$ or all gauche$^-$, the chain twists into a helix. The helix would fit into the intercalation gap, but a trans conformation at its end would almost invariably be in steric conflict with the inorganic layers.

If the signs of the OC-CO gauche torsion angles alternate, the chain loops into a structure similar to small crown ethers with the ether oxygens directed inwards. This would be consistent with strong polymer-Na^+ interactions deduced from ^{23}Na NMR.[5] However, after approximately five monomer units with alternating TTG^+ and TTG^- conformations, due to steric interactions with other portions of the chain, either a OC-CO bond would be forced into a trans conformation or a CO-CC bond would be forced into a

gauche conformation. The observed trans fraction of OC-CO bonds for the studied systems is only 10%, lower than about 25% that would be required due to these steric interactions. Therefore, a significant percentage of the CO-CC bonds are expected to be in the gauche conformation. This significant percentage would not conflict with the values predicted by the RIS description.

5.4 Summary

The conformations of the OC-CO bond of PEO intercalated in hectorite clay and in MoS_2 have been studied by double-quantum solid-state NMR. The polymer chains are confined into intercalation gaps of well-defined thicknesses of only ~0.8 nm, ~0.85 nm, and ~1.0 nm, as determined by WAXD. The OC-CO bonds are found to be 90±5% gauche, which provides valuable constraints on the possible chain conformation in the intercalation gaps.

5.5 References

(1) Wu, J.; Lerner, M. M. *Chem. Mater.* **1993**, *5*, 835.

(2) Lemmon, J. P.; Lerner, M. M. *Chem. Mater.* **1994**, *6*, 207-210.

(3) Lemmon, J. P.; Lerner, M. M. *Solid State Commun.* **1995**, *94*, 533-537.

(4) Oriakhi, C. O.; Nafshun, R. L.; Lerner, M. M. *Mater. Res. Bull.* **1996**, *31*, 1513-1520.

(5) Aranda, P.; Ruiz-Hitzky, E. *Chem. Mater.* **1992**, *4*, 1395-1403.

(6) Ruiz-Hitzky, E.; Jimemez, R.; Casal, B.; Manriquez, V.; Ana, A. S.; Gonzalez, G. *Adv. Mater.* **1993**, *5*, 738.

(7) Aranda, P.; Ruiz-Hitzky, E. *Acta Polym.* **1994**, *45*, 59-67.

(8) Vaia, R. A.; Vasudevan, S.; Krawiec, W.; Scanlon, L. G.; Gianellis, E. P. *Adv. Mater.* **1995**, *7*, 154.

(9) Giannelis, E. *Adv. Mater.* **1996**, *8*, 29.

(10) Vaia, R. A.; Sauer, B. B.; Tse, O. K.; Giannelis, E. P. *J. Polym. Sci. Part B: Polym. Phys.* **1997**, *35*, 59-67.

(11) Vaia, R. A.; Ishii, H.; Giannelis, E. P. *Chem. Mater.* **1993**, *5*, 1694-1696.

(12) Vaia, R. A.; Jandt, K. D.; Kramer, E. J.; Giannelis, E. P. *Macromolecules* **1995**, *28*, 8080-8085.

(13) Krishnamoorti, R.; Vaia, R. A.; Giannelis, E. P. *Chem. Mater.* **1996**, *8*, 1728-1734.

(14) Vaia, R. A.; Giannelis, E. P. *Macromolecules* **1997**, *30*, 7990-7998.

(15) Vaia, R. A.; Giannelis, E. *Macromolecules* **1997**, *30*, 8000-8009.

(16) Ogawa, M.; Kuroda, K. *Chem. Rev.* **1995**, *95*, 399-438.

(17) Schmidt-Rohr, K. *Macromolecules* **1996**, *29*, 3975-3981.

(18) Harris, D. J.; Bonagamba, T. J.; Schmidt-Rohr, K. *Macromolecules* **1999**, *32*, 6718.

(19) Wong, S.; Zax, D. B. *Electrochimica Acta* **1997**, *42*, 3513-3518.

(20) Divigalpitiya, W. M. R.; Frindt, R. F.; Morrison, S. R. *Science* **1989**, *246*, 369-371.

(21) Dines, M. B. *Mat. Res. Bull.* **1975**, *10*, 287-292.

(22) Dickinson, R. G.; Pauling, L. *J. Am. Chem. Soc.* **1923**, *45*, 1466-1471.

(23) Grim, R. E. *Clay Mineralogy*; 1st ed. ed.; McGraw-Hill Book Company: New York, 1953.

(24) Whittingham, M. S. *Prog. Solid. State Chem.* **1978**, *12*, 41-99.

(25) Pinnavaia, T. J. *Science* **1983**, *220*, 365-371.

(26) Schilling, F. C.; Tonelli, A. E.; Cholli, A. L. *J. Polym. Sci., Part B: Polym. Phys.* **1992**, *30*, 91-96.

(27) Yang, D.-K.; Zax, D. B. *J. Chem. Phys.* **1999**, *110*, 5325-5336.

(28) Wong, S.; Vaia, R. A.; Giannelis, E. P.; Zax, D. B. *Solid State Ionics* **1996**, *86-88*, 547-557.

(29) Papke, B. L.; Ratner, M. A.; Shriver, D. F. *J. Phys. Chem. Solids* **1981**, *42*, 493-500.

(30) Yokoyama, M.; Ishihara, H.; Iwamoto, R.; Tadokoro, H. *Macromolecules* **1969**, *2*, 184-192.

(31) Mark, J. E.; Flory, P. J. *J. Am. Chem. Soc.* **1965**, *87*, 1415-1422.

(32) Mark, J. E.; Flory, P. J. *J. Am. Chem. Soc.* **1966**, *88*, 3702-3707.

(33) Tonelli, A. E. *Macromolecules* **1990**, *23*, 3134-3137.

CHAPTER 6

CHARACTERIZATION OF PEO-PGNA BLENDS

6.1 Introduction

Recently, complexes between sodium poly(α,L-glutamate) (PGNA) and PEO were reported.[1] The crystal structure, based only on differential scanning calorimetry (DSC), circular dichroism (CD), and X-ray diffraction (XRD) peak intensities was reported. The PEO crystallite blocks were speculated to be anchored to the PGNA helical core via sodium ion–dipole interactions. The conformation of the PEO was speculated to change due to the complexation, and some of the OC-CO bonds were expected to have trans torsion angles. However, the experimental data of Pemawansa *et al.*[1] do not support the conclusions reported in the article.

In this chapter, some of the previously described experiments, including DSC, XRD, and ^{23}Na NMR, are repeated. Also, solid-state NMR is used to characterize the blends. Crystallinity of the PEO phase is determined by the ^{13}C cross-polarization/magic-angle spinning (CP-MAS) spectrum. The OC-CO conformation of PEO is determined using DQ-NMR..[2,3] Finally, spin-diffusion experiments are employed to determine the distance between the PGNA and PEO chains.

6.2 Experimental

6.2.1 Preparation of Blends

Blends were prepared by separately dissolving stoichiometric amounts of PEO and PGNA in 4:1 methanol:water, and then combining the two solutions. After stirring for 24 hours, the solvent was evaporated. The resulting film was dried under vacuum for 48 hours. Samples containing ^{13}C-^{13}C labeled PEO were prepared in an analogous fashion.

6.2.2 Wide-Angle X-Ray Diffraction

WAXD was performed using a Siemens D500 instrument with Ni-filtered Cu Kα radiation source in transmission mode.

6.2.3 Differential Scanning Calorimetry (DSC)

DSC measurements were performed with 10-mg samples loaded in Al pans on a DuPont Instruments DSC 2910. Samples were heated at 10 °C/min from 25 to 130 °C.

6.2.4 ^{13}C CP-MAS Spectrum

The CP-MAS spectrum of both a 5:1 PEO:PGNA blend and pure PEO were measured under similar conditions on a Bruker DSX-300 spectrometer. The samples were packed in 7-mm ZrO_2 rotors and spun at 6 kHz. The 90° pulse lengths were 4.2 µs for ^{13}C and 4.6 µs for ^{1}H. The ^{1}H decoupling field strength was only 80 kHz, weaker

than the decoupling power used in the experiment reported in Chapter 3. The temperature was 203 K. The recycle delay was 5 s and each spectrum is the sum of 128 scans.

6.2.5 Static DQ-NMR

The static 2D DQ-NMR spectrum was recorded on a Bruker MSL-300 spectrometer at a ^{13}C resonance frequency of 75.5 MHz in a 4.5-mm diameter coil of a static variable-temperature probe. The conditions of the experiment were exactly the same as for crystalline PEO, described in Chapter 3.

6.2.6 Spin Diffusion Experiments

The spin diffusion spectra were measured on the Bruker MSL-300 spectrometer in a 7-mm ZrO_2 rotor using the Goldman-Shen pulse sequence[4] with a 40 μs T_2 filter to initially destroy the magnetization in the rigid domains. The spinning rate was 5 kHz and the 90° pulse lengths were 4 μs for ^{13}C and 4.4 μs for ^{1}H. The recycle delay was 5 s and each spectrum is the sum of 2048 scans. Three values of spin diffusion mixing times were used: 0.5, 10, and 100 ms.

6.2.7 ^{23}Na NMR Measurements

A 5 wt. % solution of 5:1 PEO:PGNA was dissolved in benzene and injected into a 5-mm tube. The ^{23}Na spectrum was recorded in a 5-mm coil in the DSX-300

spectrometer. The typical number of scans was 128. The background signal from the glass tube was subtracted from the experimental spectra.

6.2.8 ^{13}C Solution NMR Measurements

The ^{13}C spectra were obtained at ambient temperature in a Bruker DPX-300 at a frequency of 75.5 MHz. One wt. % of 10K PEO was dissolved in a 1:1 mixture of D_2O and methanol. An aliquot of a D_2O solution containing 1 wt. % PEO and 10 wt. % PGNA were injected into the 5 mm NMR tube before each measurement. The recycle delay used for each experiment was 6 seconds, and the number of scans was typically 1024. ^{1}H NMR was used to quantify the ratio of PEO:PGNA for each concentration.

6.3 Results and Discussion

Many techniques used in the previous work[1] to determine the conformation of the PEO chains do not suggest novel chain conformations. Specifically, the DSC, WAXD, DQ-NMR, ^{23}Na, ^{13}C, and spin diffusion experiments all suggest that the blend phase separates instead of forming complexes.

6.3.1 DSC and WAXD Results

DSC showed that the melting transition of 5:1 PEO 10K – PGNA 1.5-3K is broad but has the same average melting point as neat PEO. This thermogram is consistent with the previously published DSC thermogram[1] which showed almost identical melting peaks

for the blend and neat PEO. The identical melting temperature suggests that crystalline PEO is present in the blend.

The presence of crystalline PEO is also confirmed by XRD. The peaks in the blend have identical *d* spacings as PEO. The high intensity of these peaks shows that the polymer is highly crystalline. The previously published results had observed *d* spacings of 6.58 and 6.63 Å, not significantly different from the PEO peak at 6.58 Å. Neither our measurements nor the previously published results indicate a crystalline phase with a structure significantly different from PEO. Only the relative intensities of the peaks are slightly different from the ratio found in PEO, but this does not indicate a different structure.

6.3.2 Solution NMR Results

The dynamics of the sodium counter ion was examined with ^{23}Na NMR linewidth measurements. At room temperature, the linewidths of the ^{23}Na counter ion of the PGNA are identically 1.4 kHz in neat PGNA and in a 1:5 PGNA 3K–PEO 10K blend. The identically broad linewidth suggests that the Na^+ ions are bound to the PGNA chains and not solvated by the mobile PEO chains.

The ^{23}Na linewidth of 1:5 PGNA 3K–PEO 10K dissolved in benzene was also determined. While the previous article reported no detectable signal,[1] a strong signal was observed with a 0.9 kHz linewidth. This broad linewidth indicates that the nonpolar benzene does not lead to large increases in PGNA mobility. Pemawansa *et al.*[1] suggested

that the T_1 relaxation time of the ^{23}Na ions in benzene must be extremely long; however, a value of less than 1 s was experimentally measured in this work.

Evidence for complexation was not seen in the ^{13}C solution NMR spectra, summarized by the graph in Figure 6.1. Strong interaction between PEO and a surfactant, sodium dodecyl sulfate, results in large changes of chemical shifts in both molecules.[5] For PEO, the shift was reported to change by more than 0.2 ppm with the addition of a similar concentration of SDS.

6.3.3 DQ-NMR Results

The DQ-NMR spectrum of PEO/PGNA complex is almost identical to the spectrum of neat PEO, Figure 6.2. Both spectra were obtained at 235 K. There is no evidence of any trans OC-CO bonds which would occur as two long diagonal ridges with slopes of two. The slightly broader features in the PEO-PGNA blend are likely due to the lower ^1H decoupling power level during acquisition.

6.3.4 ^{13}C CP-MAS Spectrum

Figure 6.3 shows the comparison between neat PEO and the corresponding region in a 5:1 PEO:PGNA blend. The spectra are identical, proving that a majority of PEO is in an undistorted crystalline environment. The four observed maxima, as discussed in Chapter 3, are due to packing effects in the 7_2 helical conformation. Spectra of PEO-salt blends and other complexes do not exhibit such a pattern.

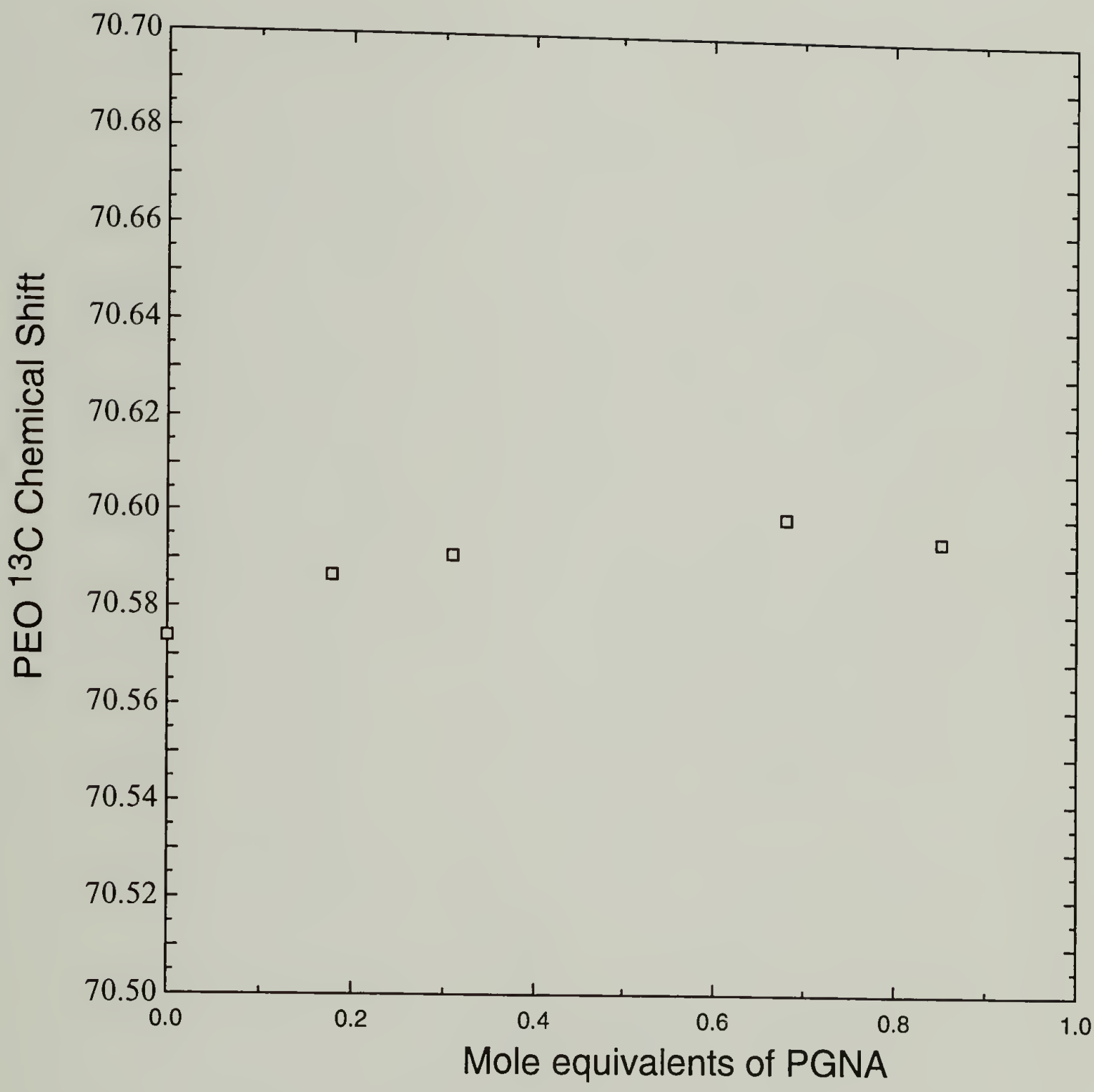

Figure 6.1: Effect of added PGNA on the chemical shift of the ^{13}C line of PEO in 1:1 D_2O:methanol.The PEO concentration was maintained at 1 wt %. The expected change of chemical shift during complexation is ~0.2 ppm. This data suggests that there was no strong complexation. The chemical shift of the methanol was used as the reference.

Figure 6.2: Comparison between DQ-NMR spectra at 235 K of (a) PGNA-PEO blend and (b) neat PEO. The lower decoupling power in the PGNA-PEO experiment leads to greater broadening in the lower part of the spectrum. The simulation, shown in (c), is consistent with both experimental spectra. No evidence of trans OC-CO torsion angles is observed.

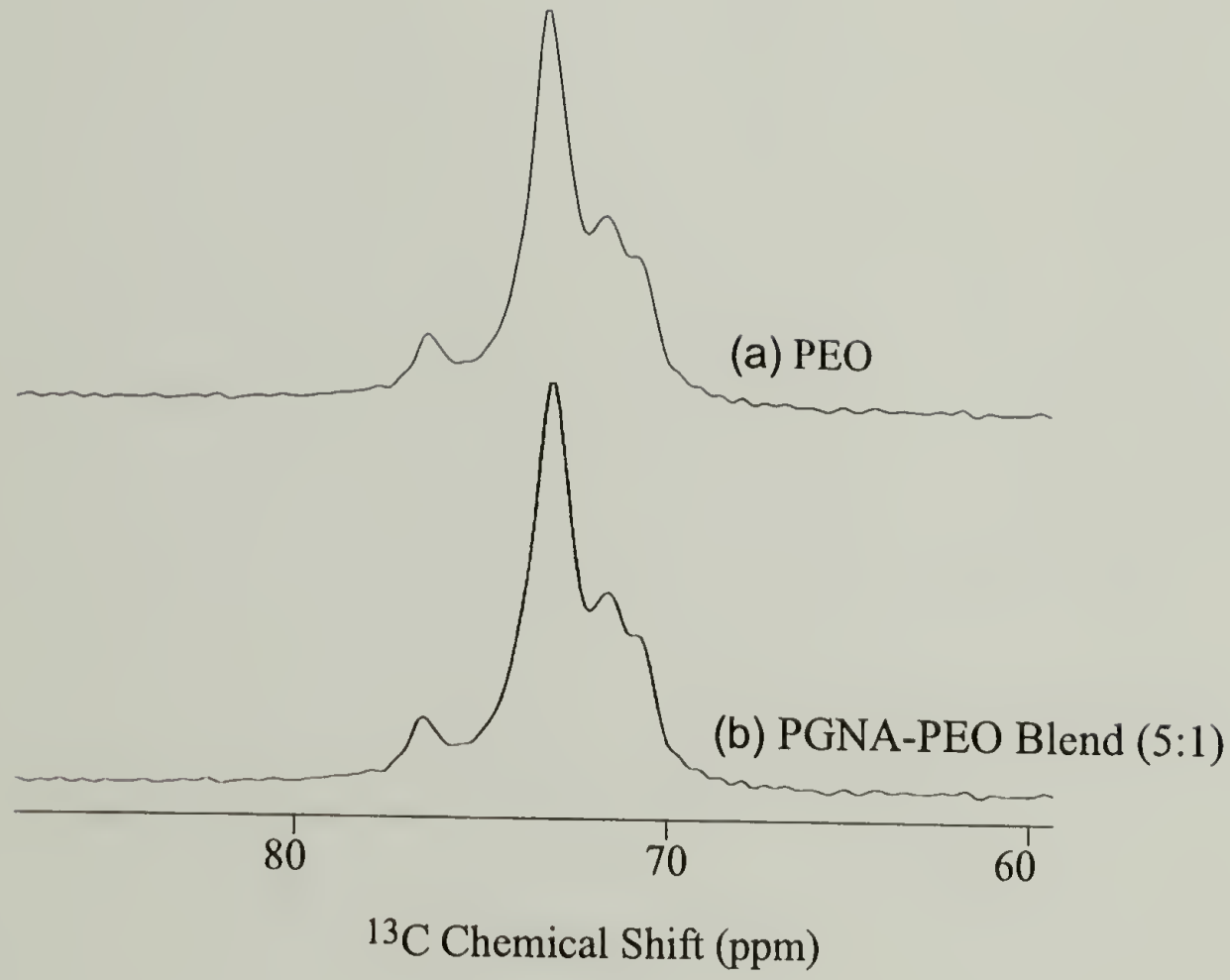

Figure 6.3: ^{13}C spectra of (a) PEO and (b) PGNA-PEO at 203 K and 6 kHz spinning rate. The spectra are broader than the results presented in Chapter 3 due to lower decoupling power. The multiple peaks are due to packing effects in the crystalline 7_2 PEO helix.

6.3.5 Spin Diffusion

The Goldman-Shen experiment initially destroyed the magnetization in the crystalline PEO and rigid PGNA phases, resulting in signal only from the amorphous PEO region. The magnetization quickly transfers from the amorphous PEO to the PGNA domain. The magnetization had equilibrated after 10 ms of spin diffusion time. This shows that the amorphous PEO regions must be less than 3 nm from the PGNA.

6.4 Summary

The results of the WAXD and DSC data for the PEO:PGNA blends are similar to the information presented by Pemawansa *et al.*[1] However, the interpretation of the results was now shown to be incorrect. The similarity between the results for PEO:PGNA blends and neat PEO clearly shows that the PEO crystallites are undisturbed and there is no significant crystalline complex. The DQ-NMR, ^{23}Na, and ^{13}C CP-MAS spectra all point to this conclusion. Furthermore, there was no evidence of strong complexation in the ^{13}C solution NMR spectra.

6.5 References

(1) Pemawansa, K. P.; Thakur, A.; Karikari, E. K.; Khan, I. M. *Macromolecules* **1999**, *32*, 1910-1917.

(2) Schmidt-Rohr, K. *Macromolecules* **1996**, *29*, 3975-3981.

(3) Harris, D. J.; Bonagamba, T. J.; Schmidt-Rohr, K. *Macromolecules* **1999**, *32*, 6718.

(4) Goldman, M.; Shen, L. *Phys. Rev.* **1966**, *144*, 321-331.

(5) Cabane, B. *J. Phys. Chem.* **1977**, *81*, 1639-1645.

CHAPTER 7

EFFECTS OF COMPOSITION ON BLOCK COPOLYMER ELECTROLYTE DYNAMICS

7.1 Introduction

Recent trends in energy technology have driven considerable interest in solid polymer electrolytes. The electrolytic properties of lithium salt-doped poly(ethylene oxide) make this polymer and derivatives favored candidates for polymer electrolytes.[1,2] Some of the primary applications for polymer electrolyte technology include high energy density lithium batteries and electrochromic devices.[3] To improve mechanical properties while retaining excellent ionic conductivity, block copolymer electrolytes have been investigated.[2,4-7] The microphase separation in those block copolymer electrolytes confers solid-like mechanical properties to the material at macroscopic scales even when both polymer blocks reside above their respective glass-transition temperatures, T_g. A low-T_g non-conductive phase has been shown to enhance the conductivity of block copolymer electrolytes.[7]

To confirm and better understand this effect of T_g of the nonconductive phase on the polymer electrolyte, we have performed solid-state nuclear magnetic resonance (NMR) linewidth and relaxation studies. The ^1H $T_{1\rho}$ rotating-frame relaxation times, and both ^1H and ^7Li linewidths were determined for several block copolymer electrolytes with different non-conductive blocks. Also differences in dynamics along the side chain in the

comb-shaped conductive block was investigated by wideline separation (WISE) experiments with a spin-diffusion mixing time.[8,9] The results of these NMR experiments are compared to the previously reported a.c. impedance spectroscopy and DSC measurements.[7]

7.2 Experimental

7.2.1 Sample Preparation

Polymers and block copolymers from poly(oligo(oxyethylene) methacrylate) macromonomer (M ~ 475 g/mol) (Polysciences), POEM, lauryl methacrylate (Aldrich), PLMA, *n*-butyl methacrylate (Aldrich), P*n*BMA, and methyl methacrylate (Aldrich), PMMA were anionically prepared in tetrahydrofuran (THF) using diphenylmethyl potassium as initiator. The syntheses and characterization of the resulting copolymers have been described previously.[7] The molecular weight characteristics, compositions and glass-transition temperatures of the polymer electrolyte materials prepared are listed in Table 7.1.

Table 7.1: Chemical structure of polymers used to prepare ionically conductive copolymers.

Polymer	Composition (v:v)	Molecular weight	Polydispersity	T_g (non-conductive block)
POEM	------	100,000 (g/mol)	1.3	
POEM-b-PLMA	53:47	64,700 (g/mol)	1.1	-35±3°C
POEM-b-P*n*BMA	50:50	77,200 (g/mol)	1.2	40±3°C
POEM-b-PMMA	51:49	52,400 (g/mol)	1.1	100±3°C

To prepare the doped samples, the block copolymer and $LiCF_3SO_3$ (lithium triflate) were first dried in a vacuum oven at 70°C for several days. The materials were then transferred into an inert atmosphere, dissolved in anhydrous THF, and solution cast into a glass dish. The relative amounts of polymer and salt were determined by the desired stoichiometric ratio of ethylene oxide units [EO] to Li^+, in this case 8:1.

7.2.2 NMR Experiments

^1H spin diffusion[10-13] was used to determine the domain size of the POEM phase in the Li^+ doped POEM-*b*-P*n*BMA and POEM-*b*-PMMA copolymers. The ^1H T_2^{-1} value was determined for the POEM phase by measuring the echo time dependence of the ^1H signal refocused by a π pulse. The effective diffusion rate was calculated based on the previously reported polymer systems with an equivalent T_2^{-1} relaxation rate.[10]

^1H linewidth and rotating-frame relaxation times, $T_{1\rho}$, and ^7Li linewidths were measured using a Bruker DSX-300 spectrometer operating at ^1H and ^7Li frequencies of 300.13 MHz and 116 MHz, respectively. The ^1H linewidth and $T_{1\rho}$ values were measured on undoped copolymers except POEM-*b*-PMMA, which does not separate into 2 domains without addition of $LiCF_3SO_3$. The ^1H experiments were performed in a 7-mm variable-temperature magic-angle-spinning (MAS) probe at spinning rate of 1 kHz. The ^7Li linewidths were determined in a 5-mm diameter coil of a static variable-temperature probe. Typical 90° pulse lengths were 4.0 μs for the ^1H

experiments and 3.0 μs for the ^{7}Li experiments. The spin lock field for the $T_{1\rho}$ experiment was 62 kHz.

Reproducible temperature determination is paramount for measuring the small differences between the copolymers. The experiments were conducted with a constant flow of N_2 gas through the liquid nitrogen-cooled heat-exchanger, and the liquid-nitrogen dewar was maintained fully filled. The temperature was calibrated with methanol twice, and the deviation between the two calibrations was less than 1 °C at all temperatures.

In order to prove that the nonexponential $T_{1\rho}$ relaxation observed for the poly(ethylene oxide), PEO, side chain is a result of the comb architecture, WISE experiments with a spin-diffusion mixing-time[9] were performed at 263 K using a Bruker MSL-300 spectrometer operating at a ^{1}H and ^{13}C frequencies of 300.13 MHz and 75.5 MHz, respectively. In the t_1 dimension, 48 slices with increments of 10 μs were acquired. The carbon and proton 90° pulse lengths were 2.8 μs and 3.6 μs, respectively. A cross-polarization time of 100 μs and a mixing-time of 100 μs were used in one experiment and a longer cross-polarization of 500 μs was used for the second WISE experiment with a mixing-time of 100 ms. The signal-acquisition time was 8 ms.

7.3 Results and Discussion

7.3.1 Domain Size Determination

^{1}H spin diffusion experiments determined the domain sizes of the POEM blocks in the POEM-*b*-P*n*BMA and POEM-*b*-PMMA diblock copolymers. The results are

shown in Figure 7.1. The decrease of the PEO signal intensity with spin diffusion mixing time was equal for both polymers; the initial decay slope was 8.5 ± 2 $ms^{-1/2}$. The diffusion rate in the POEM phase, 0.07 ± 0.03 nm^2/ms was determined based on the measured ^1H T_2^{-1} of the POEM phase, 400 ± 100 Hz^{-1}, and the curve determined by Mellinger *et al.*[10] The square root of the effective spin diffusion rate was calculated using Equation 2.4 to be 0.4 ± 0.1 $nm/ms^{1/2}$. Assuming that the diblock copolymers both have lamellar morphologies, the thickness of the POEM lamellae in both copolymers was determined based on Equation 2.5 to be 4 ± 1 nm.

7.3.2 ^{7}Li Linewidth Measurements

The ^{7}Li linewidth measurements show a small, but significant difference between $LiCF_3SO_3$ doped block copolymer electrolytes with different non-conductive phases, as shown in Figure 7.2. The segmental motion of the polymer chains averages orientation-dependent interactions of the observed nucleus with its environment. The ^{7}Li linewidth transitions occur when the motional rate exceeds the frequency width of the rigid limit spectrum (~6 kHz). The linewidths display a shift towards higher temperatures as the T_g of the poly(alkyl methacrylate) block increases; PLMA, P*n*BMA, and PMMA blocks exhibited glass-transitions at -35, 40, and 100°C, respectively. The ^{7}Li results are in agreement with the a.c. impedance spectroscopy measurements which also showed a higher ionic conductivity and lower activation energy for POEM-*b*-PLMA.[7] The specific conductivities for doped POEM, POEM-*b*-PLMA,

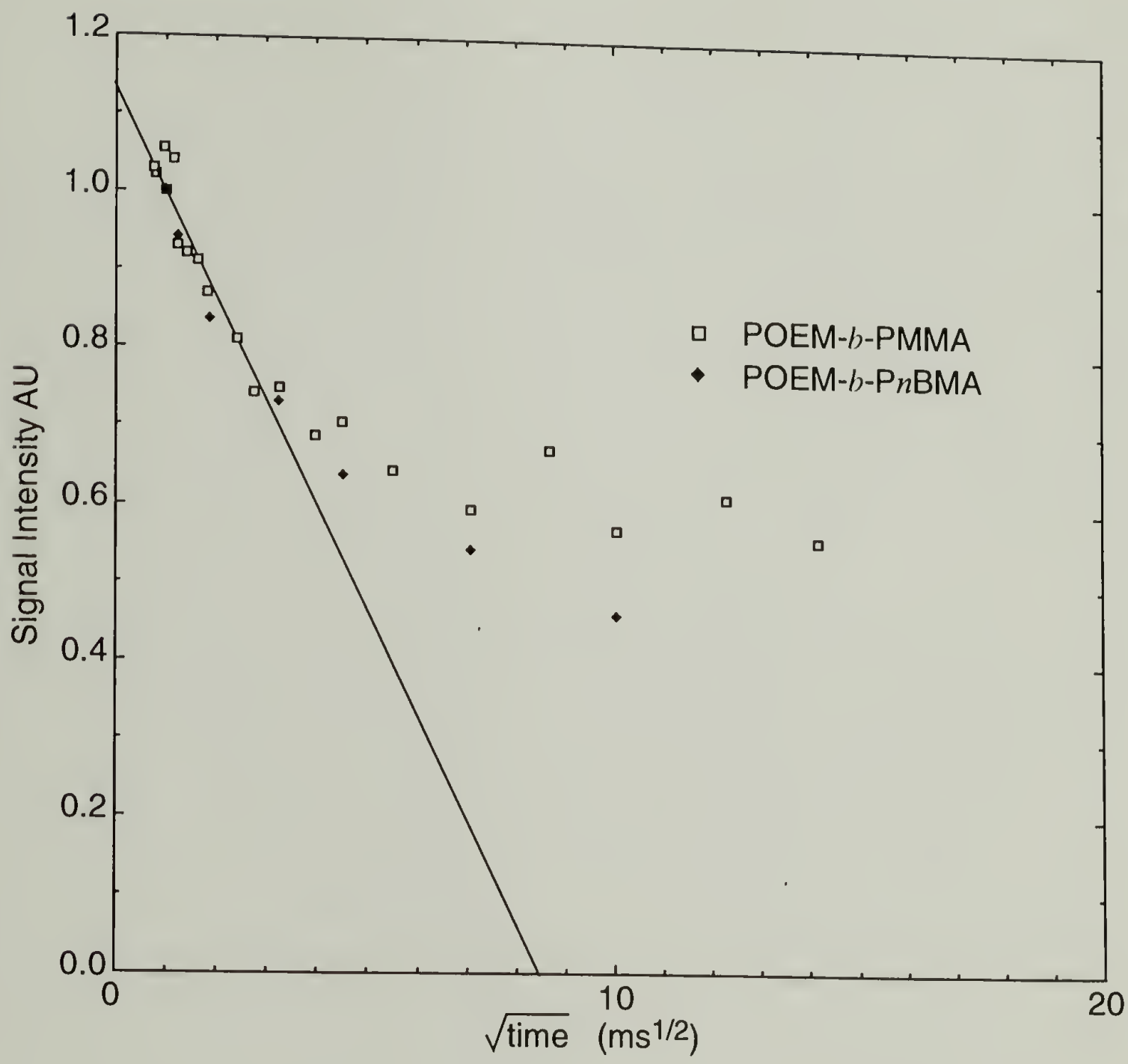

Figure 7.1: ^{1}H spin diffusion experiments to determine the domain sizes of the POEM blocks in the POEM-*b*-P*n*BMA and POEM-*b*-PMMA diblock copolymers. The slope of the initial transfer of magnetization from the excited POEM regions to the suppresed rigid component is equal in both polymers, suggesting that the domain sizes for both copolymers are approximately equal.

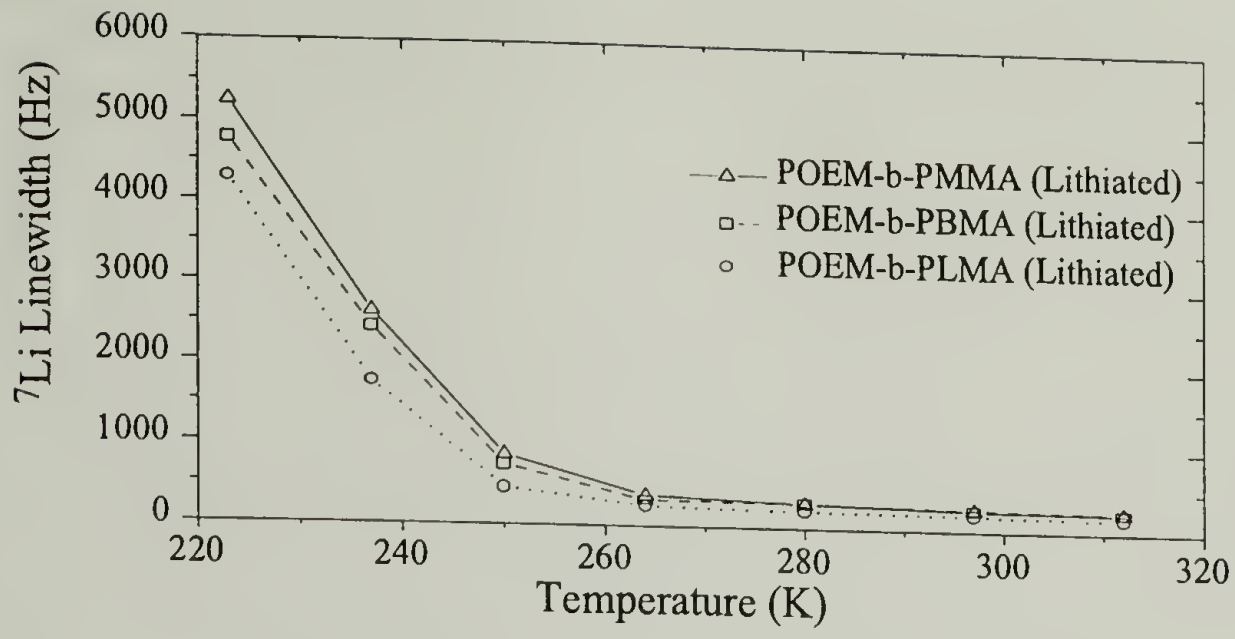

Figure 7.2: Temperature dependence of ^{7}Li linewidth in $LiCF_3SO_3$ doped POEM-*b*-PLMA, POEM-*b*-P*n*BMA, and POEM-*b*-PMMA copolymers. The T_g's of PLMA, P*n*BMA, and PMMA are -35, 40, and 100°C, respectively.

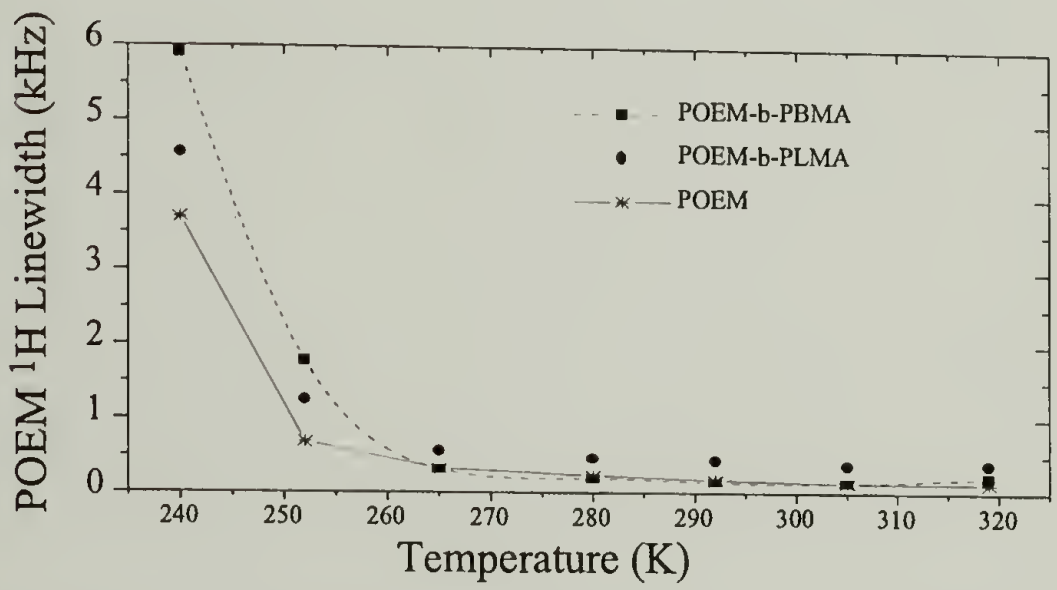

Figure 7.3: ^{1}H linewidth of peak at 4 ppm (PEO side-chain) in POEM, POEM-*b*-PLMA, and POEM-*b*-P*n*BMA copolymers. The samples were measured with a spinning rate of 1 kHz.

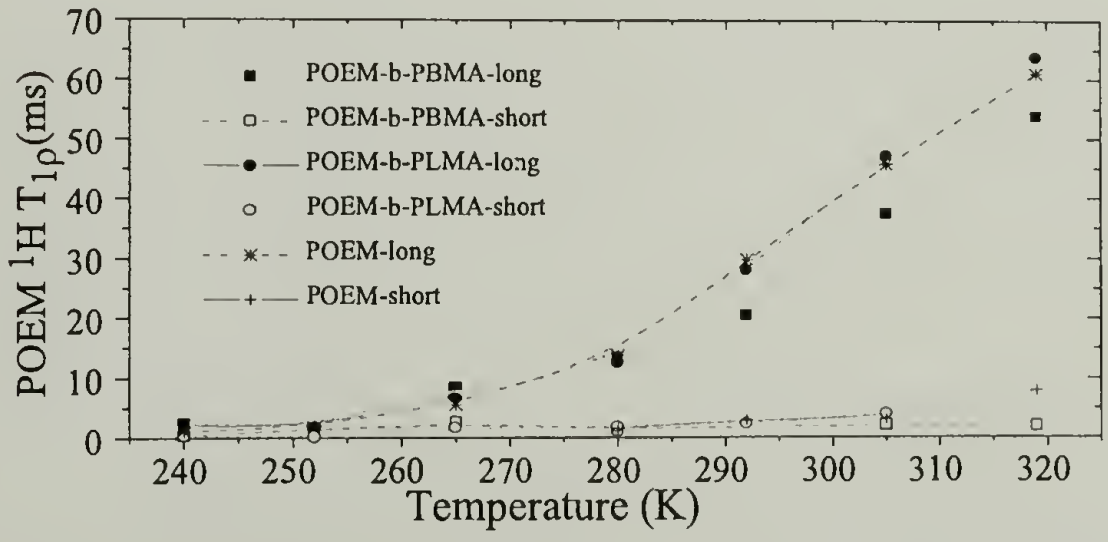

Figure 7.4: $T_{1\rho}$ measurements of peak at 4 ppm for POEM, POEM-*b*-PLMA, and POEM-*b*-P*n*BMA copolymers. The observed decay of the magnetization was fit with two exponential functions exponential equations.

POEM-*b*-P*n*BMA, and POEM-*b*-PMMA ([EO]:[Li^+] = 20:1) at 303 K were reported to be 14, 3.5, 2.0, and 1.6 x 10^{-6} S/em, respectively.[7] The conductivity curves of POEM-*b*-P*n*BMA and POEM-*b*-PMMA are shifted towards higher temperatures relative to the POEM-*b*-PLMA conductivity curve by approximately 4 °C and 6 °C, respectively. These differences are similar to the shifts of 3 °C and 5°C observed in the ^{7}Li linewidth experiments. This difference is greater than the uncertainty in temperature, ± 1 °C.

7.3.3 ^{1}H Linewidth and $T_{1\rho}$ Experiments

^{1}H linewidth measurements, shown in Figure 7.3, were performed on the undoped materials. A shift in the linewidth transition is present in this comparison as well. The differences between the POEM curve and the POEM-*b*-PLMA and POEM-*b*-P*n*BMA curves are 2 °C and 5° C, respectively.

To complement the linewidth data, ^{1}H $T_{1\rho}$ measurements were also conducted on the undoped samples. $T_{1\rho}$ reaches a minimum for motional rates near 2π x 60 kHz.[14] The rotating-frame relaxation data for the protons of the PEO side-chain could not be fit by a simple exponential decay. A bi-exponential function with both long and short $T_{1\rho}$ values was used to fit the relaxation data and these values are shown in Figure 7.4. The short $T_{1\rho}$ values are nearly independent of temperature for all samples. The long $T_{1\rho}$ relaxation times showed a trend consistent with the ^{1}H and ^{7}Li linewidth measurements: the P*n*BMBA phase decreases the mobility in the POEM phase. The $T_{1\rho}$ behavior of

POEM-*b*-PLMA and POEM homopolymer at temperatures greater than the T_g of PLMA are similar. This shows that the previously observed difference in ionic conductivity is at least partially due to slower dynamics of segments and ions in the POEM phase. The differences in POEM mobility between all samples, as shown by the three types of NMR experiments, although significant, is very small. *N.B.* POEM is a comb polymer and the mobility differences in linear block copolymers may be different. There also will be a molecular weight dependence: longer polymer chains will have less interaction with the other block.

7.3.4 WISE Experiments

The disparity between the short and long $T_{1\rho}$ components indicate that the chain dynamics of the POEM block is quite complex. To confirm the hypothesis that this difference is due to a gradient of mobility in the POEM side chain, 2D WISE experiments were conducted on the POEM-*b*-PLMA sample at 263 K. The WISE technique allows determination of ^{1}H linewidth of specific components in inhomogeneous systems. The pulse sequence is similar to the standard CP-MAS experiment with the addition of an incremented delay t_1 after the initial ^{1}H 90° pulse, thus correlating the ^{1}H wideline spectrum and the ^{13}C isotropic shifts in the ω_1 and ω_2 dimensions, respectively. The result of the WISE experiment without ^{1}H spin-diffusion effects (both short cross-polarization and mixing times), Figure 7.5 (a), shows that the PEO side chain, at 72 ppm, contains both a highly mobile and a relatively rigid (linewidth = 23 kHz) component. The WISE experiment with both long cross-polarization and mixing times

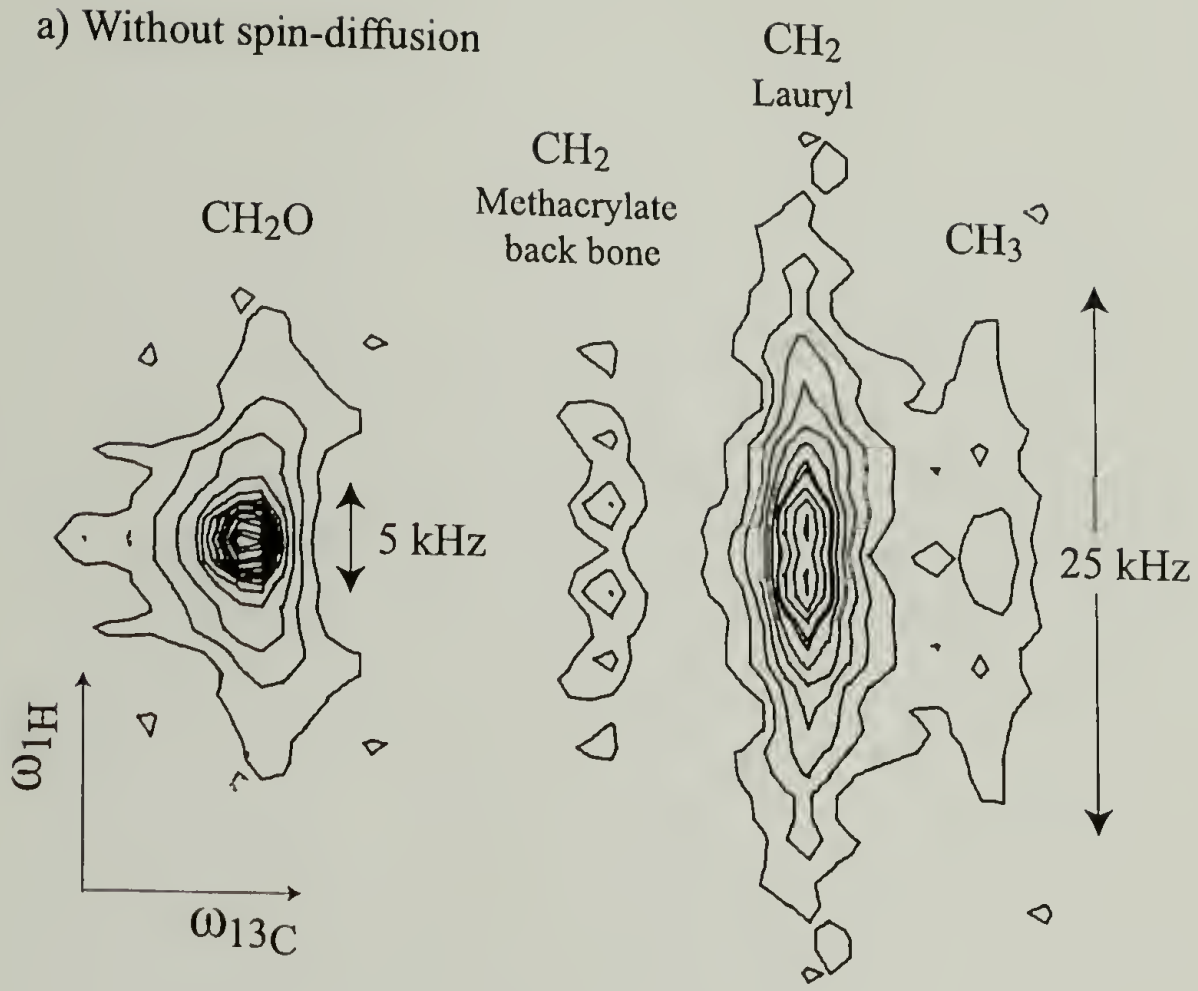

Figure 7.5: 2D WISE experiments on POEM-*b*-PLMA at 263 K with spin-diffusion mixing and cross polarization times of (a) 100 μs, 100 μs, and (b) 500 μs, 100 ms, respectively. At short CP and spin diffusion times, the signal of the more rigid units is observed selectively. The more mobile (narrow peak) component of the PEO side-chain transfers magnetization to the more rigid component during the 100 ms spin-diffusion mixing time.

(500 μs and 100 ms, respectively), are shown in Figure 7.5 (b). The magnetization is transferred through spin-diffusion from the rigid component to the mobile component. Thus, assuming Fickian diffusion, the distance between the highly mobile ethylene oxide units and the more rigid units must be less than 4 nm.

A gradient of motional rates is expected in comb polymers: the free end of the side chain has fast dynamics relative to the backbone. The similar biexponential behavior of the $T_{1\rho}$ relaxation curves for the POEM homopolymer suggests that this gradient of motion is not primarily due to the diblock structure.

7.4 Conclusions

^{1}H and ^{7}Li NMR spectroscopy has shown that the enhanced conductivity of diblock copolymer electrolytes with a low T_g non-conductive phase is at least partially due to faster chain dynamics in the conductive phase. A higher T_g non-conductive block shifts the observed dynamics curves towards a higher temperature; this shift is small (approximately 5 °C), but significant. Finally, the dynamic inhomogeneity in the POEM side chain, observed in the bi-exponential $T_{1\rho}$ decay, was determined by the WISE experiments to be on a length-scale of less than 5 nm.

7.5 Bibliography

(1) MacCallum, J. R.; Vincent, C. A. *Polymer Electrolyte Reviews*; Elsevier: Amsterdam, 1987; Vol. 1.

(2) Gray, F. M.; MacCallum, J. R.; Vincent, C. A.; Giles, J. R. M. *Macromolecules* **1988**, *21*, 392-397.

(3) Bruce, P. G.; Vincent, C. A. *J. Chem. Soc., Faraday Trans.* **1993**, *89*, 3187-3203.

(4) Khan, I.; Fish, D.; Delaviz, Y.; Smid, J. *Makromol. Chem.* **1989**, *190*, 3043.

(5) Giles, J. R. M.; Gray, F. M.; MacCallum, J. R.; Vincent, C. A. *Polymer* **1987**, *28*, 1977-1981.

(6) Li, J.; Khan, I. *Makromol. Chem.* **1991**, *192*, 3043-3050.

(7) Soo, P. P.; Huang, B. Y.; Jang, Y.-I.; Chiang, Y.-M.; Sadoway, D. R.; Mayes, A. M. *J. Electrochem. Soc.* **1999**, *146*, 32-37.

(8) Schmidt-Rohr, K.; Clauss, J.; Spiess, H. W. *Macromolecules* **1992**, *25*, 3273-3277.

(9) Schmidt-Rohr, K.; Spiess, H. W. *Multidimensional Solid-State NMR and Polymers*; Academic Press: San Diego, 1994.

(10) Mellinger, F.; Wilhelm, M.; Spiess, H. W. *Macromolecules* **1999**, *32*, 4686-4691.

(11) VanderHart, D. L.; McFadden, G. B. *Solid State Nucl. Magn. Reson.* **1996**, *7*, 45.

(12) VanderHart, D. L. *Makromol. Chem. Makromol. Symp.* **1990**, *34*, 125-159.

(13) Caravatti, P.; Neuenschwander, P.; Ernst, R. R. *Macromolecules* **1985**, *24*, 125.

(14) Johansson, A.; Tegenfeldt, J. *J. Chem. Phys.* **1996**, *104*, 5317-5325.

BIBLIOGRAPHY

Abragam, A. *Principles of Nuclear Magnetism*; Oxford University Press: Oxford, 1961.

Ahlnäs, T.; Karlström, G.; Lindman, B. *J. Phys. Chem.* **1987**, *91*, 4030-4036. "Dynamics and Order of Nonionic Surfactants in Neat Liquid and Micellar Solution from Multifield ^{13}C NMR Relaxation and ^{13}C NMR Chemical Shifts."

Aranda, P.; Ruiz-Hitzky, E. *Chem. Mater.* **1992**, *4*, 1395-1403. "PEO-Silicate Intercalation Materials."

Aranda, P.; Ruiz-Hitzky, E. *Acta Polym.* **1994**, *45*, 59-67. "New Polyelectrolyte Materials Based on Smectite Polyoxyethylene Intercalation Compounds."

Belfiore, L. A.; J., L. T.; Cheng, C.; Bronnimann, C. E. *J. Polym. Sci., Part B: Polym. Phys.* **1990**, *28*, 1261-1274. "Solid-State Phase Behavior and Molecular-Level Mixing Phenomena in a Strongly Interacting Polymer Blend."

Bennett, A. E.; Rienstra, C. M.; Auger, M.; Lakshmi, K. V.; Griffin, R. G. *J. Chem. Phys.* **1995**, *103*, 6951-6958. "Heteronuclear Decoupling in Rotating Solids."

Björling, M.; Karlström, G.; Linse, P. *J. Phys. Chem.* **1991**, *95*, 6706-6709. "Conformational Adaptation of Poly(ethylene oxide). A ^{13}C NMR Study."

Bloembergen, N.; Purcell, E. M.; Pound, R. V. *Phys. Rev.* **1948**, *73*, 679-712. "Relaxation Effects in Nuclear Magnetic Resonance Absorption."

Bloembergen, N. *Physica* **1949**, *XV*, 386-426. "On the Interaction of Nuclear Spins in a Crystalline Lattice."

Bruce, P. G.; Vincent, C. A. *J. Chem. Soc., Faraday Trans.* **1993**, *89*, 3187-3203. "Polymer Electrolytes."

Cabane, B. *J. Phys. Chem.* **1977**, *81*, 1639-1645. "Structure of Some Polymer-Detergent Aggregates in Water."

Carr, H. Y.; Purcell, E. M. *Phys. Rev.* **1954**, *94*, 630-638. "Effects of Diffusion on Free Precession in NMR Experiments."

Cheney, V. B.; Grant, D. M. *J. Am. Chem. Soc.* **1967**, *89*, 5319-5327. "Carbon-13 Magnetic Resonanee. VIII. The Theory of Carbon-13 Chemical Shifts Applied to Saturated Hydrocarbons."

Cheng, C.; Belfiore, L. A. *Polym. News* **1990**, *15*, 39-49. "Solid Statc Phase Bchavior of Strongly Interaeting Polymer Blends."

Clauss, J. S.-R., K.; Spiess, H. W. *Acta Polymer.* **1993**, *44*, 1-17. "Dctermination of Domain Sizes in Heterogcneous Polymers by Solid-Statc NMR."

Cranks, J. *The Mathematics of Diffusion*; Clarendon Press: Oxford, 1975.

Damman, P.; Point, J. J. *Macromolecules* **1993**, *26*, 1722-1728. "Crystallization and Morphology of PEO-p-Nitrophenol Molceular Complex Crystallizcd from thc Melt."

Damman, P.; Point, J. J. *Macromolecules* **1994**, *27*, 3919-3925. "Crystalline Structure of the PEO-PNP eomplex. 2. FTIR."

Damman, P.; Point, J. J. *Macromolecules* **1995**, *28*, 2050-2053. "Polymorphism of the PEO-PNP Complex."

Delaitc, E.; Point, J. J.; Damman, P.; Dosière, M. *Macromolecules* **1992**, *25*, 4768-4778. "Two Allotropie forms for thc PEO-Resorcinol Molecular Complcx."

deAzcvedo, E. R.; Hu, W.-G.; Bonagamba, T. J.; Sehmidt-Rohr, K. *J. Am. Chem. Soc.* **1999**, *121*, 8411-8412. "Centerband-Only Detection of Exchange: Efficicnt Analysis of Dynamies in Solids by NMR."

deAzevedo, E. R.; Hu, W.-G.; Bonagamba, T. J.; Schmidt-Rohr, K. *J. Chem. Phys* **(accepted)**.

Diekinson, R. G.; Pauling, L. *J. Am. Chem. Soc.* **1923**, *45*, 1466-1471. "The Crystal Strueture of Molybdenite."

Dines, M. B. *Mat. Res. Bull.* **1975**, *10*, 287-292. "Lithium Intercalation via n-Butyllithium of the Layered Transition Metal Dichalcogcnidcs."

Divigalpitiya, W. M. R.; Frindt, R. F.; Morrison, S. R. *Science* **1989**, *246*, 369-371. "Inelusion Systems of Organic Molceules in Rcstaekcd Singlc-Layer Molybdcnum Disulfide."

Dunbar, M. G.; Novak, B. M.; Schmidt-Rohr, K. *Solid State Nuclear Magn. Reson.* **1998**, *12*, 119-137. "*Trans* Content in Atactic PS cstimatcd by DQ-NMR."

Giannelis, E. *Adv. Mater.* **1996**, *8*, 29. "Polymer Layered Silicate Nanocomposites."

Giles, J. R. M.; Gray, F. M.; MacCallum, J. R.; Vincent, C. A. *Polymer* **1987**, *28*, 1977-1981. "Synthesis and Characterization of ABA Block Copolymer-Based Polymer Electrolytes."

Goldman, M.; Shen, L. *Phys. Rev.* **1966**, *144*, 321-331. "Spin-Spin Relaxation in LaF_3."

Gray, F. M.; MacCallum, J. R.; Vincent, C. A.; Giles, J. R. M. *Macromolecules* **1988**, *21*, 392-397. "Novel Polymer Electrolytes Based on ABA Block Copolymers."

Grim, R. E. *Clay Mineralogy*; 1st ed. ed.; McGraw-Hill Book Company: New York, 1953.

Gullion, T.; Schaefer, J. *J. Magn. Reson.* **1989**, *81*, 196-200. "Rotational-Echo Double-Resonance NMR."

Harris, D. J.; Bonagamba, T. J.; Schmidt-Rohr, K. *Macromolecules* **1999**, *32*, 6718. "Conformation of Poly(ethylene oxide) Intercalated in Clay and MoS_2 Studied by Two-Dimensional Double-Quantum NMR."

Harris, D. J.; Bonagamba, T. J.; Hong, M.; Schmidt-Rohr, K. *accepted to Macromolecules* **2000**.

Hong, M. *J. Magn. Reson.* **1999**, *136*, 86-89. "Solid-State Dipolar INADEQUATE NMR Spectroscopy with a Large Double-Quantum Spectral Width."

Iwamoto, R.; Saito, Y.; Ishihara, H.; Tadokoro, H. *J. Polym. Sci., Part A-2* **1968**, *6*, 1509-1525. "Structure of PEO Complexes. II. PEO-Mercuric Chloride Complex."

Jeener, J.; Meier, B. H.; Bachmann, T.; Ernst, R. R. *J. Chem. Phys.* **1978**, *71*, 4546-4553. "Investigation of Exchange Process by Two-Dimensional NMR Spectroscopy."

Johansson, A.; Tegenfeldt, J. *J. Chem. Phys.* **1996**, *104*, 5317-5325. "Segmental Mobility in Complexes of $Pb(CF_3SO_3)_2$ and PEO Studied by NMR Spectroscopy."

Kaji, H.; Schmidt-Rohr, K. **to be published.**

Khan, I.; Fish, D.; Delaviz, Y.; Smid, J. *Makromol. Chem.* **1989**, *190*, 3043.

Krishnamoorti, R.; Vaia, R. A.; Giannelis, E. P. *Chem. Mater.* **1996**, *8*, 1728-1734. "Structure and Dynamics of Polymer-Layered Silicate Nanocomposites."

Landfester, K.; Boeffel, C.; Lambla, M.; Spiess, H. W. *Macromolecules* **1996**, *29*, 5972-5980. "Characterization of Interfaces in Core-Shell Polymers by Advanced Solid-State NMR methods."

Lee, Y. K.; Kurur, N. D.; Helmle, M.; Johannessen, O. G.; Nielsen, N. C.; Levitt, M. H. *Chem. Phys. Lett.* **1995**, *242*, 304-309. "Efficient Dipolar Recoupling in the NMR of Rotating Solids. A Sevenfold Symmetric Radiofrequency Pulse Sequence."

Lemmon, J. P.; Lerner, M. M. *Chem. Mater.* **1994**, *6*, 207-210. "Preparation and Characterization of Nanocomposites of Polyethers and Molybdenum Disulfide."

Lemmon, J. P.; Lerner, M. M. *Solid State Commun.* **1995**, *94*, 533-537. "Preparation of Nanocomposites of PEO with TiS_2."

Li, J.; Khan, I. *Makromol. Chem.* **1991**, *192*, 3043-3050. "Mixed (Electronic and Ionic) Conductive Solid Polymer Matrix."

MacCallum, J. R.; Vincent, C. A. *Polymer Electrolyte Reviews*; Elsevier: Amsterdam, 1987; Vol. 1.

Maricq, M.; Waugh, J. S. *J. Chem. Phys.* **1979**, *70*, 3300-3316. "NMR in Rotating Solids."

Mark, J. E.; Flory, P. J. *J. Am. Chem. Soc.* **1965**, *87*, 1415-1422. "The Configuration of the Polyoxyethylene Chain."

Mark, J. E.; Flory, P. J. *J. Am. Chem. Soc.* **1966**, *88*, 3702-3707. "Dipole Moments of Chain Molecules. I. Oligomers and Polymers of Oxyethylene."

McBrierty, V. J.; Packer, K. J. *Nuclear Magnetic Resonance in Solid Polymers*; Cambridge University Press: London, 1993.

Mellinger, F.; Wilhelm, M.; Spiess, H. W. *Macromolecules* **1999**, *32*, 4686-4691. "Calibration of ^1H NMR Spin Diffusion Coefficients for Mobile Polymers through Transverse Relaxation Measurements."

Myasnikova, R. M.; Titova, E. F.; Obolonska, E. S. *Polymer* **1980**, *21*, 403-407. "Study of 2:1 PEO-Resorcinol Molecular Complex."

Ogawa, M.; Kuroda, K. *Chem. Rev.* **1995**, *95*, 399-438. "Photofunctions of Intercalation Compounds."

Oriakhi, C. O.; Nafshun, R. L.; Lerner, M. M. *Mater. Res. Bull.* **1996**, *31*, 1513-1520. "Preparation of Nanocomposites of Linear Poly(ethylenimine) with Layered Hosts."

Papke, B. L.; Ratner, M. A.; Shriver, D. F. *J. Phys. Chem. Solids* **1981**, *42*, 493-500. "Vibrational Spectroscopy and Structure of Polymer Electrolytes, PEO Complexes of Alkali Metal Salts."

Paternostre, L.; Damman, P.; Dosière, M.; Bourgaux, C. *Macromolecules* **1996**, *29*, 2046-2052. "Integral and Nonintegral Folding in Lamellar Crystals of Molecular Complexes of PEO."

Paternostre, L.; Damman, P.; Dosière, M. *Macromolecules* **1997**, *30*, 3946-3948. "Time-Resolved SAXS Study of the Crystallization and Melting of PEO Molecular Complexes."

Pemawansa, K. P.; Thakur, A.; Karikari, E. K.; Khan, I. M. *Macromolecules* **1999**, *32*, 1910-1917. "Preparation and Characterization of PGNA/PEO Macromolecular Complexes."

Persson, B.-O.; Drakenberg, T.; Lindman, B. *J. Phys. Chem.* **1976**, *80*, 2124-2125. "Amphiphile Aggregation Number and Conformation from Carbon-13 NMR Chemical Shifts."

Pinnavaia, T. J. *Science* **1983**, *220*, 365-371. "Intercalated Clay Catalysts."

Point, J. J.; Coutelier, C. *J. Polym. Sci.: Polym. Phys. Ed.* **1985**, *23*, 231. "Linear High Polymers as Host in Intercalates. Introduction and Example."

Point, J. J.; Jasse, B.; Dosière, M. J. *J. Phys. Chem.* **1986**, *90*, 3273-3277. "Intercalates with Linear Polymer Hosts. 2. FTIR Study of PEO-Para-Disubsituted Benzene Ontercalates."

Point, J. J.; Damman, P. *Macromolecules* **1992**, *25*, 1184-1188. "Structure of New Crystalline complex: PEO with *p*-Nitrophenol."

Ribeiro, A. A.; Dennis, E. A. *J. Phys. Chem* **1977**, *81*, 957-963. "A Carbon-13 and Proton NMR Study on the Structure and Mobility of Nonionic Alkyl Polyoxyethylene Ether Micelles."

Rienstra, C. M.; Hatcher, M. E.; Mueller, L. J.; Sun, B. Q.; Fesik, S. W.; Griffin, R. G. *J. Am. Chem. Soc.* **1998**, *120*, 10602-10612. "Efficient Multispin Homonuclear Double-Quantum Recoupling for Magic-Angle Spinning NMR: 13C-13C Correlation Spectroscopy of U-13C-Erythromyscin A."

Ruiz-Hitzky, E.; Jimemez, R.; Casal, B.; Manriquez, V.; Ana, A. S.; Gonzalez, G. *Adv. Mater.* **1993**, *5*, 738. "PEO Intercalated in Layered Chalcogenides."

Sandström, D.; Hong, M.; Schmidt-Rohr, K. *Chem. Phys. Lett.* **1999**, *300*, 213-220. "Identification and Mobility of Deuterated Residues in Peptides and Proteins by ^{2}H-^{13}C Solid-State NMR."

Schilling, F. C.; Tonelli, A. E.; Cholli, A. L. *J. Polym. Sci., Part B: Polym. Phys.* **1992**, *30*, 91-96. "A ^{13}C NMR Study of the Effect of g-Irradiation on the Chain Dynamics of PEO."

Schmidt, A.; McKay, R. A.; Schaefer, J. *J. Magn. Reson.* **1992**, *96*, 644-650. "Internuclear Distance Measurement between Deuterium and a spin-1/2 Nucleus in Rotating Solids."

Schmidt, M.; Maurer, F. H. J. *J. Polym. Sci., Polym. Phys. Edn.* **1998**, *36*, 1061-1080. "Pressure-Volume-Temperature Properties and Free Volume Parameters of PEO/PMMA Blends."

Schmidt-Rohr, K.; Clauss, J.; Spiess, H. W. *Macromolecules* **1992**, *25*, 3273-3277. "Correlation of Structure, Mobility, and Morphological Information in Heterogeneous Polymer Materials by Two-Dimensional Wideline-Separation NMR Spectroscopy."

Schmidt-Rohr, K.; Wilhelm, M.; Johansson, A.; Spiess, H. W. *Magn. Reson. Chem.* **1993**, *31*, 352-356. "Determination of Chemical-Shift Tensor Orientations in Methylene Groups by Separated-Local-Field NMR."

Schmidt-Rohr, K.; Spiess, H. W. *Multidimensional Solid-State NMR and Polymers*; Academic Press: San Diego, 1994.

Schmidt-Rohr, K. *Macromolecules* **1996**, *29*, 3975-3981. "A Double-Quantum Solid-State NMR Technique for Determining Torsion Angles of Polymers."

Schmidt-Rohr, K. *J. Magn. Reson.* **1998**, *131*, 209. "Complete Dipolar Decoupling and 2D DQ-NMR for determining segmental conformations in Polymers."

Smith, G. D.; Yoon, D. Y.; Jaffe, R. L.; Colby, R. H.; Krishnamoorti, R.; Fetters, L. J. *Macromolecules* **1996**, *29*, 3462-3469. "Conformations and Structures of PEO Melts from Molecular Dynamics Simulations and Small-Angle Neutron Scattering Experiments."

Soo, P. P.; Huang, B. Y.; Jang, Y.-I.; Chiang, Y.-M.; Sadoway, D. R.; Mayes, A. M. *J. Electrochem. Soc.* **1999**, *146*, 32-37. "Rubbery Bloek Copolymer Eleetrolytes for Solid-State Reehargeable Lithium Batteries."

Spevácek, J.; Suehopárek, M. *Macromol. Symp.* **1997**, *114*, 23-34. "Polymer-Solvent Complexes in Thermoreversible Gels and in Solids As Studied by NMR and Other Methods."

Speváeek, J.; Paternostre, L.; Damman, P.; Draye, A. C.; Dosière, M. *Macromolecules* **1998**, *31*, 3612-3616. "Solid State ^{13}C NMR study of Moleeular Complexes of PEO and Hydroxybenzenes."

Spiegal, S.; Landfester, K.; Lieser, G.; Boeffel, C.; Spiess, H. W.; Eidam, N. *Macromol. Chem. Phys.* **1995**, *196*, 985-993. "Microheterogeneities of Core-Shell Latexes Probed by ^{1}H Spin Diffusion and Transmission Eleetron Mieroseopy."

Tadokoro, H.; Chatani, Y.; Yoshihara, T.; Tahara, S.; Murahashi, S. *Makromol. Chem.* **1964**, *73*, 109-127. "Structural Studies of Polyethers, II Moleeular strueture of PEO."

Tadokoro, H.; Yoshihara, T.; Chatani, Y.; Murahashi, S. *J. Polym. Sci., Part B* **1964**, *2*, 363-368. "A Preliminary Report of Structural Studies on Polyethylene Oxide-Urea Complex."

Takahashi, Y.; Tadokoro, H. *Macromolecules* **1973**, *6*, 672-675. "Struetural studies of Polyethers. X. Crystal Strueture of PEO."

Tonelli, A. E. *Macromolecules* **1990**, *23*, 3134-3137. "Conformations and Motions of Polyethylene and Poly(oxyethylene) Chains Confined to Channels."

Vaia, R. A.; Ishii, H.; Giannelis, E. P. *Chem. Mater.* **1993**, *5*, 1694-1696. "Synthesis and Properties of Two-Dimensional Nanostructures by Direet Intercalation of Polynmer Melts in Layered Silicates."

Vaia, R. A.; Vasudevan, S.; Krawiec, W.; Seanlon, L. G.; Gianellis, E. P. *Adv. Mater.* **1995**, *7*, 154. "New Polymer Eleetrolyte Nanoeomposites: Melt Interealation of PEO in Mica-Type Silicates."

Vaia, R. A.; Jandt, K. D.; Kramer, E. J.; Giannelis, E. P. *Macromolecules* **1995**, *28*, 8080-8085. "Kineties of Polymer Melt Interealation."

Vaia, R. A.; Sauer, B. B.; Tse, O. K.; Giannelis, E. P. *J. Polym. Sci. Part B: Polym. Phys.* **1997**, *35*, 59-67. "Relaxations of Confined Chains in Polymer Nanocomposites: Glass Transition Properties of PEO Interealated in Montmorillonite."

Vaia, R. A.; Giannelis, E. P. *Macromolecules* **1997**, *30*, 7990-7998. "Lattice Model of Polymer Melt Intercalation in Organically-Modified Layered Silicates."

Vaia, R. A.; Giannelis, E. *Macromolecules* **1997**, *30*, 8000-8009. "Polymer Melt Intercalation in Organically-Modified Layered Silicates: Model Predictions and Experiment."

VanderHart, D. L.; Earl, W. L.; Garroway, A. N. *J. Magn. Reson.* **1981**, *44*, 361-401. "Resolution in ^{13}C NMR of Organic Solids Using High-Power Proton Decoupling and Magic-Angle Sample Spinning."

VanderHart, D. L. *Makromol. Chem. Makromol. Symp.* **1990**, *34*, 125-159. "Proton Spin Diffusion As a Tool for Characterizing Polymer Blends."

VanderHart, D. L.; McFadden, G. B. *Solid State Nucl. Magn. Reson.* **1996**, *7*, 45.

Whittingham, M. S. *Prog. Solid. State Chem.* **1978**, *12*, 41-99. "Chemistry of Intercalation Compounds: Metal Guests in Chacogenide Hosts."

Wong, S.; Vaia, R. A.; Giannelis, E. P.; Zax, D. B. *Solid State Ionics* **1996**, *86-88*, 547-557. "Dynamics in a Poly(ethylene oxide)-Based Nanocomposite Polymer Electrolyte Probed by Solid State NMR."

Wong, S.; Zax, D. B. *Electrochimica Acta* **1997**, *42*, 3513-3518. "What do NMR Linewidths Tell Us? Dynamics of Alkali Cations in a PEO-Based Nanocomposite Polymer Electrolyte."

Wu, J.; Lerner, M. M. *Chem. Mater.* **1993**, *5*, 835. "Structural, Thermal, and Electrical Characterization of Layered Nanocomposites Derived from Na-Montmorillonite and Polyethers."

Yokoyama, M.; Ishihara, H.; Iwamoto, R.; Tadokoro, H. *Macromolecules* **1969**, *2*, 184-192. "Structure of PEO Complexes. III. PEO-Mercuric Chloride Complex. Type II."

Yang, D.-K.; Zax, D. B. *J. Chem. Phys.* **1999**, *110*, 5325-5336. "Li^+ Dynamics in a Polymer Nanocomposite: An Analysis of Dynamic Line Shapes in Nuclear Magnetic Resonance."

Yoshihara, T.; Tadokoro, H.; Murahashi, S. *J. Chem. Phys.* **1964**, *41*, 2902-2911. "Normal Vibrations of the Polymer Molecules of Helical Conformation. IV. Polyethylene Oxide and Polyethylene-d_4 Oxide."